

Chapter 1 Introduction

1-1 A brief history of Gallium Nitride epitaxial layers

Electroluminescence is a phenomenon in which a material emits light when electricity is passed through it. Electroluminescence was one of the greatest discoveries of the twentieth century and is rivaled by other forms of luminescence, including incandescence, chemiluminescence, cathodoluminescence, triboluminescence, and photoluminescence. Electroluminescence generally involves the production of light by a material without producing heat. Electroluminescence differs from black body light emission, which is only produced by mechanical actions. Electroluminescence is produced when an electric current is passed through a semiconductor with tiny holes. As excited electrons pass over these holes, they are emitted into the free air as particles known as photons. The semiconductor is usually made of a film, whether organic or inorganic, and can be dyed by some types of metal, known as a dopant. This is the most basic principle of all LEDs and most electronic lights in general. Specifically, there is a phosphorous-based electroluminescent backlight in virtually all electronic devices that is used to illuminate the Liquid Crystal Display (LCD).

Electronic lighting technology made its appearance with the advent of semiconductors during the second part of twentieth century. The achievement of high-efficiency electroluminescence from semiconductor devices in early 1963 led to light-emitting-diode (LED) technology [1-2]. Semiconductors with electroluminescence are expected a main part in many optoelectronic systems, such as high power energy source system, optical memory system, full color scanners or high definition ROM disk systems. Recently many researchers have been done on electroluminescence, especially in Zinc selenide (ZnSe) [3], Silicon carbide (SiC) [4], and Gallium Nitride (GaN) [2].

Electroluminescence has several advantages that has led it to be used so widely in electronic devices. For example, electroluminescence requires very little current in order to

work. This is advantageous in small electronic devices because they often run on batteries that are 1.5 Volts or smaller. Electroluminescent devices can be used to produce any color and are very simple in design. Though electroluminescence can be advantageous in most cases, it does have a few disadvantages. For example, electroluminescent devices require low amounts of current but high amounts of voltage, usually between 60 and 600 Volts. In electroluminescent devices that are connected to a power line, these voltages can be provided consistently at any time of day. In battery-operated, handheld devices, however, the voltage must be provided by a converter circuit that is built into the device.

1-2 The Introduction of Light-Emitting Diodes

Light-emitting diodes (LEDs) are a typical p-n junction device used under a forward bias. The basic operating mechanisms are based on the electrical and optical properties of p-n junction and of semiconductor materials. When the diode is forward biased, electrons are able to recombine with holes and energy is released in the form of light. This effect is called electroluminescence. As shown in **Fig. 1.1[5]**, the wavelength of the light emitted, and therefore its color, depends on the band gap energy of the materials forming the p-n junction. Most commercially available LEDs are made from III-V compound semiconductors. Some II-VI compound semiconductors such as ZnS and ZnSe are used in a few LEDs emitting visible light, though these materials are not used frequently because of the difficulty of p-n junction formation**[6]**.

1-2-1 Historical Introduction

Electroluminescence was discovered in 1907 by the British experimenter H. J. Round of Marconi Labs, using a crystal of silicon carbide and a cat's-whisker detector**[7]**. Russian Oleg Vladimirovich Losev independently created the first LED in the mid 1920s**[8]**; his research was distributed in Russian, German and British scientific journals, but no practical use was made of the discovery for several decades. LED development began with infrared and red

devices made with GaAs. Rubin Braunstein of the Radio Corporation of America first reported on infrared emission from GaAs and other semiconductor alloys in 1955[9]. Braunstein observed infrared emission generated by simple diode structures using GaSb, GaAs, InP, and SiGe alloys at room temperature and at 77 K. Experimenters at Texas Instruments, Bob Biard and Gary Pittman, found in 1961 that GaAs gave off infrared light when electric current was applied. Biard and Pittman were able to establish the priority of their work and received the patent for the infrared light-emitting diode. Nick Holonyak Jr. of the General Electric Company, who is seen as the “father of the light-emitting diode”, developed the first practical visible-spectrum LED in 1962. Since then, related researches went on continually.

In 1972, J. I. Pankove et al. fabricated the first blue LED using III-nitrides materials with a Metal-*i-n* structure [10]. However, the device performance was limited by the poorly conducting *p*-type GaN. The first high-brightness blue LED was demonstrated by Shuji Nakamura of Nichia Corporation and was based on critical developments in GaN nucleation on sapphire substrates and the demonstration of *p*-type doping of GaN which were developed by Isamu Akasaki and H. Amano in Nagoya using a low-temperature buffer layer and Low-Energy Electron Beam Interaction (LEEBI) technique, respectively[11]. In 1995, Alberto Barbieri at the Cardiff University Laboratory investigated the efficiency and reliability of high-brightness LEDs and demonstrated a very impressive result by using a transparent contact made of indium tin oxide (ITO) on AlGaInP/GaAs LED. The existence of blue LEDs and high efficiency LEDs quickly led to the development of the first white LED, which employed a $Y_3Al_5O_{12}:Ce$, or “YAG”, phosphor coating to mix yellow light with blue to produce light that appears white. Nakamura was awarded the 2006 Millennium Technology Prize for his invention.

1-2-2 Advantages of the LED Lighting

LEDs offer numerous benefits due to their mode of operation:

(1) Energy Efficiency

LEDs are highly efficient. In traffic signal lights, a strong market for LEDs, a red traffic signal head that contains 196 LEDs draws 10W versus its incandescent counterpart that draws 150W. Various estimates of potential energy savings range from 82% to 93%. With the red signal operating about 50% of the day, the complete traffic signal unit is estimated to save 35-40%. An estimation had been made that replacing incandescent lamps in all of America's some 260,000 traffic signals (red, green and yellow) could reduce energy consumption by nearly 2.5 billion kWh. At the end of 1997, more than 150,000 signals were retrofitted.

(2) Long Life

Some LEDs are projected to produce a long service life of about 100,000 hours. For this reason LEDs are ideal for hard-to-reach/maintain fixtures such as exit sign lighting and, combined with its durability, pathway lighting. This service life can be affected by the application and environmental factors, including heat and if being overdriven by the power supply.

(3) Range of Colors

LEDs are available in a range of colors, including white light. **Fig. 1.2** shows the chromaticity diagram^[12]. White light can be produced through color mixing, like red/blue/green, blue/yellow, or green/yellow-green/orange/purple. In addition, through the innovative combination of various-colored LEDs, dramatic color-changing effects can be produced from a single fixture through dynamic activation of various sets of LEDs. Manufacturers such as Color Kinetics offer fixtures that employ this principle. They offer track, theatrical, underwater, outdoor and other fixtures utilizing variable-intensity LEDs that can provide more than 16.7

million colors, including white light. These fixtures can be individually controlled via a PC, DMX controller or proprietary controller to generate effects including fixed color, color washing, cross fading, and random color changing.

(4) Cool Light

In contrast to most light sources, LEDs radiate very little heat in the form of IR that can cause damage to sensitive objects or fabrics. Wasted energy is dispersed as heat through the base of the LED.

(5) Durable

LEDs are highly rugged. They feature no filament that can be damaged due to shock and vibrations. They are subject to heat, however, and being overdriven by the power supply.

(6) Small Size/Design Flexibility

A single LED is very small and produces little light overall. However, this weakness is actually its strength. LEDs can be combined in any shape to produce desired lumen packages as the design goals and economics permit. In addition, LEDs can be considered miniature light fixtures; distribution of light can be controlled by the LEDs' epoxy lens, simplifying the construction of architectural fixtures designed to utilize LEDs. A controller can be connected to an LED fixture to selectively dim individual LEDs, resulting in the dynamic control of distribution, light output and color. Finally, DC power enables the unit to be easily adaptable to different power supplies.

(7) Dimming

LEDs can very easily be dimmed either by Pulse-width modulation or lowering the forward current.

(8) On/Off Time

LEDs light up very quickly. A typical red indicator LED will achieve full brightness

in microseconds. LEDs used in communications devices can have even faster response times.

(9) Cycling

LEDs are ideal for use in applications that are subject to frequent on-off cycling, unlike fluorescent lamps that burn out more quickly when cycled frequently, or HID lamps that require a long time before restarting.

1-2-3 Applications

Many application of LEDs are very diverse but fall into three major categories: Visual signal application where the light goes more or less directly from the LED to the human eye, to convey a message or meaning. Illumination where LED light is reflected from object to give visual response of these objects. Finally LEDs are also used to generate light for measuring and interacting with processes that do not involve the human visual system. These three categories are introduced below:

(1) Signals and Large Displays

The low energy consumption, low maintenance and small size of modern LEDs has led to applications as status indicators and displays on a variety of equipment and installations. Large area LED displays are used as stadium displays and as dynamic decorative displays. Thin, lightweight message displays are used at airports and railway stations, and as destination displays for trains, buses, trams, and ferries. The single color light is well suited for traffic lights and signals, exit signs, emergency vehicle lighting, ships' lanterns and LED-based Christmas lights. Red or yellow LEDs are used in indicator and alphanumeric displays in environments where night vision must be retained: aircraft cockpits, submarine and ship bridges, astronomy observatories, and in the field, e.g. night time animal watching and military field use. Because of their long life and fast switching times, LEDs have been used for automotive high-mounted brake lights and truck and bus brake lights and turn signals

for some time. The use of LEDs also has styling advantages because LEDs are capable of forming much thinner lights than incandescent lamps. The significant improvement in the time taken to light up (perhaps 0.5s faster than an incandescent bulb) improves safety by giving drivers more time to react. Due to the relative cheapness of low output LEDs, they are also used in many temporary applications such as glowsticks and throwies and Lumalive, a photonic textile, artists have also used LEDs for LED art.

(2) Lighting

With the development of high efficiency and high power LEDs, it has become possible to incorporate LEDs in lighting and illumination. Replacement light bulbs have been made as well as dedicated fixtures and LED lamps. LEDs are used as street lights and in other architectural lighting where color changing is used. The mechanical robustness and long lifetime is used in automotive lighting on cars, motorcycles and on bicycle lights. The lack of IR/heat radiation makes LEDs ideal for stage lights using banks of RGB LEDs that can easily change color and decrease heating from traditional stage lighting, as well as medical lighting where IR-radiation can be harmful. Since LEDs are small, durable and require little power, they are used in hand held devices such as flashlights. LED strobe lights or camera flashes operate at a safe, low voltage, as opposed to the 250 volts commonly found in xenon flashlamp-based lighting. This is particularly applicable to cameras on mobile phones, where space is at a premium and bulky voltage-increasing circuitry is undesirable. LEDs are used for infrared illumination in night vision applications including security cameras. A ring of LEDs around a video camera, aimed forward into a retroreflective background, allows chroma keying in video productions. LEDs are used for decorative lighting as well. Uses include but are not limited to indoor/outdoor decor, limousines, cargo trailers, conversion vans, cruise ships, RVs,

boats, automobiles, and utility trucks. Decorative LED lighting can also come in the form of lighted company signage and step and aisle lighting in theaters and auditoriums

(3) Non-Visual Applications

Light has many other uses besides for seeing. LEDs are used for some of these applications. The uses fall in three groups: Communication, sensors and light matter interaction. The light from LEDs can be modulated very fast so they are extensively used in optical fiber and free space optics (FSO) communications. This includes remote controls, such as for TVs and VCRs, where infrared LEDs are often used. Many sensor systems rely on light as the main medium. LEDs are often ideal as a light source due to the requirements of the sensors. LEDs are used as movement sensors, for example in optical computer mice. Touch sensing: Since LEDs can also be used as photodiodes, they can be used for both photo emission and detection. This could be used in for example a touch-sensing screen that register reflected light from a finger or stylus. Many materials and biological systems are sensitive to, or dependent on light. Grow lights use LEDs to increase photosynthesis in plants and bacteria and vira can be removed from water and other substances using UV LEDs for sterilization. Other uses are as UV curing devices for some ink and coating applications as well as LED printers.

1-3 III-V Nitride Based LEDs

Creating sources of white light is the ultimate goal of solid-state lighting technology. The most challenging application for LEDs is the replacement of conventional incandescent and probably, even fluorescent lamps. Attempts to up-convert long-wavelength emission of IR LEDs to broader visible spectra were undertaken years ago by Galginaitis and Fenner (1968) [13-14]. Berggren et al. (1994) demonstrated white light-emitting devices made from electroluminescent organic semiconductors [15]. However, practical white LEDs became

feasible only after the development of high brightness blue AlInGaN emitters (Nakamura and Fasol 1997) [16]. Based on short-wavelength LEDs, white LEDs that exploit the mixture of two or three colors (dichromatic and trichromatic LEDs, respectively) are being developed. The bandgap energy of AlGaInN varies between 6.2 and 1.95 eV depending on its composition at room temperature, as shown in Fig. 1.1. Therefore, these III-V nitride semiconductors are useful for light emitting devices especially in the short wavelength region. Among AlGaInN system, GaN has been most intensively studied. GaN has bandgap energy of 3.4 eV at room temperature. Previous research on III-V nitrides has paved the way for the realization of high quality crystals of GaN, AlGaIn and InGaIn, and of *p*-type conduction in GaN and AlGaIn[17-18]. The beginning of the growth of good quality epilayers was made by Yoshida et al. [19]. They showed in 1983 that if an AlN buffer layer is grown by two step method between the GaN film and the sapphire substrate, the quality of the layers improves. Amano et al. [20] were also the first to obtain *p*-type conductivity in GaN which used Mg as an acceptor. In 1992 van Vechten et al. [21] suggested that Mg-H complexes are formed in the as grown Mg-doped GaN and therefore hydrogen passivates the Mg acceptors. Later it was found that annealing the Mg-doped GaN layers at >750 °C in nitrogen or vacuum also activates the Mg acceptors[22]. By middle 1990s so much knowledge and experience in technology had accumulated that the progress in designing and fabricating devices became very rapid. High brightness blue LEDs have been fabricated on the basis of these results, and luminous intensities over 1 cd had been achieved in 1994[23-25].

1-4 The development of Gallium Nitride epitaxial layers

The development of GaN-based devices has challenged the conventional thinking on the material requirements for successful device fabrication in several ways. With the exceptions of silicon on sapphire and GaN, no semiconductor has been commercialized exclusively using heteroepitaxial materials; all other semiconductors have employed bulk substrates. Before pn-junction GaN-based LEDs on sapphire substrates were demonstrated, good luminescence

efficiency, regardless of the semiconductor, was thought to require very low dislocation densities, less than 10^6 cm^{-2} . Researchers were surprised to measure excellent luminescence efficiency from GaN LEDs despite dislocation densities four orders of magnitude higher. Unlike the majority of semiconductors, in GaN dislocations did not seem to degrade its optical and electrical properties. That sapphire was, and remains, the most common choice for GaN based LEDs is particularly surprising, given its properties are seemingly unsuitable based on the usual assumptions made in choosing a substrate for epitaxy; it has large lattice constant and thermal expansion coefficient mismatches with GaN. [5]

Interest has always been high in the production and characterization of wide-bandgap semiconductor materials for a wide range of short-wavelength and hightemperature applications. Candidate material systems include silicon carbide (SiC), the Group II-VI semiconductors zinc sulfide (ZnS) and zinc selenide (ZnSe), and the Group IIIA nitrides. The hexagonal polytypes of SiC, although once considered excellent candidates for blue LEDs and more recently for high-temperature and high-power electronic devices, are not suitable for ultraviolet (UV) detector or emitter applications because of their indirect and comparatively low bandgaps ($E_g < 3.2 \text{ eV}$).

Recent progress[26] in developing blue-green LEDs and laser diodes in the $\text{ZnS}_x\text{Se}_{1-x}$ alloy system¹ has been restricted to high-selenium alloys with bandgaps less than 2.8 eV. Higher-bandgap alloys continue to be plagued by autocompensation effects, whereby the introduction of a dopant atom is compensated by native defects and precludes well-behaved conductivity control. Thus, the Group III-V nitrides are the preferred candidates for short-wavelength applications. InN, GaN, and AlN have direct bandgaps of 2.0, 3.4, and 6.2 eV, respectively, with corresponding cutoff wavelengths of 620, 365, and 200 nm. Since they are miscible with each other, these nitrides form complete series of indium gallium nitride ($\text{In}_{1-x}\text{Ga}_x\text{N}$) and aluminum gallium nitride ($\text{Al}_x\text{Ga}_{1-x}\text{N}$) alloys, and it should be possible to develop detectors with wavelength cutoffs anywhere in this range.[26]

1-5 An Overview of the Dissertation

The primary contents of this dissertation are subjects which are relating to the mechanical properties and nanotribological characterization of GaN epitaxial layers on different axis sapphire substrate, including the contact-induced deformation behaviors, the repetition pressure-induced impairment behaviors, and nanotribological characterization behaviors.

There five chapters in this dissertation. In chapter 1, a brief history of the progress of lighting devices is presented. We also make a complete introduction about the LED, which contains history, advantages, applications, development of III-V nitride-based LEDs, and several key issues we might experience while studying it.

Chapter 2 reviews the GaN films including its characteristics, growth methods, and applications. Besides, the nanoindentation and nanoscratch principle and technique were introduced.

Chapter 3 introduces the experimental procedure and apparatus. The designed deposition parameters for different axis structures of GaN films were exhibited. Finally, the detail parameters of nanoindentation and nanoscratch for measuring mechanical properties and nanotribological characterization were shown, respectively.

Chapter 4 analyzes mechanical properties and nanotribological characterization of GaN films qualitatively and quantitatively. The ‘pop-in’ event was explained by the interaction of the deformed region, produced by the indenter tip, with the inner threading dislocations in the GaN films. In addition, the nanotribological behavior and deformation characteristics of the GaN films were investigated by nanoscratch technique and atomic force microscopy (AFM).

Finally, chapter 5 summarizes the major results of this study and points out several research areas which need further attention.

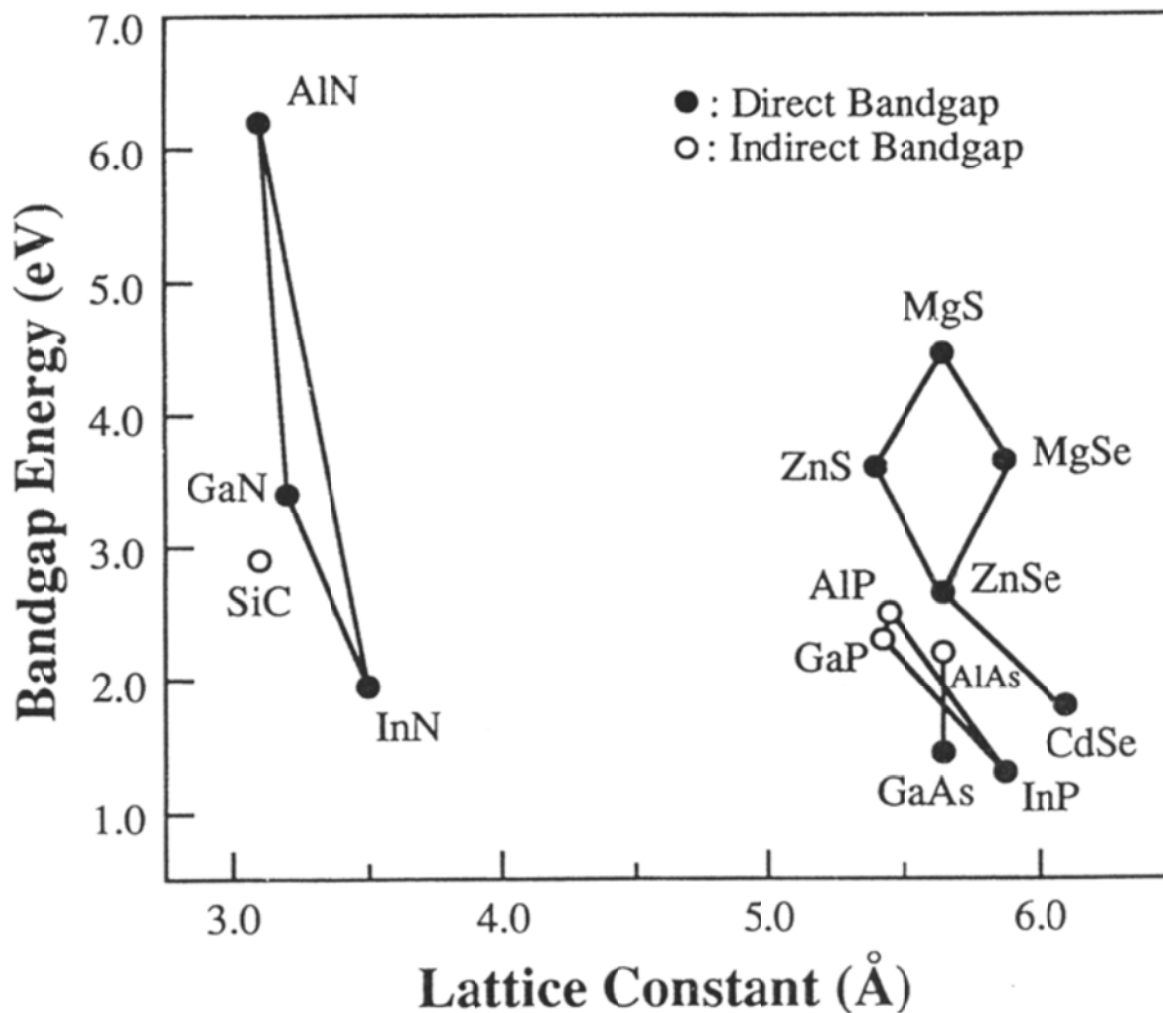


Figure 1.1 Bandgap energy of various materials for visible emission devices as a function of their lattice constant[5].

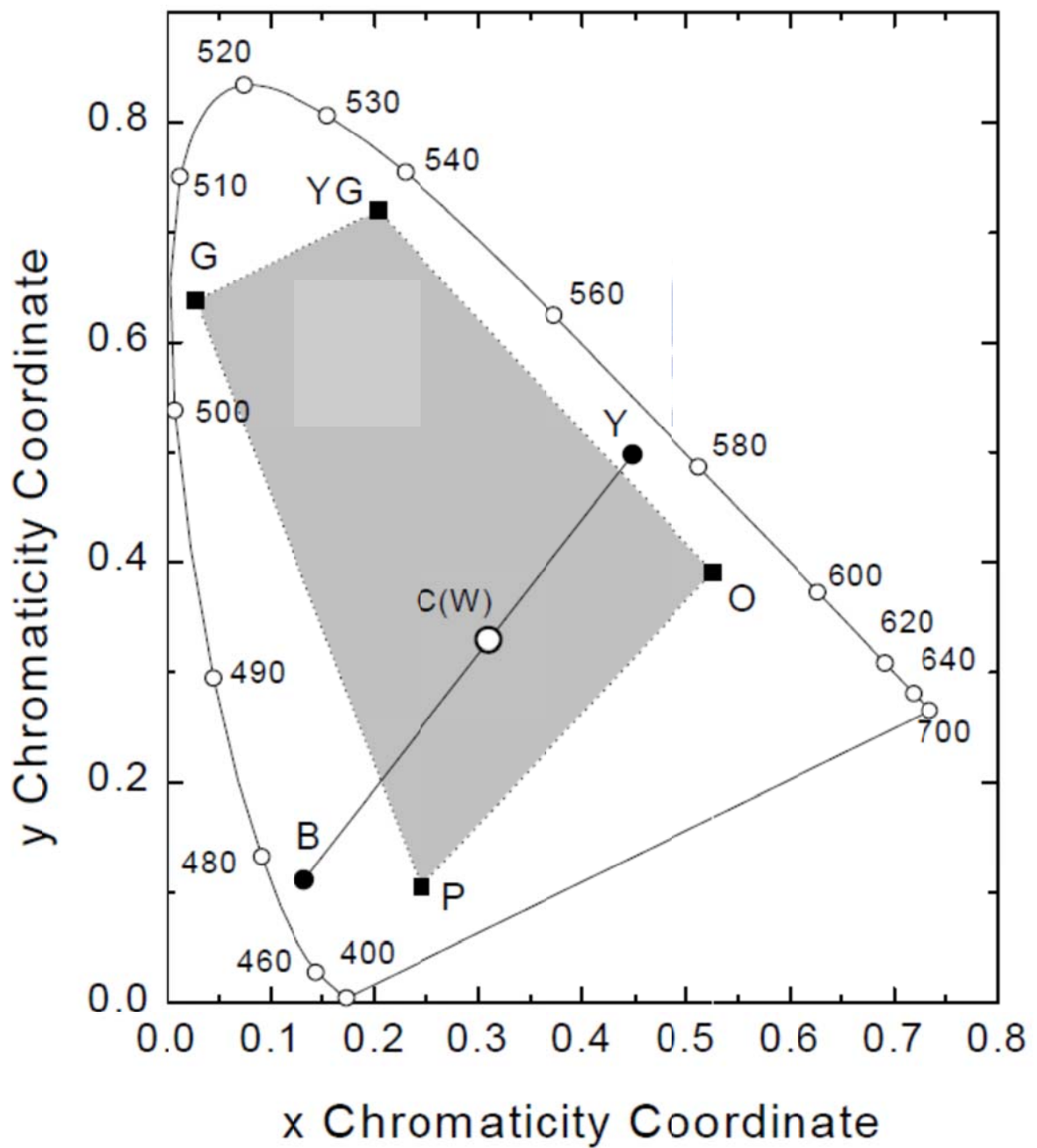


Figure 1.2 Chromaticity diagram. White light can be produced through color mixing, like red/blue/green, blue/yellow, or green/yellow-green/orange/purple[12].

Chapter 2 Literature review

2-1 Introduction

Gallium nitride is a highly attractive material of groups III–V nitride semiconductors, because it is great potential for the development of optoelectronic devices in blue/green light emitting diodes, semiconductor lasers, and optical detectors. The fabrication of optoelectronic devices based on GaN films requires to be understood in the mechanical properties as well as its optical and electrical properties [22, 27–30], that is to say, the mechanical damages of GaN films, such as film cracking and interface delamination caused by thermal stresses, chemical–mechanical polishing, usually suppress the processing yield and application reliability of microelectronic devices.

The heteroepitaxy using typical substrates (e.g., sapphire) with high lattice mismatch is discussed in early report. GaN films on sapphire substrates exhibits large lattice mismatch (about 14.5%) causing in-plane tensile strain in the GaN layers. In fact, the most common orientation of sapphire used for GaN is the c-axis sapphire. And, the lattice mismatch of the GaN films on a-axis $[11\bar{2}0]$ sapphire is less (2%) than that on c-axis $(0\ 0\ 0\ 1)$ sapphire (13.9%), which promises for excellent quality of GaN growth with improved surface morphology [31]. Here, compared to bulk single crystals, the deformation properties of thin films can serve strongly correlate to the geometrical dimensions and the materials defect structure. The misfit dislocations at the interface play an important role such as carrier mobility, and luminescence efficiency.

2-2 Physical properties, and development of GaN films

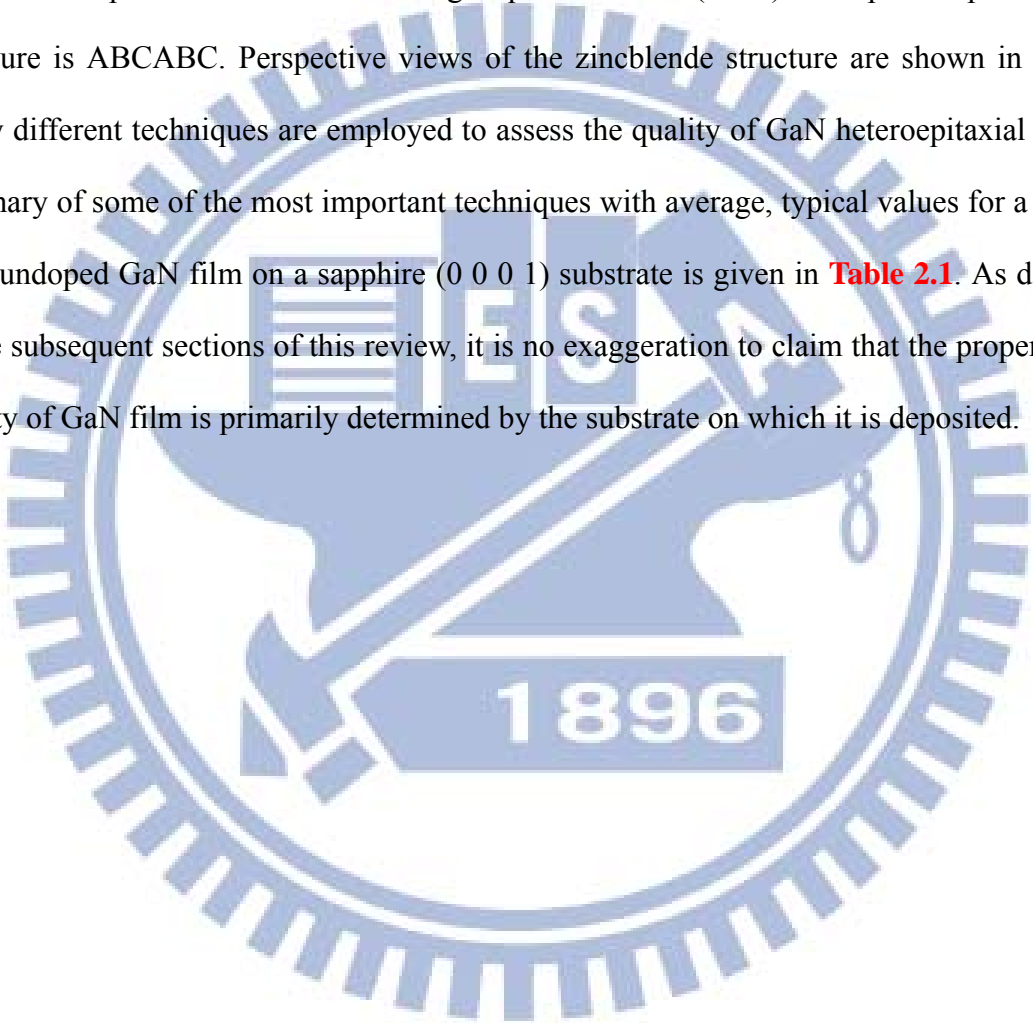
2-2-1 Physical properties of GaN films

The physical properties of GaN make it an attractive semiconductor for many electronic [32] and optoelectronic devices [33]. Its wide, direct energy band gap makes it suitable for short wavelength emitters (LEDs and diodes lasers) and detectors. The wide energy band gap and good thermal stability of GaN is also advantageous for high-temperature and high power electronics. Gallium nitride forms solid solutions with AlN and InN, making a wide range (1.9–6.2 eV) of energy band gaps possible. This ability to form alloys is essential for producing specific wavelengths for emitters, and for creating heterojunctions with potential barriers into the device structures. Heat dissipation in devices is facilitated by GaN's high thermal conductivity compared to silicon and gallium arsenide. Both n- and p-type conductivities are possible in GaN. Because the group III nitrides have a noncentrosymmetric structure and significantly ionic chemical bonding, they are strongly piezoelectric, and also undergo spontaneous polarization [34-35]. These effects can be advantageously employed, to increase the sheet carrier concentration in heterostructure transistor [36]. A summary of the physical properties of gallium nitride is given in **Table 1**. The thermal expansion coefficients of semiconductors including GaN depend on the temperature, and here only changes in lattice constants for certain temperature range are listed in this paper. The temperature-dependent data of thermal expansion coefficient for various substrates including GaN, AlN, 6H-SiC, 3C-SiC, GaAs, Al₂O₃, ZnO, and MgO can be found in [42].

Gallium nitride normally has a wurtzite structure, with the space group of P6₃mc (no. 186). The wurtzite structure consists of alternating biatomic close-packed (0 0 0 1) planes of Ga and N pairs stacked in an ABABAB sequence. Atoms in the first and third layers are directly aligned with each other. **Fig. 2.1** displays the perspective views of wurtzite GaN along [0 0 0 1], [11 $\bar{2}$ 0] and [1 0 $\bar{1}$ 0] directions, where the large circles represent gallium atoms and the small circles nitrogen. The close-packed planes are the (0 0 0 1) planes. The

group III nitrides lack an inversion plane perpendicular to the c-axis, thus, crystals surfaces have either a group III element (Al, Ga, or In) polarity (designated (0 0 0 1) or (0 0 0 1)A) or a N-polarity (designated (0 0 0 1) or (0 0 0 1)B). An excellent review on crystal polarity is given by Hellman [48].

The zincblende structure (see Table 2.2 the space group is F43m) of GaN can be stabilized in epitaxial films. The stacking sequence for the (1 1 1) close-packed planes in this structure is ABCABC. Perspective views of the zincblende structure are shown in **Fig. 2.2** Many different techniques are employed to assess the quality of GaN heteroepitaxial films. A summary of some of the most important techniques with average, typical values for a thin (<5 mm) undoped GaN film on a sapphire (0 0 0 1) substrate is given in **Table 2.1**. As described in the subsequent sections of this review, it is no exaggeration to claim that the properties and quality of GaN film is primarily determined by the substrate on which it is deposited.



2-2-2 The development of Gallium Nitride films

The development of GaN-based devices has challenged the conventional thinking on the material requirements for successful device fabrication in several ways. With the exceptions of silicon on sapphire and GaN, no semiconductor has been commercialized exclusively using heteroepitaxial materials; all other semiconductors have employed bulk substrates. Before pn-junction GaN-based LEDs on sapphire substrates were demonstrated, good luminescence efficiency, regardless of the semiconductor, was thought to require very low dislocation densities, less than 10^6 cm^{-2} [49-50]. Researchers were surprised to measure excellent luminescence efficiency from GaN LEDs despite dislocation densities four orders of magnitude higher. Unlike the majority of semiconductors, in GaN dislocations did not seem to degrade its optical and electrical properties. That sapphire was, and remains, the most common choice for GaN based LEDs is particularly surprising, given its properties are seemingly unsuitable based on the usual assumptions made in choosing a substrate for epitaxy; it has large lattice constant and thermal expansion coefficient mismatches with GaN.

Interest has always been high in the production and characterization of wide-bandgap semiconductor materials for a wide range of short-wavelength and hightemperature applications. Candidate material systems include silicon carbide (SiC), the Group II-VI semiconductors zinc sulfide (ZnS) and zinc selenide (ZnSe), and the Group IIIA nitrides. The hexagonal polytypes of SiC, although once considered excellent candidates for blue LEDs and more recently for high-temperature and high-power electronic devices, are not suitable for ultraviolet detector or emitter applications because of their indirect and comparatively low bandgaps ($E_g < 3.2 \text{ eV}$).

Recent progress in developing blue-green LEDs and laser diodes in the $\text{ZnS}_x\text{Se}_{1-x}$ alloy system¹ has been restricted to high-selenium alloys with bandgaps less than 2.8 eV. Higher-bandgap alloys continue to be plagued by autocompensation effects, whereby the introduction of a dopant atom is compensated by native defects and precludes well-behaved

conductivity control. Thus, the Group IIIA nitrides are the preferred candidates for short-wavelength applications. Indium nitride (InN), gallium nitride (GaN), and aluminum nitride (AlN) have direct bandgaps of 2.0, 3.4, and 6.2 eV, respectively, with corresponding cutoff wavelengths of 620, 365, and 200 nm. Since they are miscible with each other, these nitrides form complete series of indium gallium nitride ($\text{In}_{1-x}\text{Ga}_x\text{N}$) and aluminum gallium nitride ($\text{Al}_x\text{Ga}_{1-x}\text{N}$) alloys, and it should be possible to develop detectors with wavelength cutoffs anywhere in this range.[26, 49, 51]

Improvements in the growth and characteristics of gallium nitride[52] have resulted in significant inroads in device technology.[53] For example, high-efficiency blue-emitting metal insulator semiconductor LEDs[54] have been fabricated, and, with the advent of magnesium-doped p-type material, violet-emitting pn-junction LEDs[55] have been developed. Prototype GaN metal semiconductor field-effect transistors have also been reported.[56] In addition, high-quality, low-aluminum-content GaN/ $\text{Al}_x\text{Ga}_{1-x}\text{N}$ heterostructures have been produced that exhibit quantum confinement effects by photoluminescence,[57] stimulated emission under photon pumping,[58] and electron mobility enhancement.[59] Violet-emitting $\text{In}_{1-x}\text{Ga}_x\text{N}/\text{GaN}$ LEDs with external quantum efficiencies of 0.22% have been made,[60] as have double-heterostructure blue- and green-emitting $\text{In}_{1-x}\text{Ga}_x\text{N}/\text{Al}_y\text{Ga}_{1-y}\text{N}$ LEDs with external quantum efficiencies as high as 2.7%.[61] High-brightness blue, green, and yellow LEDs based on $\text{Al}_x\text{Ga}_{1-x}\text{N}/\text{In}_{1-x}\text{Ga}_x\text{N}$ quantum well structures have recently been reported.[62] Finally, stimulated emission by current injection from an $\text{Al}_x\text{Ga}_{1-x}\text{N}/\text{GaN}/\text{In}_{1-x}\text{Ga}_x\text{N}$ device has been observed.[63-64]

Along with this progress in light-emitting and microwave devices, a small but significant interest has grown in the development of photodetectors using the $\text{Al}_x\text{Ga}_{1-x}\text{N}$ alloy system. Khan et al.[65] developed a metal–semiconductor–metal detector based on insulating GaN and obtained a responsivity of 2000 A/W (amperes of photocurrent per unit incident photon power) at 365 nm under an applied bias of 5 V. They recently reported an improved responsivity of 3000 A/W by employing an enhanced mobility GaN/ $\text{Al}_x\text{Ga}_{1-x}\text{N}$ heterostructure.[66] However, their detector performance varied from sample to sample, depending on the quality of the material. One main problem associated with GaN-based detectors has been their slow response times, originating from the high defect density of the starting material, which can also directly affect the stability and linearity of the devices.

A semiconductor-based photoconductive detector can be viewed as a radiation-sensitive resistor,[67] as shown schematically in Fig. 2.3. In such a resistor, the current is generated by incoming photons that excite electrons from the valence to the conduction band and by at least some carriers being collected by one of the electrodes. Simply put, the photon-induced current I_{ph} is given by

$$I_{\text{ph}} = q\eta A\Phi g, \quad (1)$$

where

q = electronic charge,

η = quantum efficiency (i.e., number of carriers generated per incident photon in the primary absorption process),

A = device area exposed to incident radiation,

Φ = incident flux, and

g = photoconductive gain.

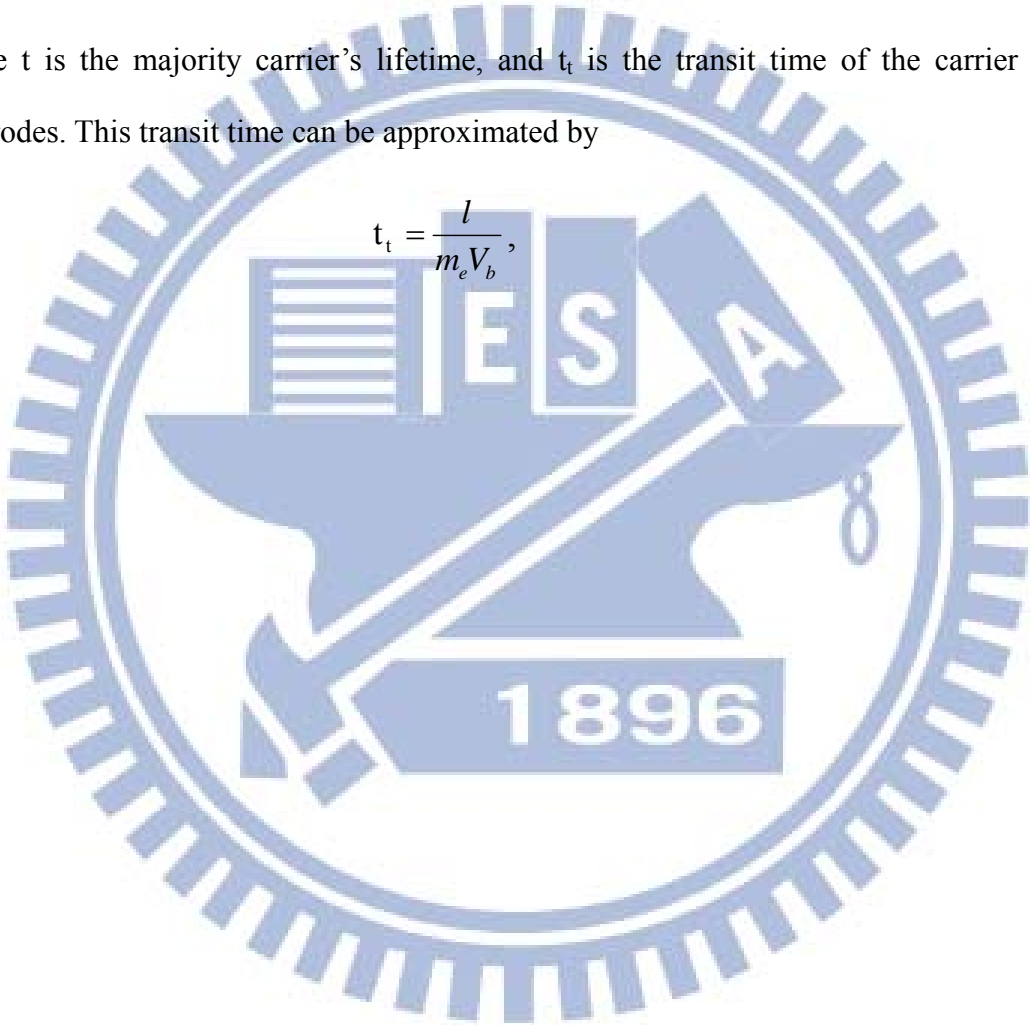
The two parameters influenced by the material characteristics are the quantum efficiency and the photoconductive gain.

In its simplest form, the photoconductive gain is given by

$$g = \frac{t}{t_t}, \quad (2)$$

where t is the majority carrier's lifetime, and t_t is the transit time of the carrier between electrodes. This transit time can be approximated by

$$t_t = \frac{l}{m_e V_b}, \quad (3)$$



2-3 Formation of Gallium Nitride films

Because bulk gallium nitride crystals are not commercially available, most researchers have relied on heteroepitaxy, which is crystal growth on substrates of another material, for device fabrication. Most often, the lattice constant mismatch has been the primary criteria for determining the suitability of a material as a substrate for GaN epitaxy. A wide variety of materials have been studied for GaN epitaxy including insulating metal oxides, metals, metal nitrides, and other semiconductors. A summary of crystal structure and lattice constants of some of the candidate substrate materials for GaN epitaxy is given in **Table 3**.

In practice, properties other than the lattice constants including the material's crystal structure, surface finish, composition, reactivity, chemical, thermal, and electrical properties, are also important in determining its suitability as a substrate, as these greatly influence the resulting properties of the epitaxial layer, sometimes in unexpected ways. The substrate employed determines the crystal orientation, polarity, polytype, the surface morphology, strain, and the defect concentration of the GaN film. Thus, the substrate properties may ultimately determine whether the device achieves its optimal performance. The influence of the substrate on the polarity and polarization of the group III nitride epitaxial layer is particularly important. The chemical reactivity and the conditions required for good quality epitaxy depend on the polarity of the crystal. In many cases, the substrate controls the crystal polarity and the magnitude and sign (tensile or compressive) of the strain incorporated into the epitaxial layers, and thereby the extent of the polarization effect. Considerable variations are possible using a variety of epitaxial growth techniques, as evidenced from the case of sapphire, where epitaxial GaN films of either polarity can be controllably produced (see the subsection on sapphire). Nevertheless, the choice of substrate does provide limits on what can be done in subsequent processing.

Thus far, the vast majority of substrates studied produce $[0\ 0\ 0\ 1]$ oriented GaN, as this orientation is generally the most favorable for growing smooth films. However, interest in

GaN epitaxial layers with other orientations is increasing to eliminate the polarization effects. Such effects can be deleterious for some optoelectronic devices, causing red shifts in emission. In addition, piezoelectric effects in quantum wells can cause a spatial separation of electrons and holes, thereby decreasing the recombination efficiency [68].

2-3-1 Structure and properties of Sapphire substrate

Sapphire, single crystal aluminum oxide, was the original substrate used in Maruskas and Tietjen's pioneering study of GaN epitaxy by hydride vapor phase epitaxy (HVPE) in 1969 [73], and it remains the most commonly employed substrate for GaN epitaxy. The large lattice constant (15% mismatch of sapphire (Al_2O_3) with GaN leads to high dislocation density (10^{10} cm^{-2}) in the GaN epitaxial film [73]. These high defect densities reduce the charge carrier mobility, reduce the minority carrier lifetime, and decrease the thermal conductivity, all of which degrade device performance. Sapphire's coefficient of thermal expansion is greater than GaN, thus, producing biaxial compressive stress in the layer as it cooled from the deposition temperature. For thick films, the stress can cause both the film and the substrate to crack [74]. The thermal conductivity of sapphire is low (about 0.25 W/cm K at 100°C), thus, it is relatively poor at dissipating heat compared to other substrate materials. The cleavage planes of epitaxial GaN layer do not parallel to those of sapphire, making laser facet formation difficult. Sapphire is electrically insulating, thus, all electrical contacts must be made to the front side of the device, reducing the area available for devices and complicating device fabrication. In addition, there is evidence that oxygen from the sapphire causes unintentional doping in the GaN layer, raising its background electron concentration [75]. Sapphire has the space group of $R\bar{3}c$ (no. 167) and is mainly composed of ionic bonds. The single crystal can be described by both rhombohedral unit cells with volume 84.929 \AA^3 and hexagonal unit cell with volume 254.792 \AA^3 [76], which is displayed in Fig. 3. In the rhombohedral unit cell, there are 4Al^{3+} ions and 6O^{2-} ions, and 10 ions in total. In the

hexagonal unit cell, there are 12Al^{3+} ions and 18O^{2-} ions, and 30 ions in total. The unit cell described in terms of hexagonal Miller-Bravais indices consists of six close packed (0 0 0 1) planes of O^{2-} ions, sandwiching 12 planes of Al^{3+} ions that occupy two thirds of the available octahedral voids created by the O^{2-} ions. The unreconstructed basal c-plane perspective views for both unit cells are shown in **Fig. 2.4**, where the polyhedra are the cell boxes. The faceting of sapphire crystal is shown in **Fig. 2.5**. All common surfaces employed for GaN epitaxy including the (0 0 0 1) and (1 1 0 0) are non-polar. Thus, the polarity of the GaN epitaxial film is primarily controlled by the process conditions to which it is subjected. **Table 5** shows the physical, chemical, thermal, mechanical and optical properties of sapphire.

2-3-2 Growth mechanisms

Epitaxial films have been grown on substrates of several orientations, and the resulting orientations are presented in Table 6. By far, the most common orientation of sapphire used for GaN is the c-plane sapphire. GaN epitaxy on c-plane sapphire results in c-plane oriented films, but with a 30° rotation of the in-plane GaN crystal directions with respect to the same directions in the sapphire. The 30° rotation of the (0 0 0 1) nitride plane with respect to the sapphire (0 0 0 1) occurs to reduce the lattice constant mismatch; the mismatch would be 30% without this rotation. With a proper nitridation and an optimized LT buffer layer of either AlN or GaN, very smooth GaN films can be obtained. The c-plane sapphire is very difficult to cleave, especially with a smooth cleave plane surface on the edge of the GaN layer. This is made worse by the 30° rotation of the AlN and GaN c-plane relative to the sapphire c-plane, such that the natural cleavage planes of the nitride and sapphire are not aligned. Stocker et al. [78] reported that c-plane sapphire cleaves along both the a- and m-planes, with roughly parallel cleaving of the m- and a-planes in the GaN film respectively. Large steps (90 nm) were produced on the surface of the m-plane of the GaN which were unsuitable for laser diode fabrication, hence, cleaves along the a-plane of sapphire unsuitable. Much smaller

striations occurred on the a-plane of GaN, making it a more promising for fabricating lasers. Cleaving c-plane sapphire along its m-plane to expose the a-plane in the GaN remains an area of active research. GaN films grown on a-plane sapphire are also oriented in the $[0\ 0\ 0\ 1]$ direction, and have the advantage that they are easily cleaved, along r-plane. This is potentially advantageous for forming edge-emitting lasers. Although the lattice mismatch for GaN films on a-plane sapphire is less (2%) than on c-plane sapphire (13.9%), no significant differences in GaN film quality have been reported between these two substrates. Nakamura et al. [79] has reported a pulsed MQW laser with cleaved facet mirrors fabricated in GaN on a-plane sapphire, which might be a promising for production of nitride-based lasers on a large scale.

The r-plane of sapphire is unusual, as it is one of only a few substrates capable of producing GaN or AlN films with orientations other than the c-axis normal to the substrate. For either GaN or AlN epitaxy on r-plane $(1\bar{1}0\ 2)$ sapphire, the a-axis $[1\ 1\bar{2}\ 0]$ orientation is produced. This is the preferred orientation for AlN-based surface acoustic wave devices, as it produces the electromechanical coupling coefficient. For on-axis sapphire substrates with this orientation, the AlN films are universally rough, forming a peak and valley morphology, bounded by $(01\bar{1}0)$ and $(0\ 1\bar{1}\ 2)$ facets. The roughness generally increases and becomes more severe as the film thickness increases. By using r-plane sapphire substrates misoriented with a 48 tilt toward the $[1\bar{1}01]$ negative a-direction, Shibata et al. [80] improved the quality of AlN films by suppressing the formation of inverted twins.

From the viewpoints of lattice mismatch and crystal symmetry, $(1\ 0\ \bar{1}\ 0)$ sapphire (m-plane) seems the most suitable for GaN growth. However, the c-axis of GaN film grown on a $(10\bar{1}0)$ sapphire substrate has a non-zero inclination with respect to the c-axis of the sapphire substrate. Thus, twins may be generated, and the structure and surface morphology of GaN films becomes poor quality. This is a major disadvantage of a $(1\ 0\ \bar{1}\ 0)$ plane compared to a $(0\ 0\ 0\ 1)$ plane.

Tripathy et al. [81] compared the quality of GaN layers with the same thickness (1.2 μm) grown on c-, a-, r-, and m-plane sapphire substrates by MBE. GaN layers were smooth and flat on c-plane sapphire, somewhat rougher on a-plane, and rough on r-plane and m-plane sapphire. Only (0 0 0 2) and (0 0 0 4) XRD diffraction peaks were seen from GaN on c-plane and a-plane sapphire substrates due to the smooth surface morphology. The layers grown on r-plane and m-plane had mixed orientations, with both (0 0 0 2) and (1 1 $\bar{2}$ 0) diffraction peaks. From the smallest width of XRD rocking curve and narrow band PL spectrum, GaN on c-plane sapphire suggested the best crystalline quality. Although the PL intensities are comparable to that grown on c-plane sapphire, strong in-plane anisotropy of optical response was found in GaN grown on a-, r-, and m-plane sapphire substrates. Matsuoka and Higiwara [82] observed a significant improvement in the quality of GaN films deposited on m-plane sapphire substrates misoriented by 15–20°. This misorientation suppressed twinning and enabled the growth of smooth, single crystal GaN films. Although the dislocation density was still 50% higher than on c-plane sapphire, this is still a notable improvement over previous efforts [82].

2-4 The nanoindentation technique for measuring mechanical properties of thin films

Indentation has been the most commonly used technique to measure the mechanical properties of materials because of the ease and speed with which it can be carried out. Traditional indentation testing involves optical imaging of the indent. This clearly imposes a lower limit on the length scale of the indentation. During the past two decades, the scope of indentation testing has been extended down to the nanometer range. This has been achieved principally through the development of instruments capable of continuously measuring load and displacement throughout an indentation [83-86]. A schematic representation to nanoindenter apparatus is shown in Fig. 2.6.

Diamond is the most frequently used indenter material, because its high hardness and elastic modulus minimize the contribution of the indenter itself to the measured displacement [83]. For probing properties such as hardness and elastic modulus at the smallest possible scales, the Berkovich triangular pyramidal indenter is preferred over the four-sided Vickers or Knoop indenter because a three-sided pyramid is more easily ground to a sharp point [83, 86]. The shape is shown in Fig. 2.7. Another three-sided pyramidal indenter, the cube corner indenter, can displace more than three times the volume of the Berkovich indenter at the same load, thereby producing much higher stresses and strains in the vicinity of the contact and reducing the cracking threshold. This makes this indenter ideal for the estimation of fracture toughness at relatively small scales [87-88]. The spherical indenter initiates elastic contact and then causes elastic-plastic contact at higher loads. This indenter, then is well suited for the examination of yielding and work hardening.

The nanoindentations were sufficiently spaced (50 μm) to prevent from mutual interactions. In order to obtain “film-only” properties, a commonly used rule of thumb is to limit the indentation depth to less than 10 % of the films thickness [89-90]. The deformation pattern of an elastic-plastic sample during and after indentation and a

typical load–displacement curve and are shown in **Fig. 2.8** and **Fig. 2.9**, respectively. Hardness and Young’s modulus were determined using the Oliver and Pharr analysis **[85]**. Hardness (H) means the resistance to local plastic deformation of materials, which has been conventionally obtained by measuring the projected contact area, A_c :

$$H = \frac{P}{A_c} \quad (4)$$

where P is the load. Elastic modulus E can be obtained from the contact stiff, using the following relation:

$$S = \beta \frac{2}{\sqrt{\pi}} E_r \sqrt{A_c} \quad (5)$$

$$\frac{1}{E_r} = \frac{1 - \nu_i^2}{E_i} + \frac{1 - \nu^2}{E} \quad (6)$$

Where S is the experimentally stiffness, and β is a constant that depends on the geometry of indenter and $\beta=1.034$ **[91]**. E_r stands for the reduced modulus. E_i and ν_i are Young’s modulus and Poission’s ratio of indenter, respectively. E and ν are the same parameters for the specimen. The load and stiffness are directly measured during an indentation, contact area A_c and contact depth h_c has relation $A_c = 24.56h_c^2$ **[92, 100]**. By inserting the calculated contacted area into Eqs.(5) and (6), the hardness and elastic modulus were evaluated. For diamond which is the usual material of a Berkovich indenter, $E_i = 1141$ GPa and $\nu_i = 0.07$ **[89]**. As the commonly done, we assume that ν is 0.3.

2-5 The nanoscratch technique for measuring nanotribological characterization of thin films

Recently, improvements in the processing quality, quantity and variety of thin films have led to increased interest in their potential as engineering materials and have increased the need for a full properties. The latter is of interest since the generally high hardness values of thin films would make them candidates for high wear applications. However, it has been argued that hardness alone does not determine the wear resistance; in addition to resistance to indentation, crack nucleation and propagation are also responsible for wear. Existing results of wear studies often lead to conflicting reports of the wear resistance of thin films. This discrepancy in wear data and its interpretation could be due to oversight of the importance of small differences in processing conditions, which could generate differences in the quality and structure of the alloys. One of the main reasons for the divergence in wear values is the wide variety of acceptable wear tests, which can give significantly different results depending on test conditions such as sliding vs. abrasive wear, sliding load and speed, and surface roughness. The use of indentation to measure mechanical properties can be recalled to the contact theory originally considered in the late 19th century by Hertz [93] and Boussinesq [94]. Hertz analyzed the problem of the elastic contact between two spherical surfaces with different radii and elastic constants. His solutions form the basic theory in contact mechanics and provide the analysis of non-rigid indenters. Boussinesq developed a method based on potential theory for computing the stresses and displacements in an elastic body loaded by a rigid axisymmetric indenter. His method has subsequently been used to derive solutions for cylindrical and conical indenters. Another major contribution was made by Sneddon [95], who derived general relationships among the load, displacement, and contact area for any punch that can be described as a solid of revolution of a smooth function. Oliver and Pharr [96] made a critical improvement to the indentation technique, who applied Snedden's formulation to determine the contact area at maximum load even if the contact area changes

during unloading. Their analytic procedure is to fit a power law function to the unloading segment, which yields the contact stiffness as slope of this function at maximum load. This slope is used to determine the actual contact depth so that it is finally possible to derive the indentation modulus and the indentation hardness.

In experiments, indentation tests were first performed by Brinell [83, 97-98], using spherical and smooth balls from ball bearings as indenters to measure the plastic properties of materials. The Brinell's test was quickly adopted as an industrial test method soon after its introduction and prompted the development of various macro and micro indentation tests [99]. During the past two decades, the scope of indentation tests have been extended down to the nanometer range, such as the measurement of mechanical properties of nanocomposites and nanometer thin films. This has been achieved principally through the development of instruments capable of continuously measuring load and displacement throughout an indentation. Oliver and Pharr [96] and Pharr [86, 100] proposed the significant technique to determine the hardness and elastic modulus directly from the loading displacement curve instead of measuring the indentation area. In recent years, Bhushan et al. [98, 101-102] proved the mechanical properties are size-dependent in the nanoindentation, which has received much attention. X. Li, Z.C. Li, and C. R. Taylor et al. [87-88, 103-105] used the nanoindentation to estimate the fracture toughness of ultrathin films, which cannot be measured by conventional indentation tests.

In addition, it is well known that the mechanochemical reaction of the contact surface between the tip end and the surface plays an important role in nanomachining processes because a friction force (or surface force) increases with the impact of a van der Waals force, a meniscus force, and an electrostatic force on the nano/micro scale. Borosilicate is stable chemically because it mainly consists of silicate, whereas silicon easily combines with oxygen or hydrogen. Accordingly, if a silicon-silicon bond is destructed by diamond tip sliding, oxide or hydro-oxide is apt to be generated in reaction to oxygen or hydrogen in the atmosphere.

Specifically, Ando and Kaneko [106] revealed that a silicon protuberance formation is deduced to be the mechanochemical reaction of silicon to diamond tip sliding through the microfriction experiments [106-107]. They also have reported that the protuberance do not occur under vacuum and dry nitrogen conditions. Miyake and Kim [107] have introduced AFM nanoprotuberance processing technology for monocrystal silicon. They have controlled the height of protuberances and the depth of grooves by varying the applied normal load and diamond tip radius under ambient conditions, room temperature with humidity ranging between 60 and 80%. [108]

Nanoscratch testing is a versatile tool for analysis of both thin films and bulk materials. Nanoscratch provides the capability to investigate modes of deformation and fracture that are not possible using standard indentation techniques. Nanoscratching is accomplished by applying a normal load in a controlled fashion while measuring the force required to move the tip laterally across the sample. By selecting the appropriate normal loading profile and lateral displacement pattern, many different types of tests can be performed. The damage incurred from the test is then typically observed using optical or SPM imaging. The schematic of the nanoscratch machine is shown in Fig. 2.10, which basically includes a probe supported by a 2D transducer. The friction coefficient (f) is defined as

$$f = P_x / P_z \quad (7)$$

where P_x denotes the lateral load and P_z indicates the normal load. [109]

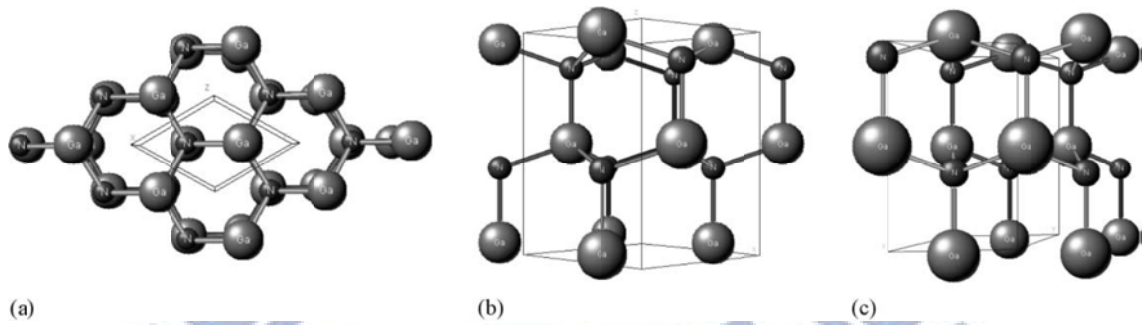


Fig.2.1 Perspective views of wurtzite GaN along various directions: (a) $[0\ 0\ 0\ 1]$; (b) $[1\ 1\ \bar{2}\ 0]$; (c) $[1\ 0\ \bar{1}\ 0]$. [31]

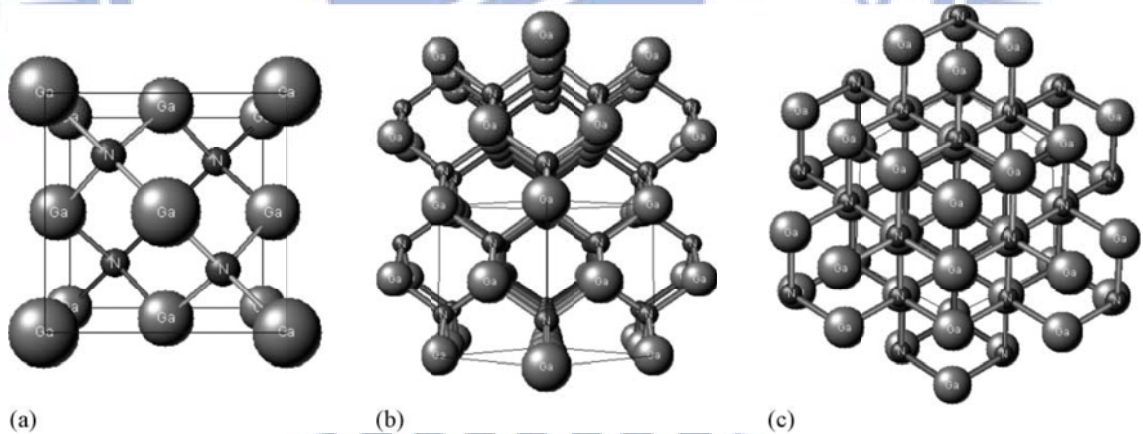


Fig. 2.2 Perspective views of zincblende GaN along various direction: (a) $[1\ 0\ 0]$ ($1\ \times\ 1\ \times\ 1$ unit); (b) $[1\ 1\ 0]$ ($2\ \times\ 2\ \times\ 2$ units); (c) $[1\ 1\ 1]$ ($2\ \times\ 2\ \times\ 2$ units). [31]

Table 2.1 Properties of GaN on sapphire (0 0 0 1) substrate.

Property	Value	Reference
Energy band gap (eV) (300 K)	3.44	[37]
Maximum electron mobility (cm ² /V s)		
300 K	1350	[38]
77 K	19200	[38]
Maximum hole mobility (300 K) (cm ² /V s)	13	[39]
Controlled doping range (cm ⁻³)		
n-type	10 ¹⁶ to 4x10 ²⁰	[40]
p-type	10 ¹⁶ to 6x10 ¹⁸	[40]
Melting point (K)	>2573 (at 60 kbar)	[41]
Lattice constants(300 K)		
a (nm)	0.318843	[42]
c (nm)	0.518524	[42]
Percentage change in lattice constants (300–1400 K)	$\Delta a / a_0$ 0.5749, $\Delta c / c_0$ 0.5032	[42]
Thermal conductivity (300 K) (W/cm K)	2.1	[43]
Heat capacity (300 K) (J/mol K)	35.3	[44]
Modulus of elasticity (GPa)	210 ± 23	[45]
Hardness (nanoindentation, 300 K) (GPa)	15.5 ± 0.9	[46]
Hardness (Knoop, 300 K) (GPa)	10.8	[46]
Yield strength (1000 K) (MPa)	100	[47]

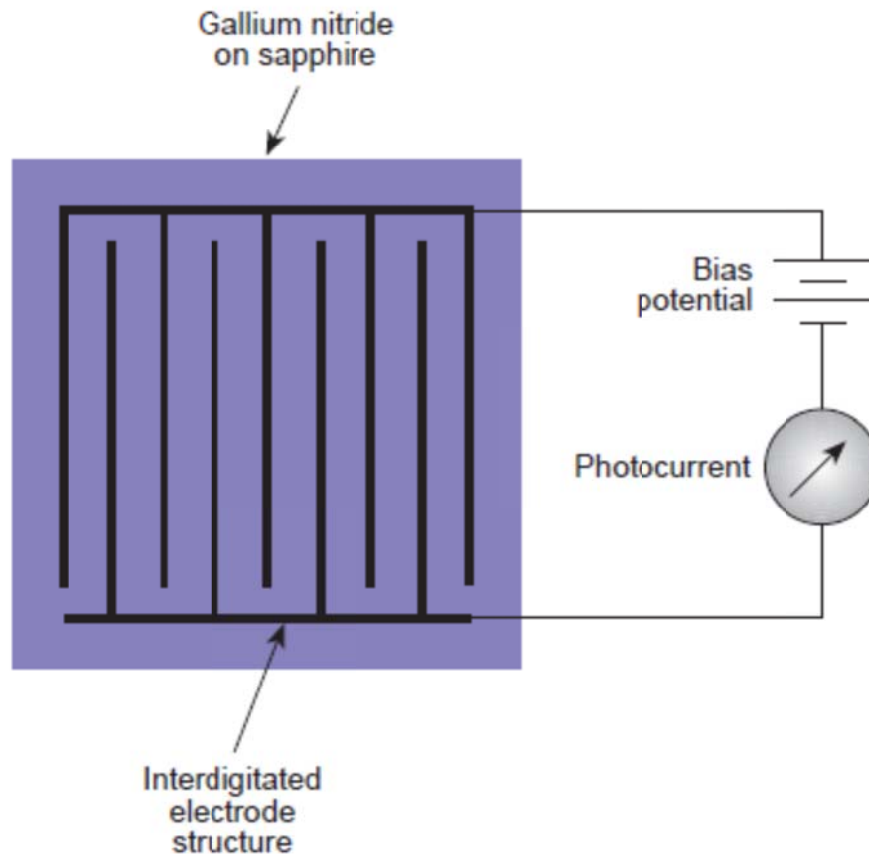


Fig. 2.3 A diagram of a typical photoconductor circuit.[67]

Tab. 2.2 Substrate candidates for GaN epitaxy.[31]

Material	Structure	Space group	Lattice constants (nm)		
			a	b	c
Semiconductors					
w-GaN	Wurtzite	P63mc	0.31885		0.5185
zb-GaN	Zincblende	F43m	0.4511		
r-GaN	Rock salt	Fm3m	0.422		
w-AlN	Wurtzite	P63mc	0.31106		0.49795
zb-AlN	Zincblende	F43m	0.438		
r-AlN	Rock salt	Fm3m	0.404		
ZnO ^[69,70]	Wurtzite	P63mc	0.32496		0.52065
β -SiC	3C (ZB)	F43m	0.43596		
SiC	4H (W)		0.3073		1.0053
SiC	6H (W)	P63mc	0.30806		1.51173
GaAs	Zincblende	F43m	0.56533		
GaP ^[71,72]	Zincblende	F43m	0.54309		
Si	Diamond	Fd3m	0.54310		
Oxides and sulphides					
Al ₂ O ₃ (sapphire)	Rhombohedral	R3c	0.4765		1.2982

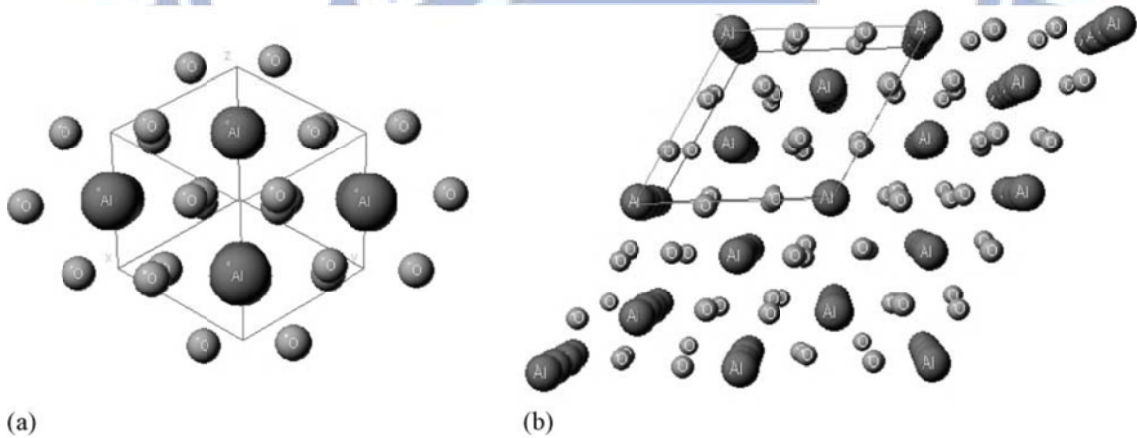


Fig. 2.4 Perspective views in $(2 \times 2 \times 1)$ unit cells: (a) along the $[0 \ 0 \ 0 \ 1]$ direction in a rhombohedral unit cell; (b) along the $(0 \ 0 \ 0 \ 1)$ direction in hexagonal unit cell. [31]

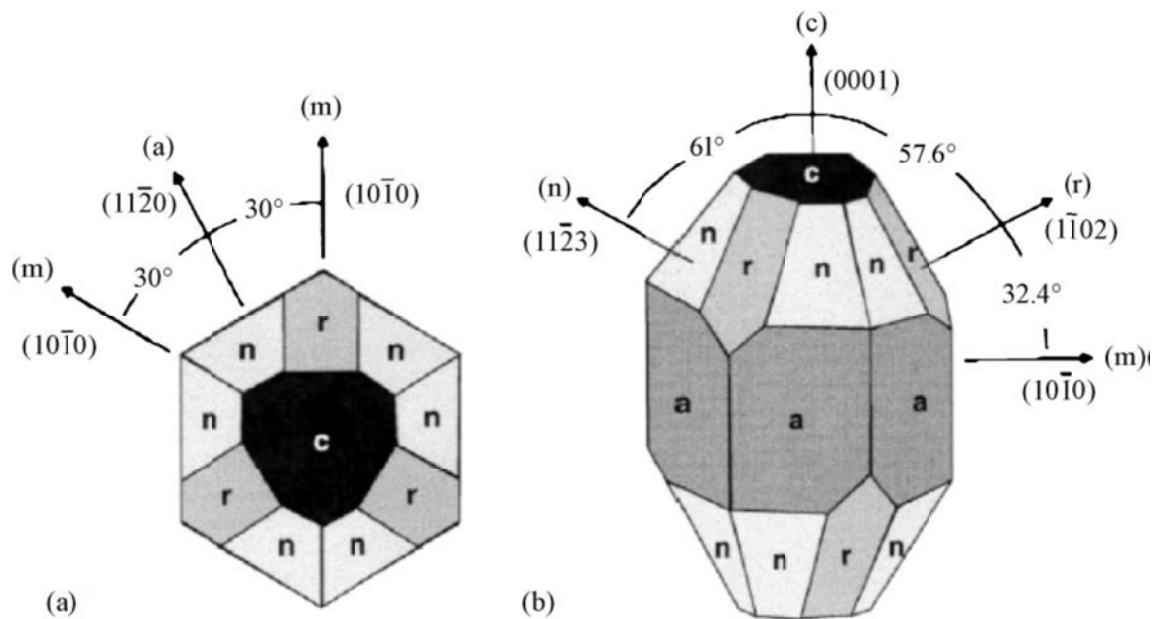


Fig. 2.5 Common facets of sapphire crystals: (a) view down c-axis; (b) surface planes. [77]

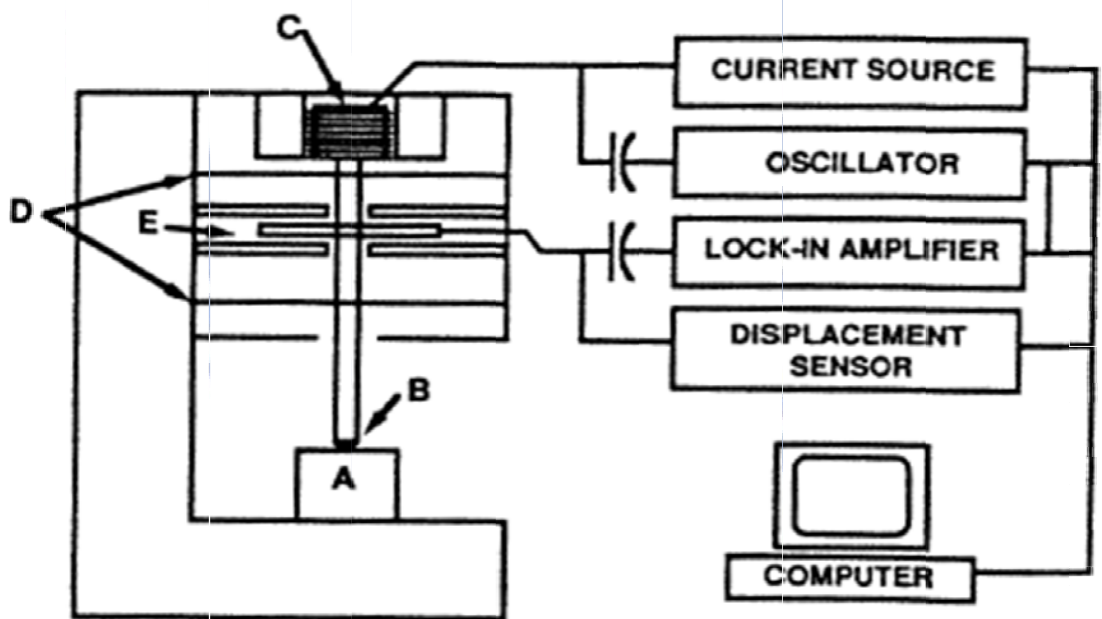


Fig. 2.6 A schematic representation of nanoindenter apparatus. (A) sample; (B) indenter; (C) load application coil; (D) indentation column guide springs; (E) capacitive displacement sensor [85].

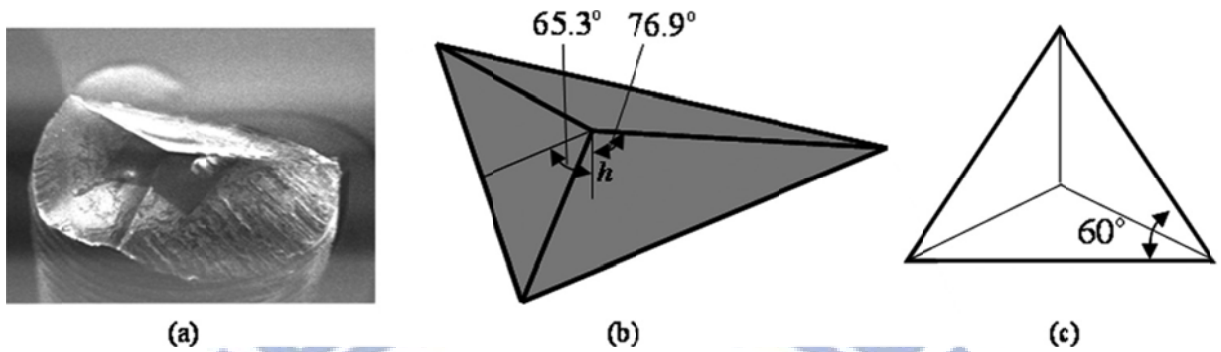


Fig. 2.7 The standard Berkovich tip. [113]

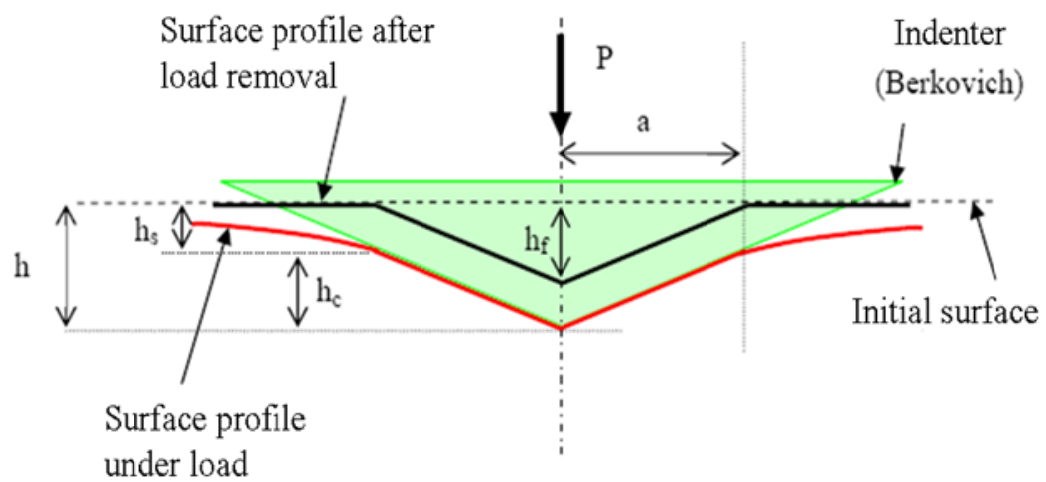


Fig. 2.8 The deformation pattern of an elastic-plastic sample during and after indentation. [85,112]

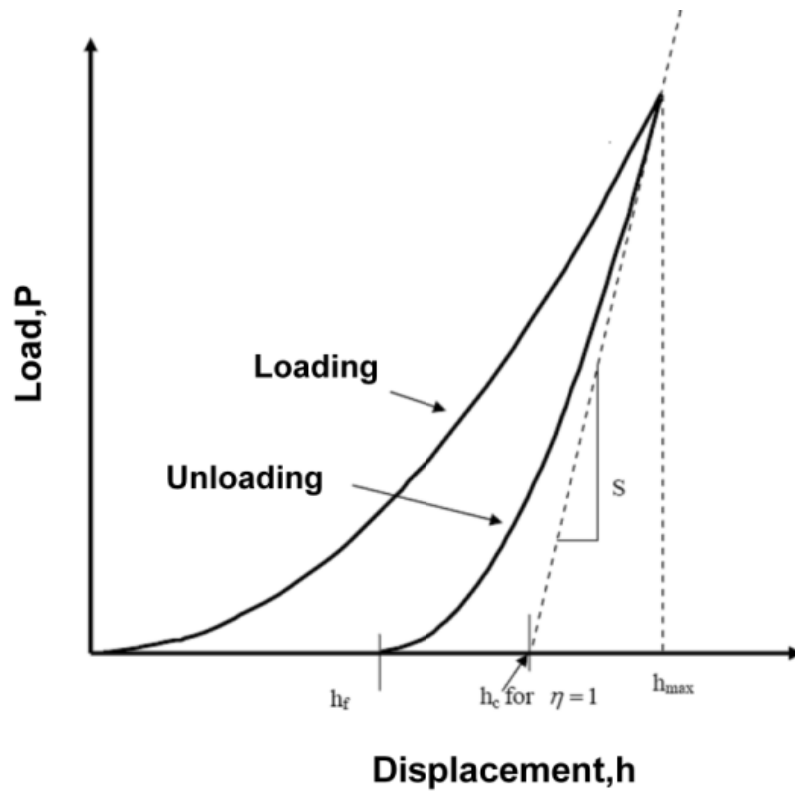


Fig. 2.9 Schematic illustration of indentation load–displacement data showing important measured parameters. [85,112]

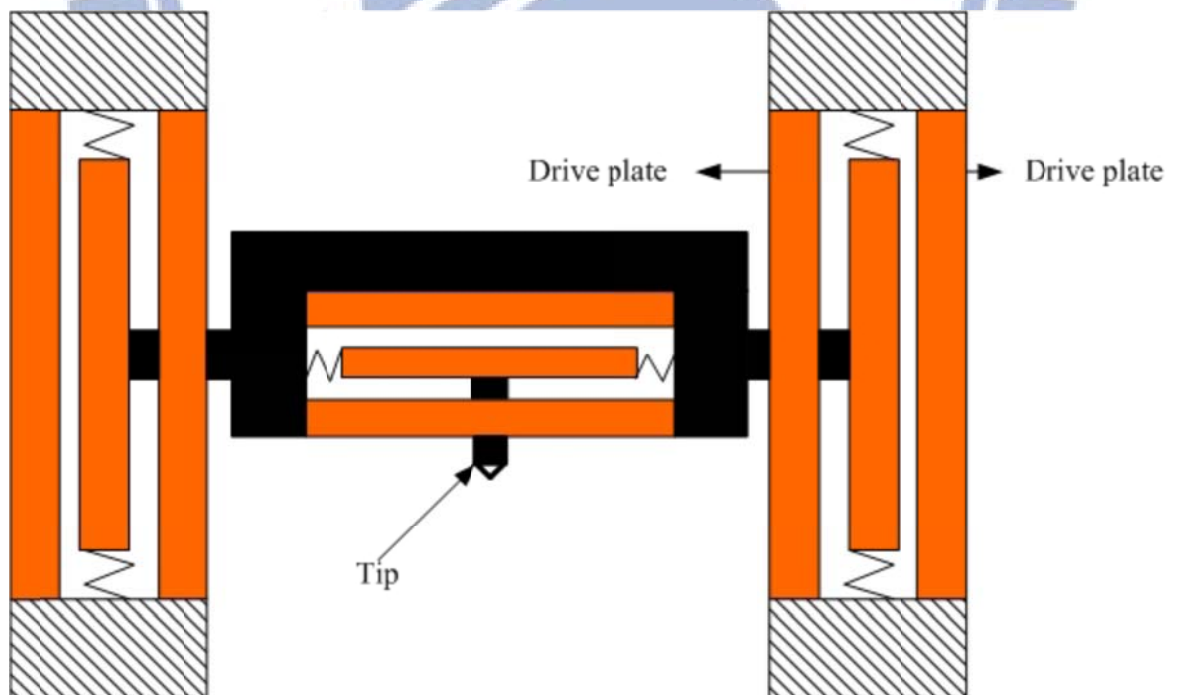


Fig. 2.10 Sketch of nanoscratch. [109]

Chapter 3 Experimental Apparatus and Procedures

3-1 Experimental procedures

In the experiment, the parameter and primary design are show in Fig. 3.1.

3-2 The process of the GaN films growth

3-2-1 Sapphire substrate preparation

The substrates used in experiments were 2-inch A-plane ($1\ 1\ \bar{2}\ 0$) and C-plane($0\ 0\ 0\ 1$) orientated sapphire wafer with thickness $420 \pm 25\mu\text{m}$.

3-2-2 GaN films deposition

Sapphire wafer was introduced into load-lock chamber of metal-organic chemical vapor deposition (MOCVD). To fabricate the GaN films, a 10-nm-thick AlN buffer layer was grown on the sapphire substrate, and then both GaN films (thickness: ca. 2 μm) were grown on top of the buffer layer through MOCVD at 1100 °C, using triethylgallium (TEGa), trimethylaluminum (TMAI), and ammonia (NH_3) as the gallium, aluminum, and nitrogen sources, respectively. The GaN films grown on c-plane (0001) and a-plane ($1\ 1\ \bar{2}\ 0$) sapphire had a [0001] orientation and a [$1\ 1\ \bar{2}\ 0$] orientation.

3-3 Surface morphologies measurement

In this section, the measurement methods used to characterize the material of GaN grown by ULVAC MBE system are described.

3-3-1 Field emission scanning electron microscope (FE-SEM)

The FE-SEM consists of a field emission electron source rather than a thermionic emission source used in a Thermal Tungsten wire SEM. A FE-SEM is therefore has a cold cathode. This SEM provides higher resolution imaging with higher beam density (brightness), and longer tip life. The primary electrons enter a specimen surface with energy of 0.5 to 30 keV to generate many low energy secondary electrons. The second electrons emission depends largely on the accelerating voltage of the primary electrons and also the probing incident angle on the specimen

surface. In general, a large quantity of secondary electrons is generated from the protrusions and the circumferences of objects on the specimen surface, causing them to appear brighter than smooth portions. Under a constant accelerating voltage, an image of sample surface can thus be constructed by measuring the secondary electron intensity as a function of the position of scanning primary electron beam. In this study, JEOL-JSM7001F FE-SEM is used routinely to check the GaN surface morphology as well as the film thickness.

3-3-2 Atomic force microscope (AFM)

AFM is used to check the surface topography of a material by measuring the interaction force between the AFM's probe and surface structure. The AFM probe consists of a sensitive 19 cantilever and a sharp tip (tip radius <10 nm) capable of obtaining the detail surface morphology of a material surface on the atomic scale if the scanning condition is carefully controlled. In general, the AFM is reliable to achieve lateral and vertical resolutions down to about 2 nm and 0.05 nm, respectively, in the ambient air environment. In this study, AFM Digital Instruments DI 5000 system from Digital Instrument was employed to examine the surface information, such as morphology, roughness and density of pits, from the GaN material grown by MBE. This information provides the indications of the material quality and is a useful means to tune the growth condition.

3-4 Mechanical properties measurement

The mechanical properties of GaN films on a-axis sapphire substrate were investigated by nanoindentation system. The nanoindentation measurements used a diamond Berkovich indenter tip (tip radius ~50 nm), suggesting that plastic deformation can be generated at very small load. The Hardness data obtained with Berkovich indenter can be transformed to Vickers hardness because of the same shape of a three-sided pyramid, which means a similar area-to-depth function [110-111]. In continuous contact stiffness measurement (CSM) test, a series of continuous load-unload indents were measured at the

penetration depth of 15, 40, and 300 nm. Each indentation was separated by 30 μm to avoid possible interference between neighboring indents. Here, all indents were performed at room temperature. The analytic method developed by Oliver and Pharr was adopted to determine the hardness (H) and Young's modulus (E) of the GaN films from the load – displacement curves [85, 112]. In addition, the cyclic nanoindentation deformation behaviors of the GaN films/a-axis sapphire substrate were conducted under force contact stiffness measurement (FSM) technique with repetition pressure-induced impairment at the constant load of 50 mN. In FSM measurement, each indentation location was separated by 30 μm in order to avoid possible interference between neighboring indents. Hence, the CSM mode can obtain hardness and Young's modulus relative to the indentation depth and is used in this experiment [85, 91, 113-114]. The instrument was calibrated by using a standard fused silica sample before measuring the mechanical characterizations of GaN epitaxial layers. The drift rate preset to < 0.05 nm/s before the beginning of each indentation. Frequency of 45 Hz was used to avoid the sensitivity to thermal drift and loading resolution was 50 μN [91, 115]. Ten indents were made on samples to minimize the deviation of the results.

3-5 Nanotribological characterization measurement

The nanotribological properties of GaN films on A- and C-axis sapphire substrate were determined by combining AFM (Digital Instruments Nanoscope III) together with a nanoscratch measurement system (Hysitron), operated at a constant scan speed of $2 \text{ } \mu\text{m s}^{-1}$. For the GaN epilayer/sapphire systems, constant forces of 2000, 4000, and 6000 μN were applied. The maximum load was then maintained while forming 10- μm -long scratches. Surface profiles before and after scratching were obtained by scanning the tip at a 0.02-mN normal load (i.e., a load sufficiently small that it produced no measurable displacement). After scratching, the wear tracks were imaged using AFM.

3-6 Cathodoluminescence properties measurement

The cathodoluminescence properties of GaN epilayers with cyclic nanoindentation deformation of the GaN epilayers/a-axis sapphire substrate were determined by cathodoluminescence (CL) mapping. The cathodoluminescence (CL) mapping acquired at a wavelength of 550 nm from an indented GaN films indented was characterized using a CL apparatus (HORIBA Co., Ltd.). The room-temperature CL measurements were performed using an electron beam energy of 20 keV. The CL light was dispersed by a 2400 nm grating spectrometer and detected by a liquid N₂-cooled charge-coupled device.

3-7 Experimental apparatus

(a) Metal-organic chemical vapor deposition (MOCVD)

MOCVD system features include:

1. Wafer size: 2".
2. Number of wafer: up to 6.
3. Stainless Steel or Quartz Chamber.
4. IR or RF heating.
5. Chamber temperature control: 1300
6. Wafer Rotation.
7. Pressure Control: 0 ~ 800 Torr.
8. Deposited materials: III-V. (GaN, GaAs, AlGaN, InP, etc)

(b) Field emission scanning electron microscope (FE-SEM)

JEOL-JSM7001F was used routinely to check the nanoindentation mark of GaN surface morphology as well as the thin film.

(c) Atomic force microscope (AFM)

Digital Instruments DI 5000 was utilized to observe the 3D surface morphologies and roughness of the GaN epilayers.

(d) Nano Indenter XP instrument

Nano Indenter XP instrument (MTS Cooperation, Nano Instruments Innovation Center, TN, USA) was utilized to investigate the hardness and elastic modulus of the GaN epilayers.

(e) Hysitron Triboscope instrument

Hysitron Triboscope instrument was utilized to investigate the Nano Indent, Nano Dynamic Mechanical Analyzer (Nano-DMA), Nano Scratch, and Wear test of thin film.

(f) Crygenic Cathodoluminescence system instrument

Crygenic Cathodoluminescence system instrument (JEOL, JSM7001F) to investigate the cathodoluminescence properties of GaN films with cyclic nanoindentation deformation of the GaN films/a-axis sapphire substrate.

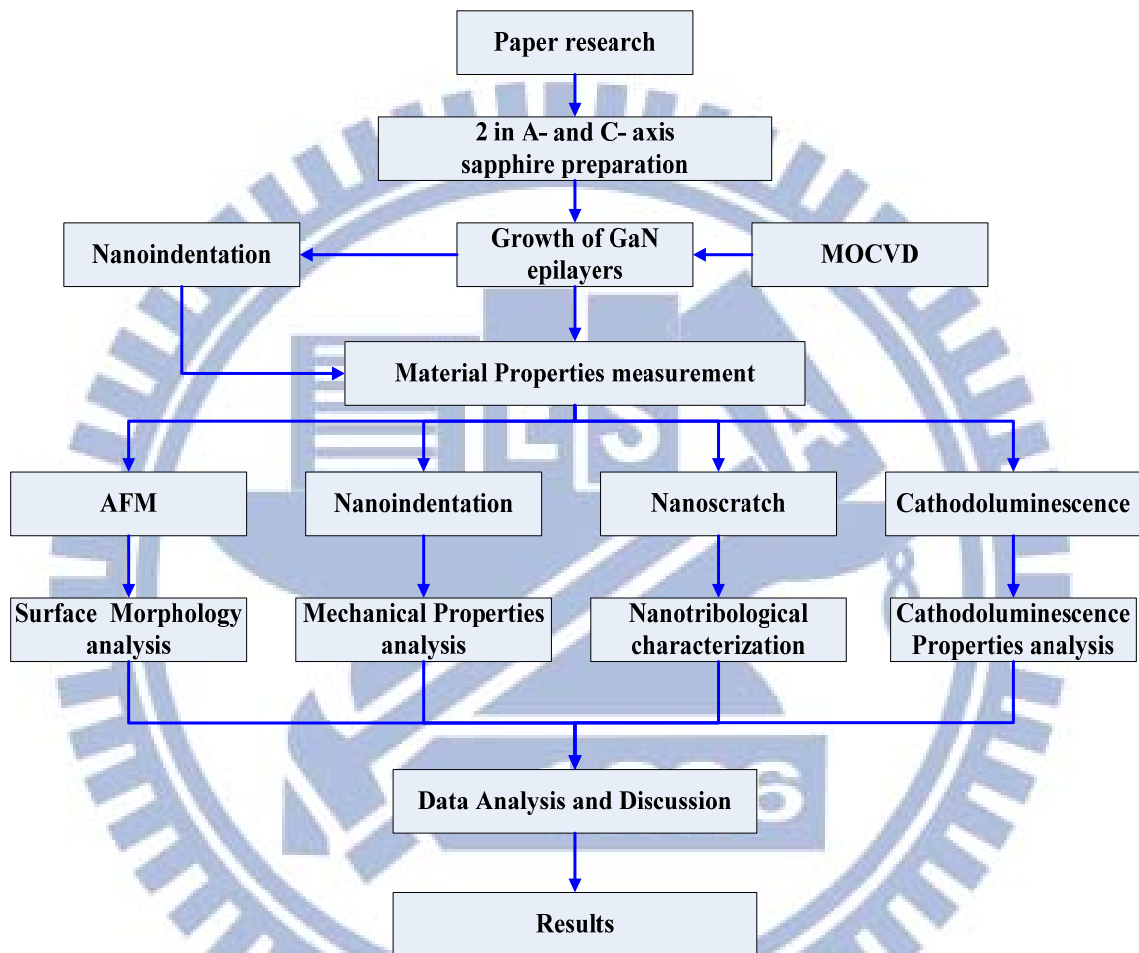


Fig. 3.1 The parameter and primary design.

Chapter 4 Primary result

4-1 Investigation of contact-induced deformation behaviors of the GaN films/a-axis sapphire substrate

4-1-1 Motivation

The mechanical damages of GaN films, such as film cracking and interface delamination caused by thermal stresses, chemical–mechanical polishing, usually suppress the processing yield and application reliability of microelectronic devices. The heteroepitaxy using typical substrates with high lattice mismatch is discussed in early report. GaN films on sapphire substrates exhibits large lattice mismatch (about 14.5%) causing in-plane tensile strain in the GaN layers. In fact, the most common orientation of sapphire used for GaN is the c-axis sapphire. And, the lattice mismatch of the GaN films on a-axis($11\bar{2}0$) sapphire is less (2%) than that on c-axis (0001) sapphire(13.9%), which promises for excellent quality of GaN growth with improved surface morphology [31, 116]. Here, compared to bulk single crystals, the deformation properties of thin films have strongly correlation to the geometrical dimensions and the materials defectstructure. The misfit dislocations at the interface play an important role such as carrier mobility, and luminescence efficiency. In this respect, nanoindentation has proven to be a powerful technique for probing the information on the mechanical properties of GaN films with characteristic dimensions in the sub-micron regime, such as hardness and Young's modulus [117-118]. During indentation load of GaN films, the nanoindentation-induced discontinuity (so-called 'pop-in') in the load–displacement curve has been observed in elsewhere investigation. The slip band movement [45, 119-120] and dislocation nucleation mechanism [117,121] have been proposed to explain this 'pop-in' event. Most of the studies were carried out on c-axis GaN films or bulk single crystals [85, 122-123]. Comparatively, the GaN films was observed in their mechanical damages, however the detail work in the a-axis GaN films is still not yet unclear.

In this paragraph, significant investigation of the mechanical characterizations on GaN films is motivated. The pressure-induced impairment of GaN films/a-axis sapphire substrate has been investigated by using nanoindentation technique and atomic force microscope (AFM).

4-1-2 Results and discussion

The load-indentation depth data for the grown GaN epilayers by MOCVD with 2 μm thickness on a-axis sapphire substrate is discussed, the multiple discontinuities during loading were clearly revealed in **Fig. 4.1(a)**. The hardness and elastic modulus as a function of indentation depth can be obtained from the CSM measurements, as illustrated in **Fig. 4.1(b)** and **(c)**, respectively. The hardness and elastic modulus of the GaN films/a-axis sapphire substrate are determined to be 15.9 ± 0.8 and 394.6 ± 12 GPa, respectively. **Table 4.1** displays some of relevant data for comparison [119, 124, 129]. It is believed that the discrepancies among the mechanical parameters obtained by various indentation methods are mainly due to the specific tip–surface contact configuration and stress distribution inherent in the different plane sapphire substrate. At beginning, the ‘pop-in’ event took place at a depth of 16 nm (at a critical load of 0.16 mN) was observed and, the contact stress has is 35.26 GPa (see the inset in **Fig. 4.1(b)**). The critical contact stress of the penetration depth in 16 nm is required to cause the initial ‘pop-in’ event in the a-axis GaN film. This case is relatively large with that of GaN film on c-axis sapphire substrates (23 nm; at a load of 0.48 mN; contact stress 22.5 GPa) [125]. The phenomenon suggested that the low indentation load (0.45 mN) serve the Berkovich tip in the increasing stress on the film’s surface than the Berkovich tip on the GaN film’s surface. In fact, the data obtained from Berkovich diamond indenter in our result were also very large with that of spherical tip (140 nm; at a load of 30 mN; contact stress 9 GPa) as reported in the other study [124]. Therefore, the initial sudden displacement discontinuity generally accompany with maximum shear stress generated under the indenter

and, is more than that of the remaining other ‘pop-ins’. It is also observed that the corresponding indentation depth versus hardness data from the hardness value increased highly about 36 GPa before the ‘pop-in’ event at 16 nm (see the inset in **Fig. 4.1(a)**). The fact was attributed from the sharper tip that induces plasticity at a shallow indentation depth. Therefore, the hardness values can be calculated accurately [119]. It is suggested that the ‘pop-in’ events partially induce from the heteroepitaxial thin film, which can also be attributed to the inner-defects of GaN films.

Evidently, due to the soft GaN film grown epitaxially on a hard sapphire substrate, it is easy to find that the differences in lattice parameter and thermal expansion coefficients between the film and substrate. This may introduce a misfit strain at the interface, and then the strain is released by generating threading dislocations in the GaN films [126-127]. In the experiment of indentation loading, the deformed region was punched out on the top edge from the indenter tip; the threading dislocation may be to cause a sudden increase in plasticity, therefore the sudden discontinuity in the load-indentation depth curve is showed. Navamathavan *et al.* [125] concluded that the threading dislocation in the GaN films/c-axis sapphire substrate can suddenly propagate after acquiring threshold energy from the deformed region. This is the reason why the multi ‘pop-ins’ of the GaN films is occurred. However, some of the threading dislocations terminate as they yet to reach the film surface [128]. At the same time, the GaN films/a-axis sapphire substrate can be interacted by indenter tip to appear deformed zone, the threading dislocations then excuse into films through certain depths, afterward causing the ‘pop-in’ event. It is conjectured that the mechanism of the event is caused by slip bands [119-120, 124], and/or dislocation nucleation [117].

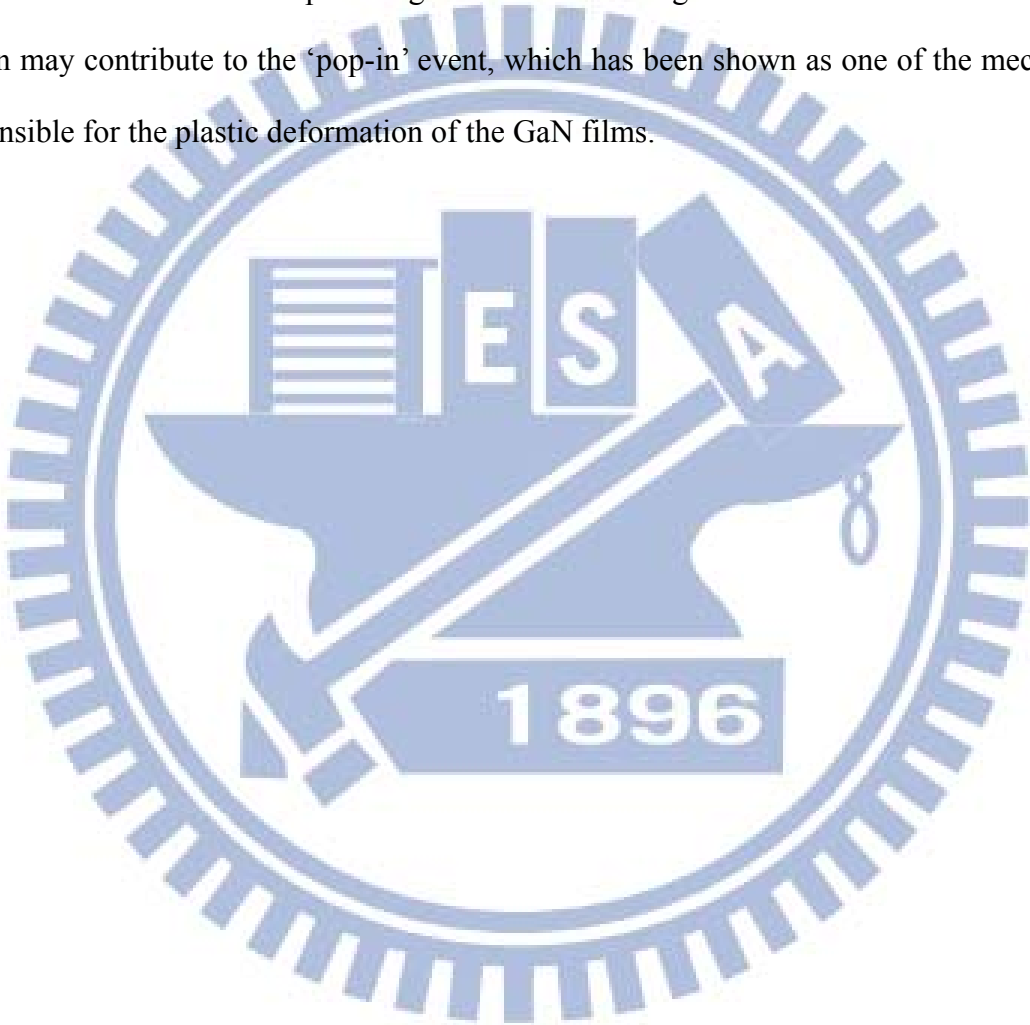
In **Fig. 4.2(a)**, the AFM image of the residual indentation mark is revealed that none of crack and particle even occurred after the indentation depth. From the section view of the indentation mark, **Fig. 4.2(b)** shows the residual volume from the edge of indentation. Dislocation-induced ‘pop-in’ event tends to associated with two distinct deformation

behaviors before (pure elastic behavior) and after (elastoplastic behavior) the phenomenon. It is speculated that the multiple ‘pop-in’ events are revealable over the indentation load and penetration depth. It is suggested that the initial ‘pop-in’ event is owing to the role of dislocation. Therefore, this could be explored that the occurrences of a discontinuity in the load-indentation depth curve. For this case, the investigation of initial deformation is measured under critical depth, which films deformed elastically and no residual deformation is observed (**Fig. 4.3(a)**). At the same time, while the indentation is stopped after the exactly ‘pop-in’ distance, the residual mark depth is observed as shown in **Fig. 4.3(b)**. This leads to larger deviations in the penetration depth versus indentation load curves. We suggested that the ‘pop-in’ event of the GaN films could be contributed from an entirely plastic deformation case. The present results are similar with the work that the GaN films can be elastically flexure before the ‘pop-in’ event [125].

From above results and discussion, the primary deformation mechanism of the GaN films is due to dislocation nucleation and propagation along the easy slip systems. The mechanisms of responsible for the dislocation recovery appears to be associated with the activation of dislocations sources bring by loading-unloading cycle of the GaN films. The plastic deformation prior to loading-unloading cycle is associated with the individual movement of a small number of new nucleation, large shear stress is quickly accumulated underneath the indenter tip. When the local stress underneath the tip reaches at high level cycles, a burst of collective dislocation movement on the slip systems is activated, resulting in a release of local stress [125]. The extensive interactions between the dislocations slipped along the GaN surface, confined the slip bands and resulted in a ‘pop-in’ event due to the deformed and strain-hardened lattice structure.

4-1-3 Conclusion

In this part of experimental results, the contact-induced deformation behaviors of the GaN films/a-axis sapphire substrate were investigated by nanoindentation and AFM technique. The deformation mechanisms of the GaN films result in a ‘pop-in’ event during loading-unloading cycle, especially lead to deviations in the penetration depth versus indentation load curves. The punching out of the threading dislocations beneath the deformed region may contribute to the ‘pop-in’ event, which has been shown as one of the mechanisms responsible for the plastic deformation of the GaN films.



4-2 Investigation of repetition pressure-induced impairment behaviors of the GaN films on a-axis sapphire substrate

4-2-1 Motivation

In terms of GaN film, the mismatch of lattice constants and thermal expansion coefficients in this heteroepitaxy serve high dislocation densities and high level of residual strain in the postgrowth of thin film, which affects its mechanical properties and *etc.* [22,30, 61, 130-133]. The mechanical damages of GaN films, such as film cracking and interface delamination caused by thermal stresses, usually suppress the processing yield and application reliability of microelectronic devices. In this scenario, to access accounting precise in the mechanical properties of GaN remains a challenge. It has been made to develop processes to grow thick GaN films and subsequently separate them from their substrates as evidenced [31, 134-138]. Notice that, GaN film on sapphire substrates exhibits large lattice mismatch (about 13.9 %) causing in-plane tensile strain in the GaN film. The most common orientation of sapphire used for GaN is the c-axis sapphire. In fact, the lattice mismatch of the GaN film on a-axis (11 $\bar{2}$ 0) sapphire is less (2 %) than that on c-axis (0001) sapphire (13.9 %), which promises for excellent quality of GaN growth with improved surface morphology [31].

Above of them, compared to bulk single crystals and the deformation mechanism of the films can serve highly correlate to the geometrical dimensions and the materials defect-structure. The misfit dislocations at the interface of GaN films, however, can play an important role of carrier mobility and luminescence efficiency, *etc.* As a consequence, nanoindentation has proven to be a powerful tools for probing the information on the mechanical properties of GaN films with characteristic dimensions in the sub-micron regime, such as hardness and Young's modulus [117-118, 139-151]. In terms of indentation load on GaN films, the nanoindentation-induced discontinuity in the load-displacement curve has been revealed. The slip band movement [45, 119, 142-143] and dislocation nucleation mechanism [117, 140, 144] to explain this pop-in event on c-axis GaN films or bulk single

crystals have been investigated [122, 145]. In our prior article, the proposal of a-axis GaN films had been attempts in pop-in study [146], but for reasons that are unclear from repetition pressure-induced impairment events.

In this paragraph, the pressure-induced impairment of GaN films/a-axis sapphire substrate has been investigated by using nanoindentation, AFM, and CL mapping. A significant investigation of the mechanical characterizations on GaN films is motivated here.

4-2-2 Results and discussion

In term of indentation, residual impression of repeated indent mark was examined by tapping mode 3D-AFM to check for the evidence of slip, cracking, and pile-up/sink-in phenomenon. Shown in Fig. 4.4 are typical amplitude-mode AFM images of a (a) typical cycle, (b) three, (c) six, and (d) nine loading/reloading cycles to maintain a maximum load of 25 mN. In Fig. 4.4(a), AFM image clearly illustrated that slightly activation of pyramidal slip near the indent mark, which occurs at typical cycle nanoindentation, is suppressed in the GaN films. A comparison of three and six loading/reloading cycles nanoindentation images [Fig. 4.4(b)-(c)] gives a gradation of protrusion that mean some pyramidal slip nucleation rather than that of typical cycle one. It is suggested that the slip mechanism can be responsible for the pile-up events during the loading of GaN. Furthermore, the AFM image of the residual indentation mark at nine loading/reloading cycles is revealed that the pyramidal slip and partially crack [Fig. 4.4(d)]. The dislocation-induced ‘pop-in’ event tends to be associated with two distinct deformation behaviors before (pure elastic behavior) and after (elastoplastic behavior) the phenomenon. The hardness (H) and elastic modulus (E) as a function of indentation depth can be obtained from the FSM measurements; for the measured results of the GaN films/A plane sapphire substrate, H were 16.4 ± 0.2 , 15.6 ± 0.1 , 16.6 ± 0.2 , 26.5 ± 0.8 GPa, while E were 409.7 ± 12 , 400.7 ± 11 , 383.5 ± 9 , 758.8 ± 18 GPa, respectively. The soft GaN films was grown epitaxially on a hard sapphire substrate, it is tend to find that the differences in lattice parameters and thermal expansion coefficients between the film and

substrate. It may introduce a misfit strain at the interface and the strain is released by generating threading dislocations in the GaN films [126-127, 147-148]. From the plane view of the indentation mark, Fig. 4.4 shows the residual volume from the edge of indentation. There is massive material transfer from below the indented zone to the sides of the indentation mark. Navamathavan *et al.* [149] revealed that the residual impression of the indentation mark by Berkovich indenter tip. The pile-up event on the morphological surface is clearly observation from SEM technique. Barsoum *et al.* also reported [150] that pop-ins event and the cracks under a Berkovich indenter were observed. While the indenter suddenly to penetrate into the basal planes, they must rupture [Fig. 4.4(d)]. Since the rupture is associated with the repeated indenter cycles, the relatively large displacements at low stresses below the bend are most probably related to the back and forth motion of delaminated. It is believed that the discrepancies in the mechanical parameters obtained by repeated indentation methods are mainly due to the specific tip–surface contact configuration and stress distribution inherent in the system of GaN films/a-axis sapphire.

In Fig. 4.5, the CL mappings acquired at a wavelength of 550 nm from a GaN films indented were presented at (a) typical, (b) three, (c) six, and (d) nine loading/reloading cycles, respectively. These CL images reveal the distribution of indentation-induced extended defects; the cube-corner indenter form and these extended defects reflect some of the radial symmetry of the stress field [Fig. 4.5(a)-(c)]. In contrast, another luminescence/topography distribution CL image revealed a crack line that formed after nine loading/reloading cycles [Fig. 4.5(d)]. Slip enhancement may contribute to the crack that can be observed during loading/reloading and, the mechanism may be due to the plastic deformation [141]. In the GaN films, the indented area below the propagation of dislocations is observed by CL image that also revealed a detectable reduction in the intensity of the CL emission [148-151]. In the case of six loading/reloading cycles, only a small percentage of indentations was plastically deformed [Fig. 4.5(c)]. CL imaging could distinguish between the indentations that had undergone

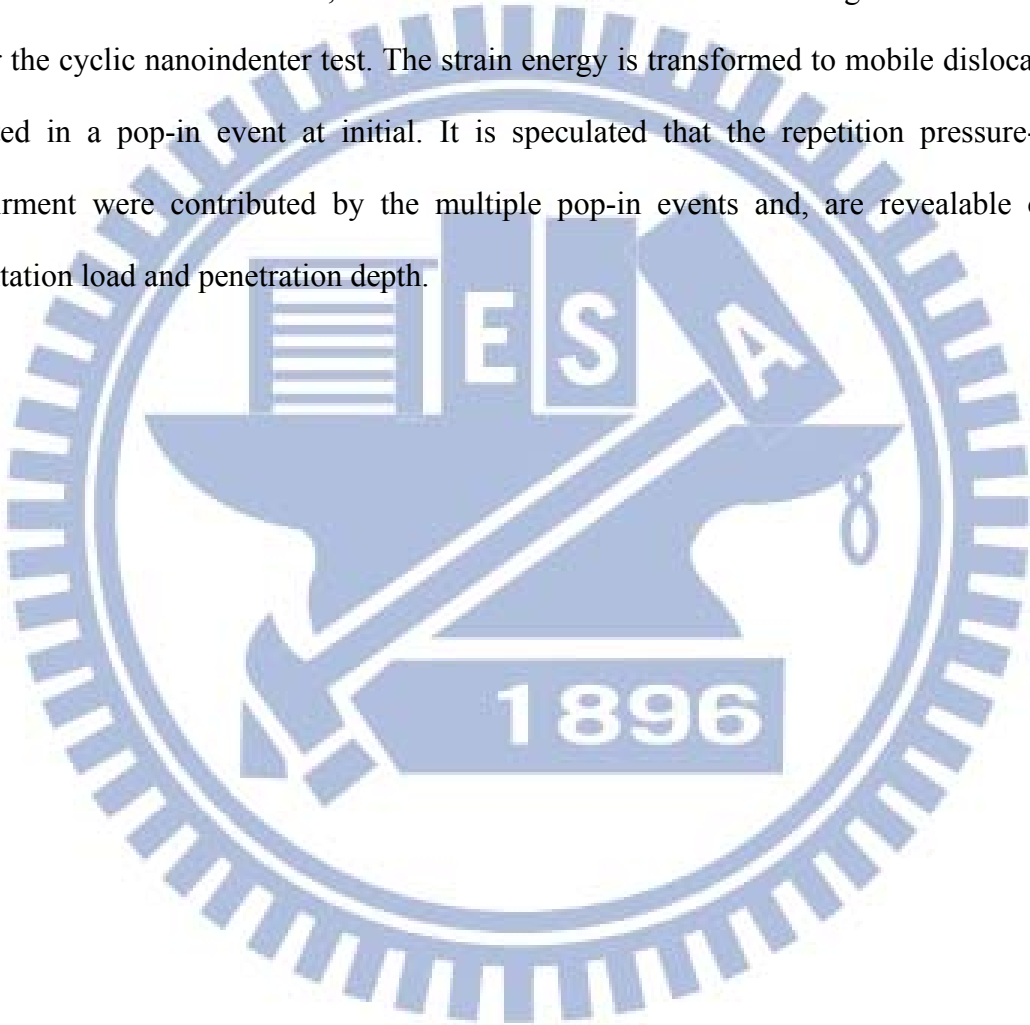
several degree of plastic deformation, which location was purely in the elastic regime [Fig. 4.5(d)]. As a result, it is detected an observable CL impression only after the pile-up event, providing convincing evidence that the phenomenon involves the nucleation of slip as the deformation mode.

Above of them, the load-indentation behaviours for the GaN films on the A plane sapphire are revealed in Fig. 4.6. At beginning, the FSM serves the typical-load vs. penetration depth of GaN film [Fig. 4.6(a)]. After the three cycles, the load vs. penetration depth of GaN film is recorded; the repetition pressure-induced curve means gradually elastic deformation. The repetition pressure-induced under three and six loading/reloading cycles nanoindentation images [Fig. 4.6(b)-(c)] gives a more suffer in strain hardening compared with that of typical one [Fig. 4.6(a)]. It is noted that the strain hardening is consist of the decreased in the penetration depth. While Fig. 4.6(d) is superimposed, it becomes evident that the crack and the increased penetration depth are almost identical at CL imaging [Fig. 4.5(d)]. From Barsoum *et al.* [118], noted that all slips are basal and the stress-strain curves both before and after the pop-ins for both C and A orientations presumably were almost perfectly superimposable in sapphire. It is thus reasonable to implicate basal slip for the deformation in the A orientation. The corresponding penetration depth vs. repetition cycles concluded in Fig. 4.7; the strain hardening of GaN films partially induce as the penetration depth are observed to decrease from typical to six loading/reloading cycles, but nine loading/reloading cycles. Consequently, the system (GaN films/a-axis sapphire) can be interacted by indenter tip to appear deformed zone, the threading dislocations then excursion into films through certain depths, afterward causing the pop-in event occurred. It is conjectured that the mechanism of the event is caused by slip bands [119, 124, 152-154], and/or dislocation nucleation [117, 155]. However, the inner failure of the GaN films is observed while crack is suddenly occurred at the condition of nine loading/reloading cycles. It is speculated that the repetition pressure-induced impairment during loading were contributed by the multiple pop-in events

and, are revealable over the indentation load and penetration depth [40, 44]. From the previous reported [118, 156-157], they discussed that the deformation mechanisms in freestanding films. The successive indentations in the same location generated a series of hysteresis loops in which the first loop was slightly open, but subsequent loops were perfectly superimposable. For this case, the investigation of initial deformation of GaN films is measured under cyclic nanoindentation, which films deformed elastically and residual deformation is observed. This leads to larger deviations in the penetration depth vs. cyclic nanoindentation. The mechanisms of responsible for the dislocation recovery appears to be associated with the activation of dislocations sources bring by loading-unloading cycle of the nanoindentation tip upon GaN films. The plastic deformation prior to loading-unloading cycle is associated with the individual movement of a small number of new nucleation, and large shear stress is quickly accumulated underneath the indenter tip. When the local stress underneath the tip reaches at high level cycles, a burst of collective dislocation movement on the slip systems is activated, resulting in a release of local stress. The extensive interactions between the dislocations slipping along the GaN surface, therefore, confined the slip bands resulted in a pop-in event due to the deformed and strain-hardened lattice structure. It is suggested that the primary deformation mechanism of the GaN films may due to dislocation nucleation and propagation along the easy slip systems.

4-2-3 Conclusion

In this part of experimental results, the deformation mechanisms of the GaN films were observed in the form of a pop-in event during loading-unloading cycle, especially leading to deviations in the penetration depth vs. cyclic nanoindentation loading-unloading. A CL images study of the indentation impressions show the clear evidence on the observation of the defects transform. In addition, the transformation of strain hardening of GaN is occurred under the cyclic nanoindenter test. The strain energy is transformed to mobile dislocation and resulted in a pop-in event at initial. It is speculated that the repetition pressure-induced impairment were contributed by the multiple pop-in events and, are revealable over the indentation load and penetration depth.



4-3 Investigation of nanotribological behaviors of the GaN films/a- and c-axis sapphire substrate

4-3-1 Motivation

The misfit dislocations at the interface play an important role in carrier mobility, luminescence efficiency, *etc.* However, the mechanical damages of GaN films, such as film cracking and interface delamination caused by thermal stresses, chemical-mechanical polishing, usually suppress the processing yield and application reliability of microelectronic devices [84, 159-161]. The measurements have been made possible by the development of instruments that continuously measure force and displacement as an indentation is made [162-165]. The slip band movement [117, 119, 166-167] and dislocation nucleation mechanism [45, 168] have been proposed to explain this ‘pop-in’ event. Most of the studies were carried out on c-axis GaN films or bulk single crystals [122, 169]. In this respect, the nanoscratch technology that directly processes the surface of materials by using a diamond particle or tip of nano size has been conducted by many researchers on the grounds of advantages such as the free selection of materials, the easy alternation of designs and convenient initial facilities [170-171]. H and residual stress are significant parameters for tribological coatings [172-173]. Comparatively, GaN films grown on c- and/or a-axis sapphire substrates, not yet evidenced in the nanotribological behavior up to now.

In this paragraph, significant investigation of the nanotribological characterizations on GaN films is motivated. The pile-up induced impairment of GaN films/c- and/or a-axis sapphire substrate has been investigated by using nanoscratch system and atomic force microscope (AFM).

4-3-2 Results and discussion

The GaN films were deposited onto different sapphire substrates using MOCVD. Sapphire substrate surfaces have a specific epitaxial orientation (c- and a-axis), resulting in aspect-oriented nuclei. **Fig. 4.8** presents AFM images obtained after operating the nanoscratch measurement system at ramped loads of 2000, 4000, 6000 μN ; the images correspond to surface profiles on the GaN films. The nanoscratch depth is related to both the type of GaN epilayer (c- or a-axis sapphire) and the applied ramped load were found. **Fig. 4.8(a)** reveals that the surface of the GaN/c-axis sapphire underwent sample pile-up on surface areas during slip processing at a ramped load at 2000 μN . Between the groove and the film, the surface material appears to reveal the effects of elasticity as a result of elastic deformation during the nanoscratch tests. **Fig. 4.8(b)-(c)** evinces that the transition is affected by the contact pressure, the changing from purely elastic to elastoplastic contact upon doubling the ramped force of 4000 μN . **Fig. 4.8(d)** displays the surface of the GaN/a-axis sapphire that underwent sample pile-up on the surface areas during slip processing at a ramped load of 2000 μN ; it reveals that the surface material also exhibited an elastic reaction as a result of elastic deformation between the groove and film. **Fig. 4.8(e)-(f)**, however, reveals that a transition from purely elastic to elastoplastic contact occurred only upon initially applying the ramped force of 4000 μN ; subsequently, it became a complete plastic contact. In the ductile-regime machining part (elastoplastic deformation) of the scratch track, it is observed a slightly machined surface without cracks (**Fig. 4.8(e)-(f)**), because elastic-plastic deformation occurred. In the brittle transition part of the scratch track, it is also observed several brittle regions. The brittle regime machining part of the scratch track exhibited a deep profile. The bulge edge scenarios provided evidence for a significant reduction relative to the applied load at 2000 μN in the average scratch depth on the GaN/c-axis sapphire (**Fig. 4.8(a)-(c)**). Furthermore, the nanoscratch deformation of the GaN/a-axis sapphire samples (**Fig. 4.8(e)-(f)**) in terms of the deep profiles of their nanoscratch traces, presumably because the GaN/a-axis sapphire sample

featured weak bonds relative to those of the GaN/c-axis sapphire sample. The deep profile distribution of the a-axis GaN sample suggests that it was softer than its c-axis counterpart. Thus, the transition from purely elastic to elastoplastic contact was revealed in the nanoscratch traces and in the depth of the pile-up.

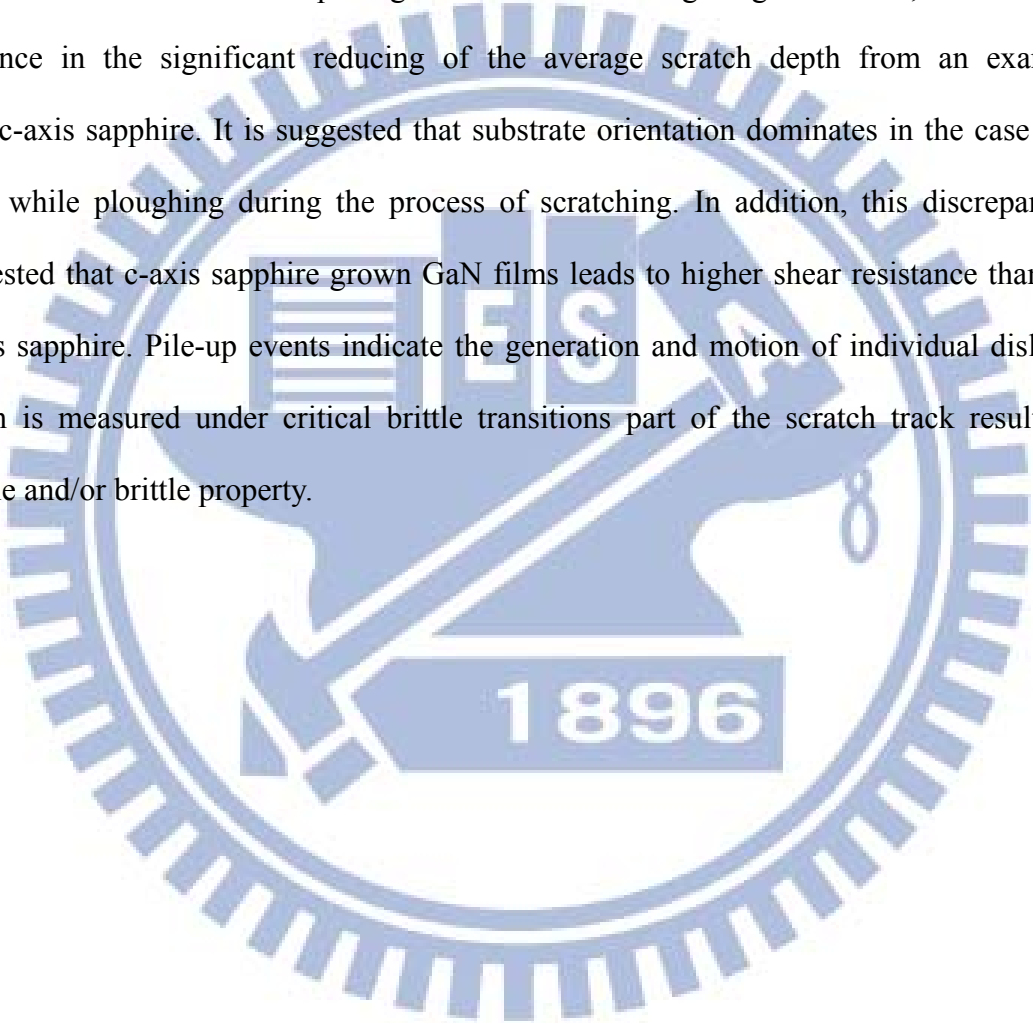
Fig. 4.9 presents typical profiles of the coefficient of friction (μ), obtained as the ratio of the in situ-measured tangential force to the applied ramped load, plotted with respect to the scratch duration at ramped loads of 2000, 4000, 6000 μN . The μ profiles of the GaN samples oscillated relatively regularly because of weak or strong bonds and cohesive failure from the period of transition of the GaN samples were found. Accordingly, the friction force revealed that a sliding mechanism was in operation, with the more strongly adhesive film providing a slighter fluctuation in its μ profile during the nanoscratch tests (**Fig. 4.9(a)**). Hence, the nanoscratch deformation of the GaN/a-axis sapphire sample resulted in μ profiles that featured rather irregular oscillation (**Fig. 4.9(b)**). Thus, lower adhesion reflects the presence of interlinks and rearrangements under a higher ramped load, not only involving the weaker GaN bonds but also resulting in higher values of the depth profile and the μ values (**Table 4.2**).

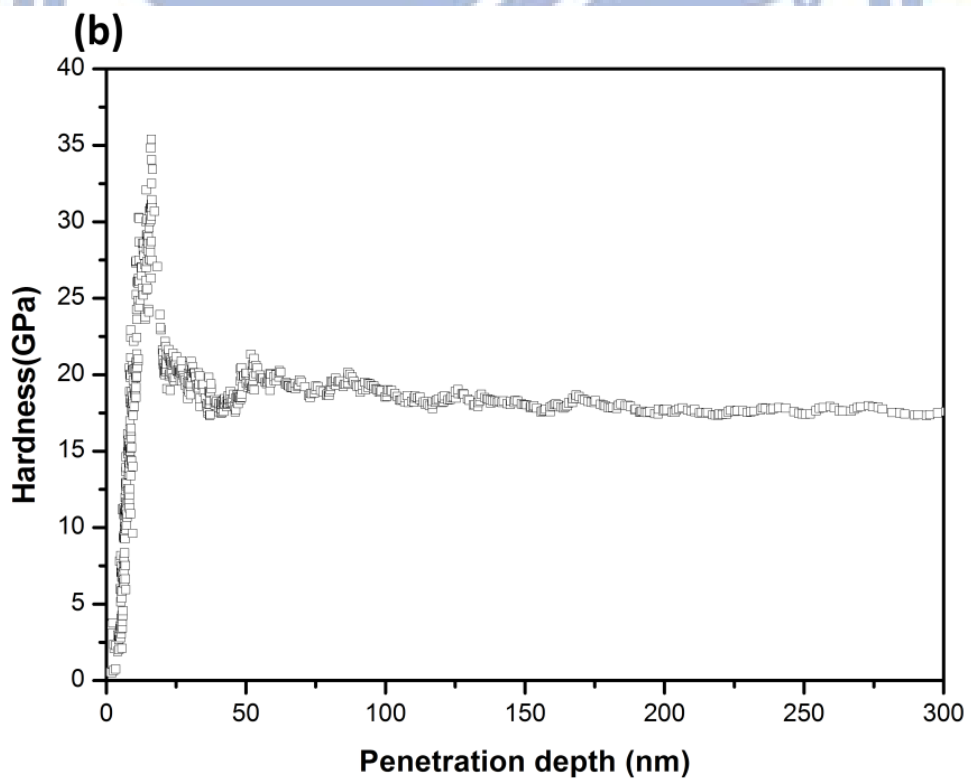
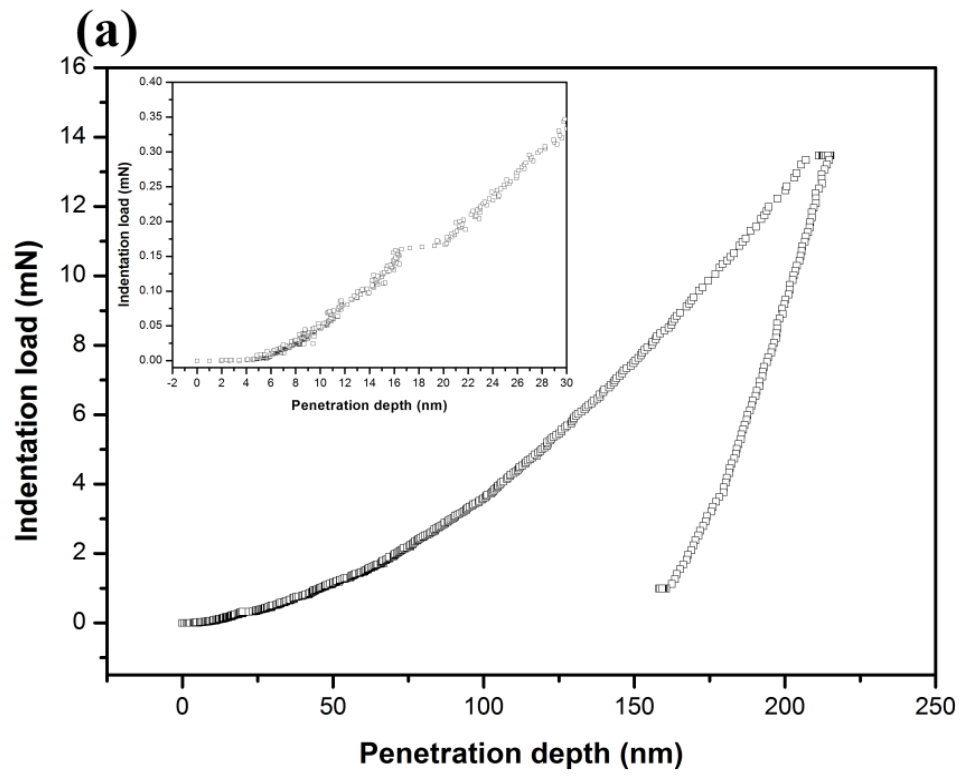
The fluctuation profile from a nanoscratch tests does not depend exclusively on the plasticity or the value of H; it is also related to the adhesive strength between the film and the substrate. While the contact area between the tool and the GaN surface increases, the pressure under the tool becomes insufficient to drive the transformation to a denser crystal structure. Thus, the deformation theory cannot be accommodated in a ductile manner. From studies of nanomachining processing, both tribological and chemical effects, rather than physical deformation and fracture, are believed to become dominant. In this scenario, the average measured residual stress in the cracking zone is much lower than that in the crack-free zone, because the elastic strain is released by cracking. From the nanotribological point of view, curvature and/or distribution in the values of l signal the onset of adhesive failure, such as cracking or delamination resulting from the interaction between the sliding stylus and the

debris formed on the nanoscratch track [174-175]. Several factors can affect the value of H of a film, including the packing factor, stoichiometry, residual stress, preferred orientation, and grain size. In the experiments, the orientation of the GaN sample not only affected its nanotribological performance but also its scratching resistance; thus, the volume of the removed material from nanoscratch tests can be measured to determine the role of the orientation of the GaN sample. This approach can be used to explain the nanotribological behavior of the GaN sample; for example, the profile of GaN/a-axis sapphire sample reveals more serious wear of the components (Fig. 4.8) and more unwanted self-excited oscillations (Fig. 4.9) than that of the GaN/c-axis sapphire sample. Thus, the GaN/c-axis sapphire sample revealed relatively small oscillations with respect to the ramped load. Taken together, our findings reveal that the nanoscratch deformation of the GaN samples was influenced primarily by the orientation of the sapphire substrate. The mechanisms for the dislocation recovery from elastic and/or plastic deformation appear to be associated with the activation of dislocation sources brought about by the nanoscratching of the GaN sample. The plastic deformation prior to nanoscratching was associated with the individual movement of a small number of new nucleation sites; large shear stress was quickly accumulated underneath the indenter tip. When the local stress underneath the tip reached high-level cycles, a burst of collective dislocation movement on the slip system was activated, resulting in a release of local stress. The extensive interactions between the dislocations slipping along the surface of the GaN/a-axis sapphire sample, therefore, confined the brittle transition part of the scratch track, resulting in ductile and/or brittle properties because of the deformed and strain-hardened lattice structure.

4-3-3 Conclusion

In this part of experimental results, the contact-induced deformation behaviors of the GaN films/c- and a-axis sapphire substrate were investigated by a combination of nanoscratch and AFM techniques. It is separated that the three part of scratch process including the ductile-regime, brittle transition (elastic–plastic deformation), and brittle-regions were observed. From the AFM morphological studies in the bulge edge scenarios, results are given evidence in the significant reducing of the average scratch depth from an example of GaN/c-axis sapphire. It is suggested that substrate orientation dominates in the case of GaN films while ploughing during the process of scratching. In addition, this discrepancy was suggested that c-axis sapphire grown GaN films leads to higher shear resistance than that of a-axis sapphire. Pile-up events indicate the generation and motion of individual dislocation, which is measured under critical brittle transitions part of the scratch track resulted in a ductile and/or brittle property.





(continues)

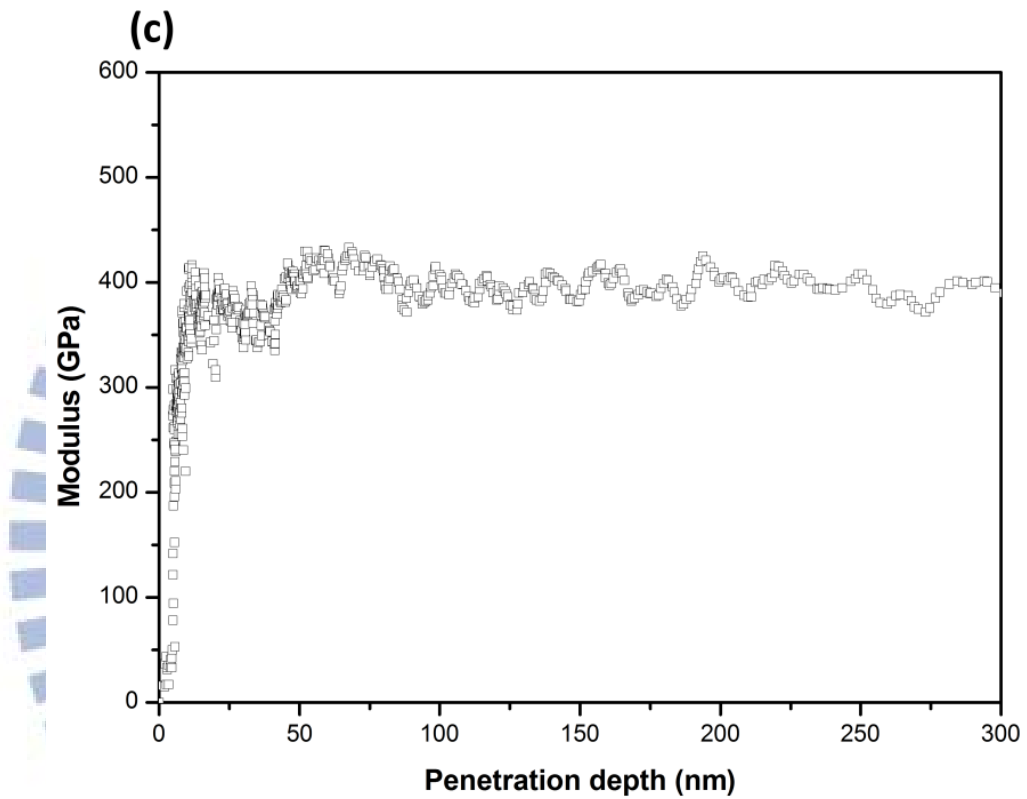


Fig. 4.1 Nanoindentation test results: (a) a typical load-displacement curve (Inset: the typical load-displacement curve illustrates the drastic variation at the critical depth of first ‘pop-in’ at 16 nm); (b) hardness-displacement curve; (c) modulus-displacement curve for GaN films/a-axis sapphire substrate.

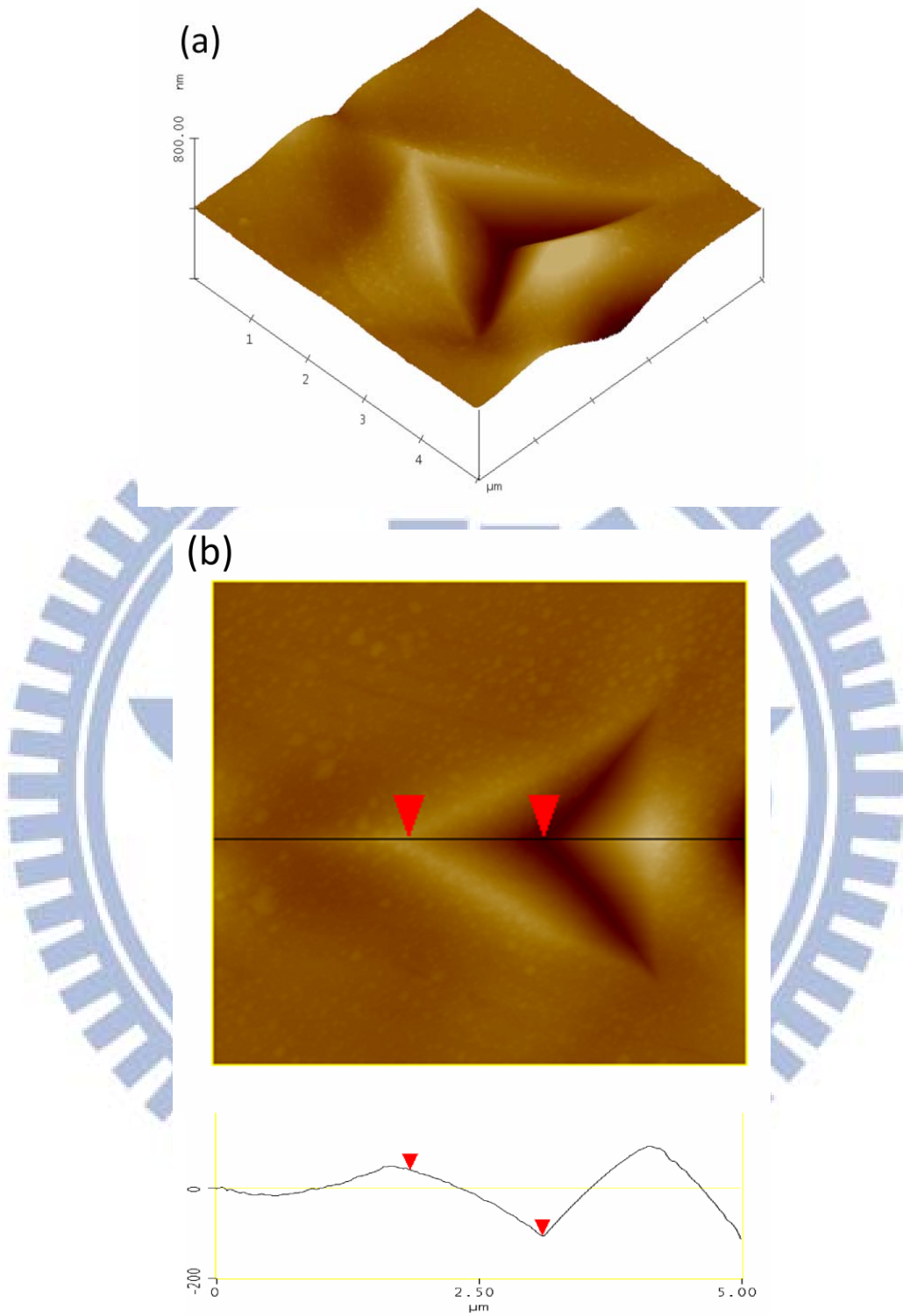


Fig. 4.2 (a) The AFM image of the residual indentation mark is revealed that none of crack and particle even occurred after the indentation depth; (b) the residual volume from the edge of indentation.

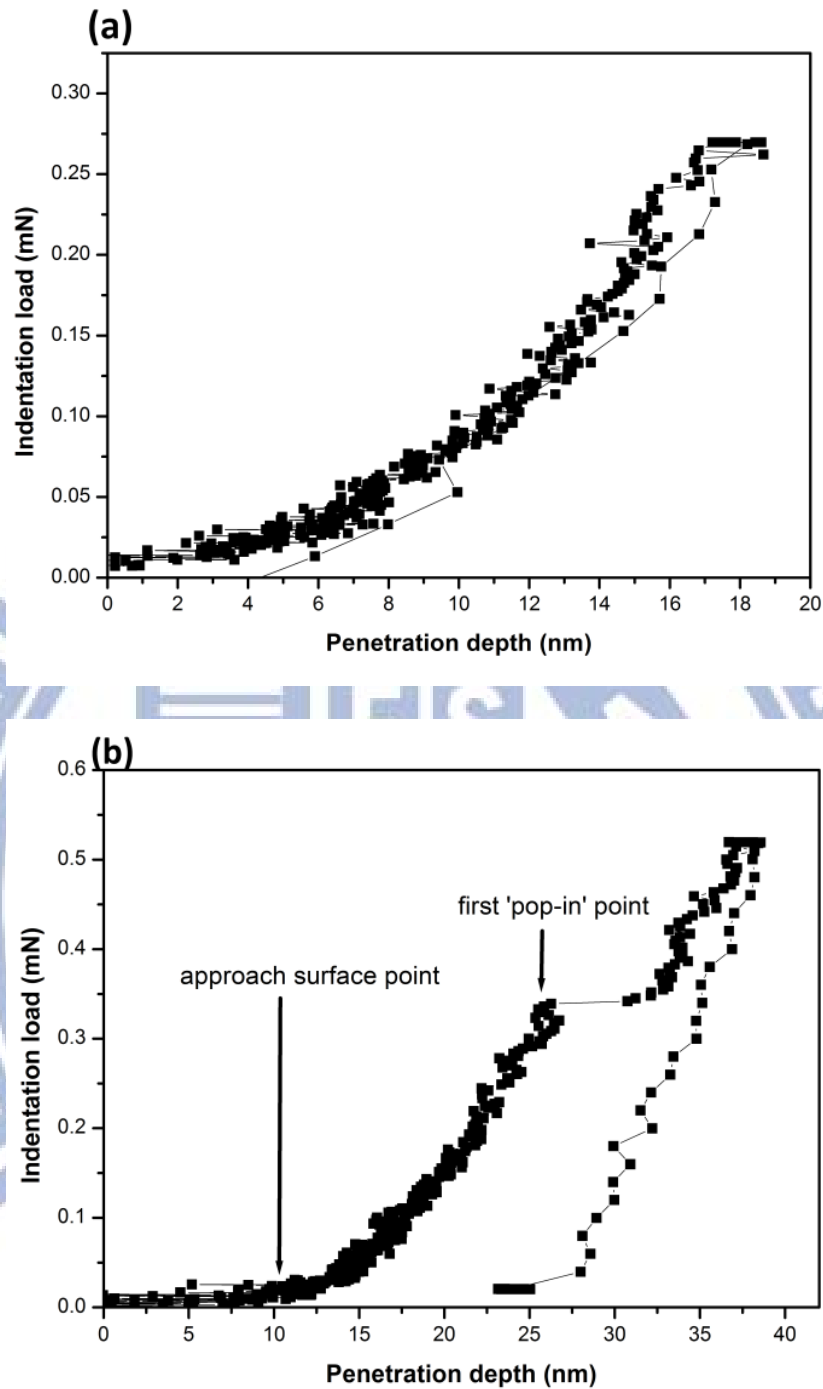
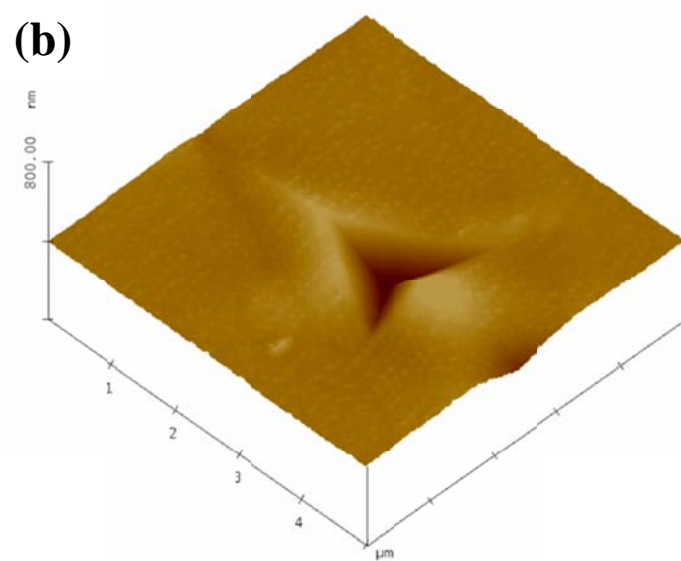
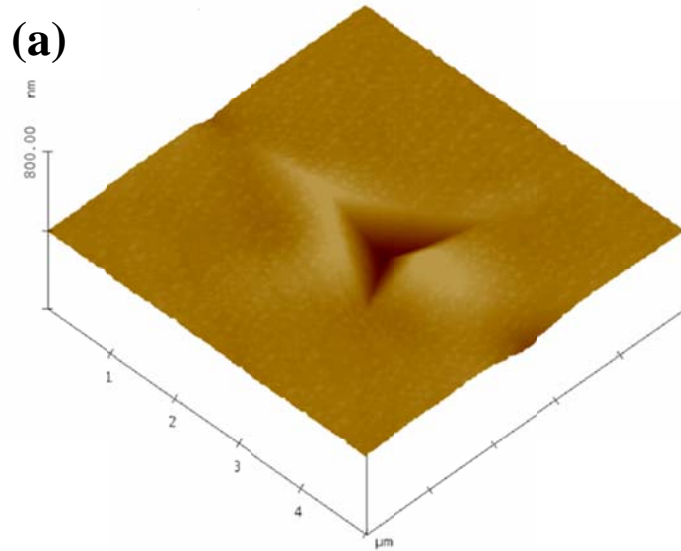


Fig. 4.3 (a) A typical load-displacement curve for just before the critical 'pop-in' depth (14 nm) shows the elastic recovery; (b) A typical load-displacement curve for just after the critical 'pop-in' depth shows sudden discontinuity and produced produced residual impression of about 26 nm.



(continues)

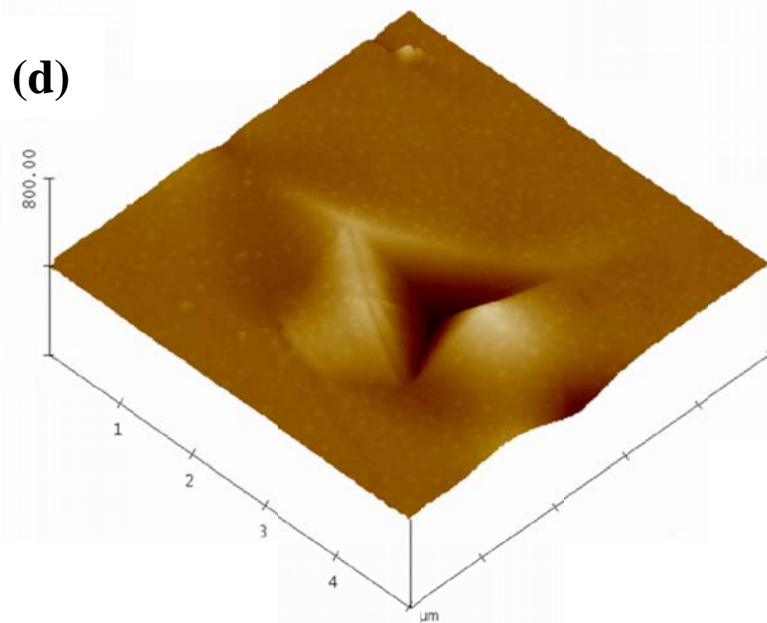
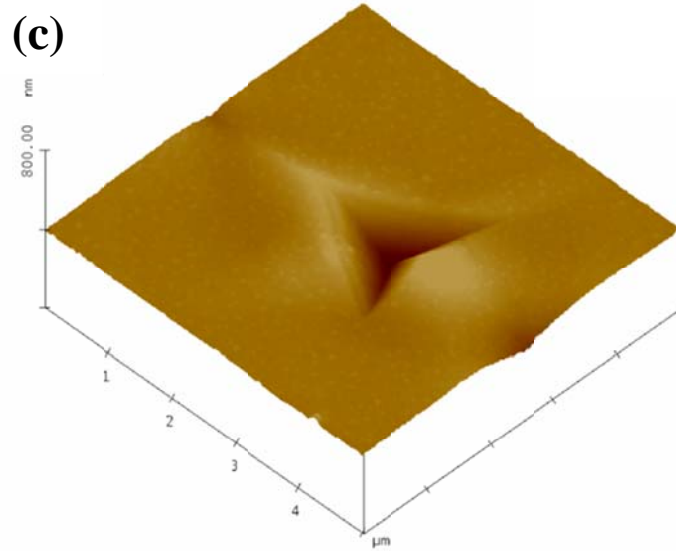
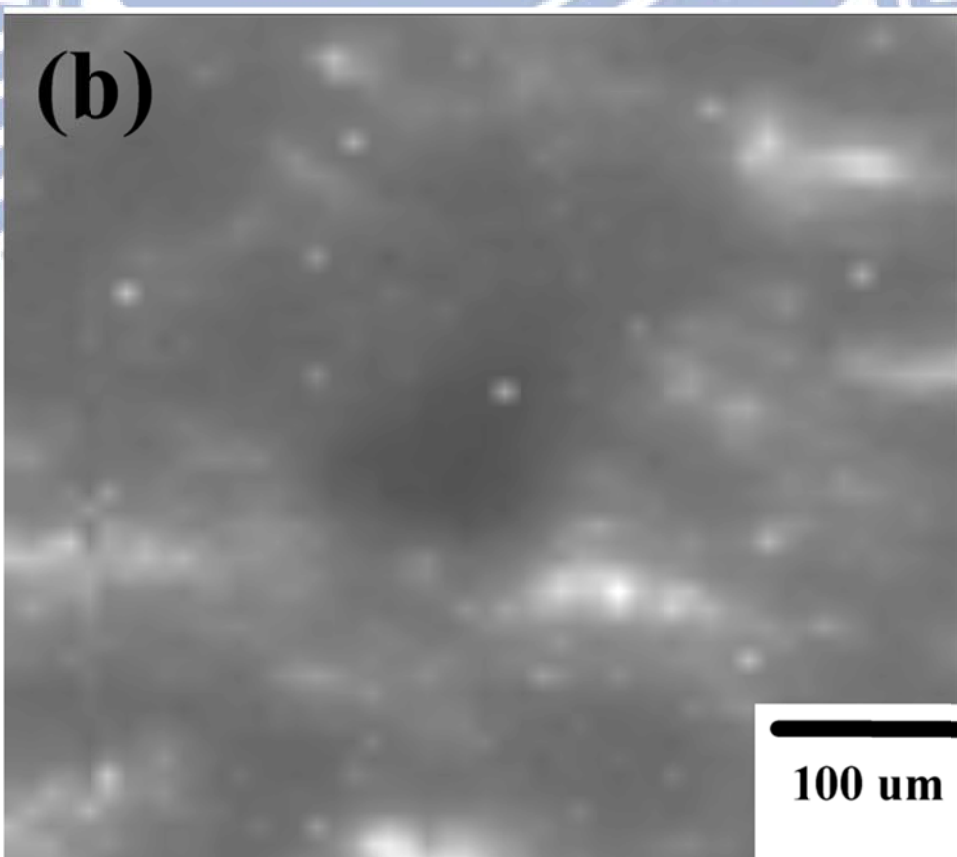
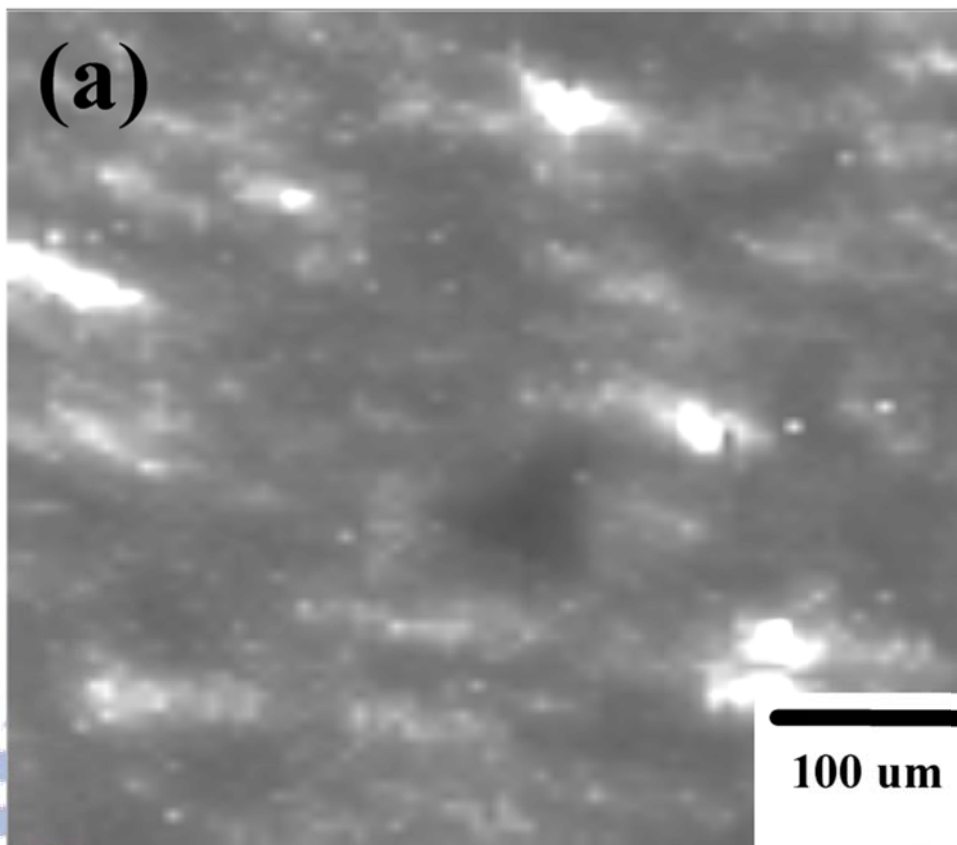


Fig. 4.4 AFM images of indented GaN film/a-axis sapphire surfaces: (a) typical, (b) three, (c) six and (d) nine loading/reloading cycles, respectively.



(continues)

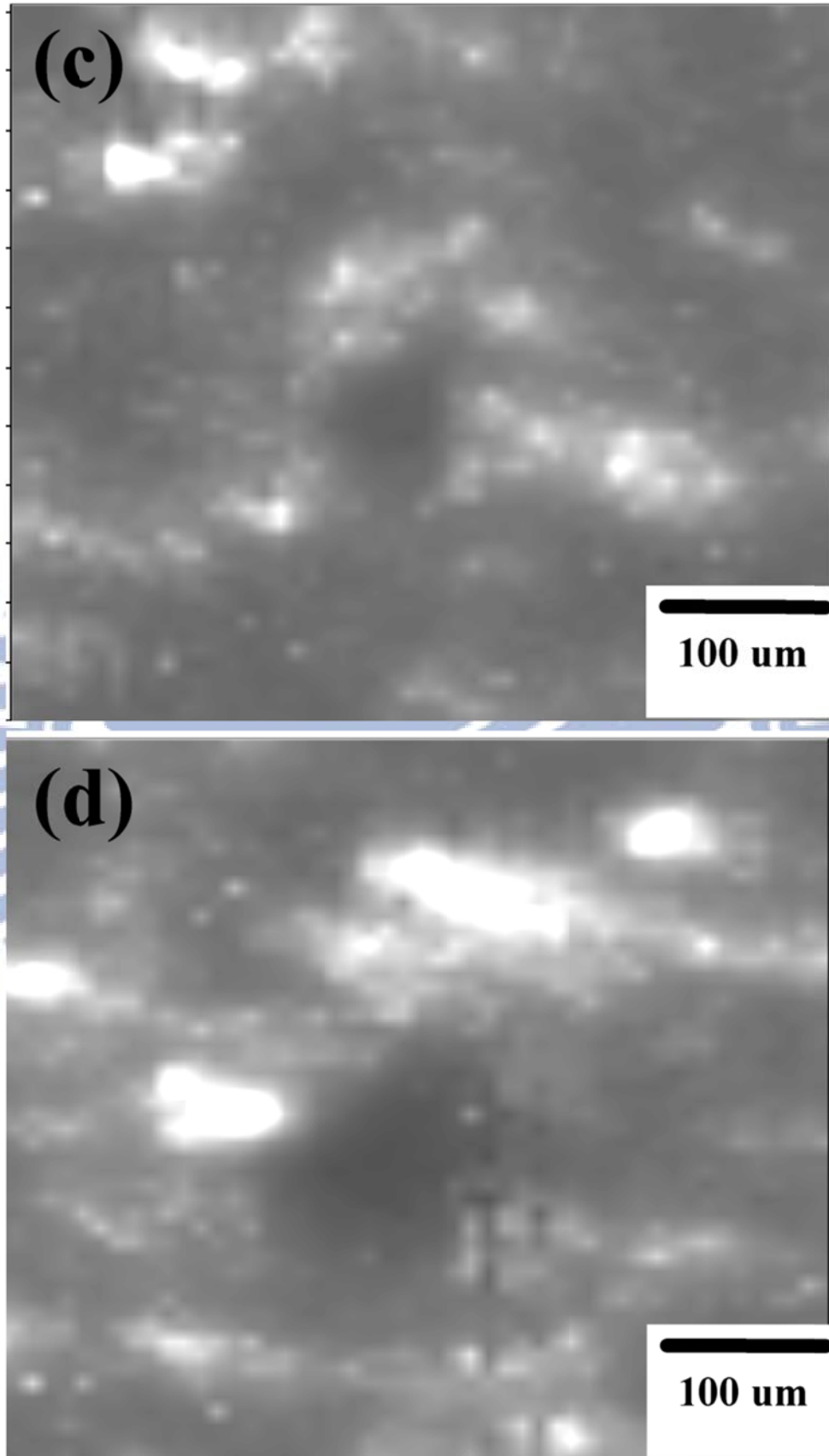


Fig. 4.5 The CL mapping acquired at a wavelength of 550 nm from an indented GaN films: (a) typical, (b) three, (c) six and (d) nine loading/reloading cycles, respectively.

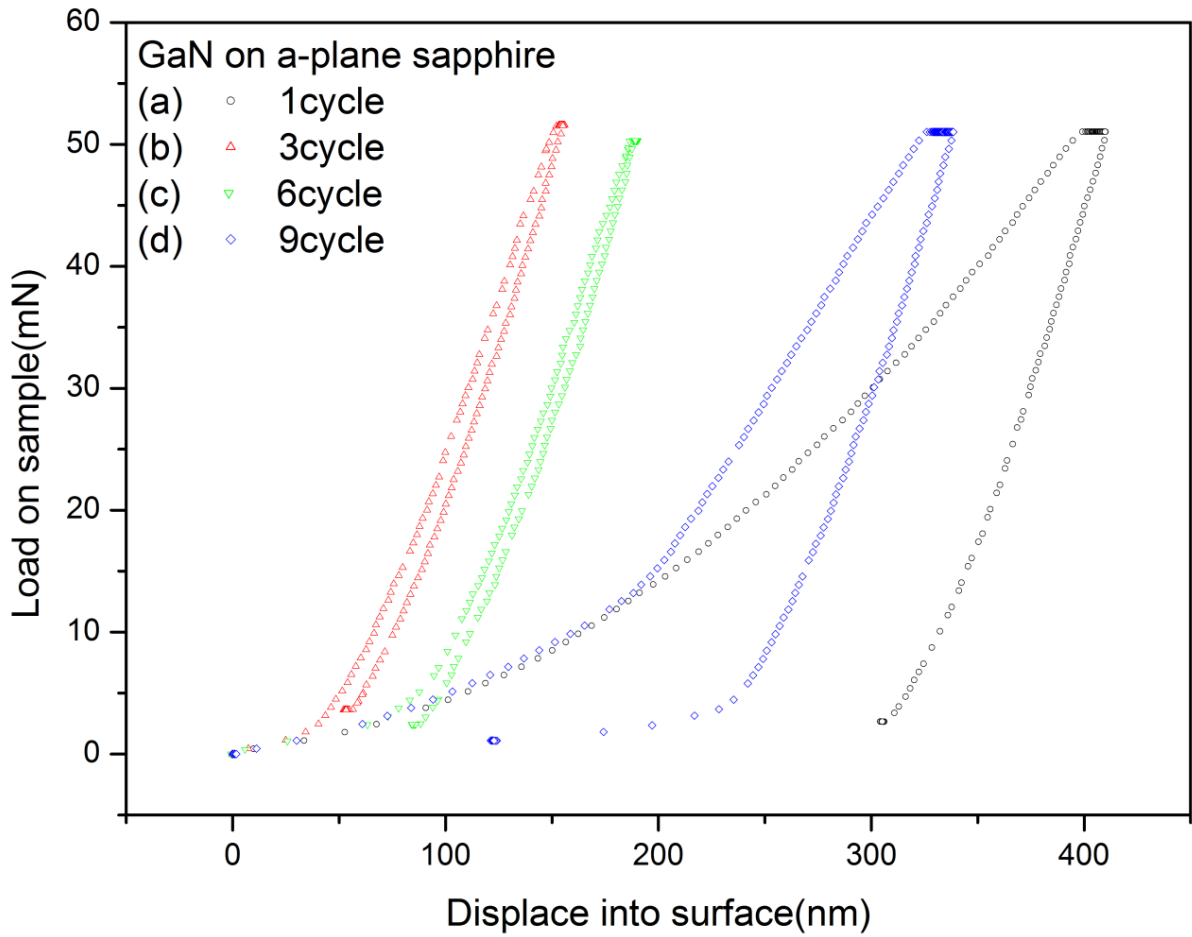


Fig. 4.6 The typical load vs penetration depth curve of GaN epilayers: (a) typical, (b) three, (c) six and (d) nine loading/reloading cycles, respectively.

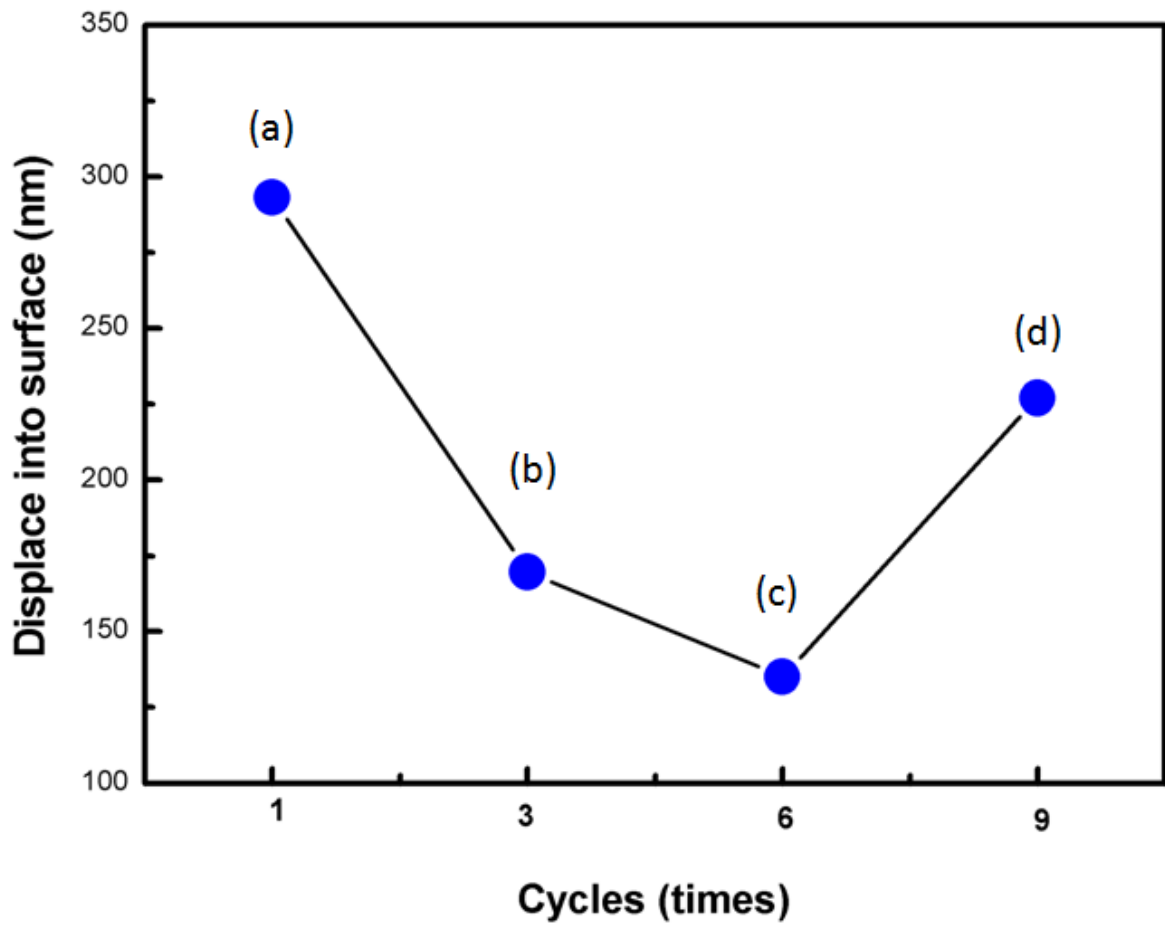


Fig. 4.7 The penetration depth vs loading/reloading of GaN epilayers: (a) typical, (b) three, (c) six and (d) nine loading/reloading cycles, respectively.

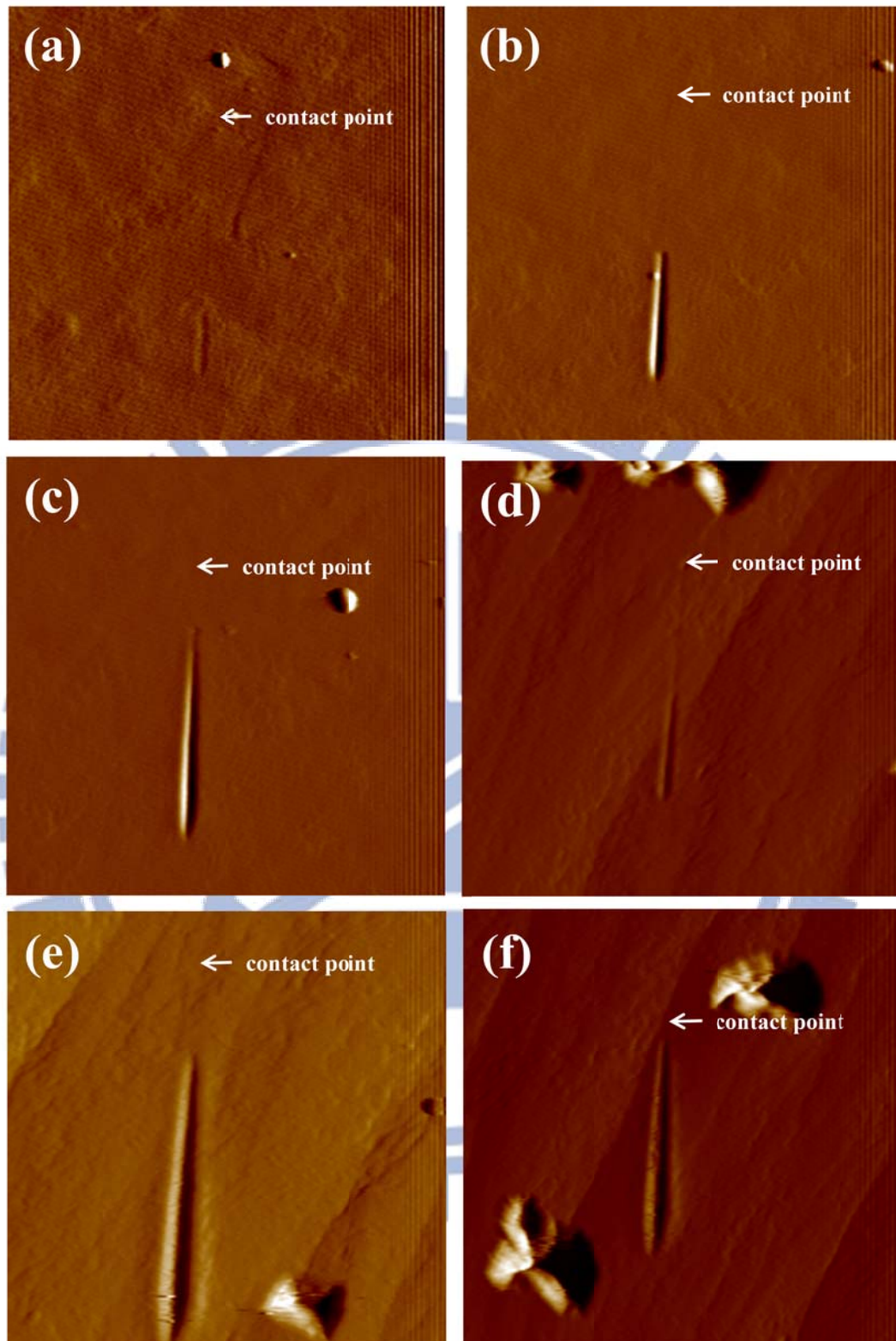


Fig. 4.8 3D AFM images of scratch tracks formed in GaN films on sapphire substrates:
 (a) 2000 uN ramped force, c-axis sapphire; (b) 4000 uN, c-axis sapphire ; (c) 6000 uN, c-axis sapphire; (d) 2000 uN ramped force, a-axis sapphire; (e) 4000 uN, a-axis sapphire ; (f) 6000 uN, a-axis sapphire.

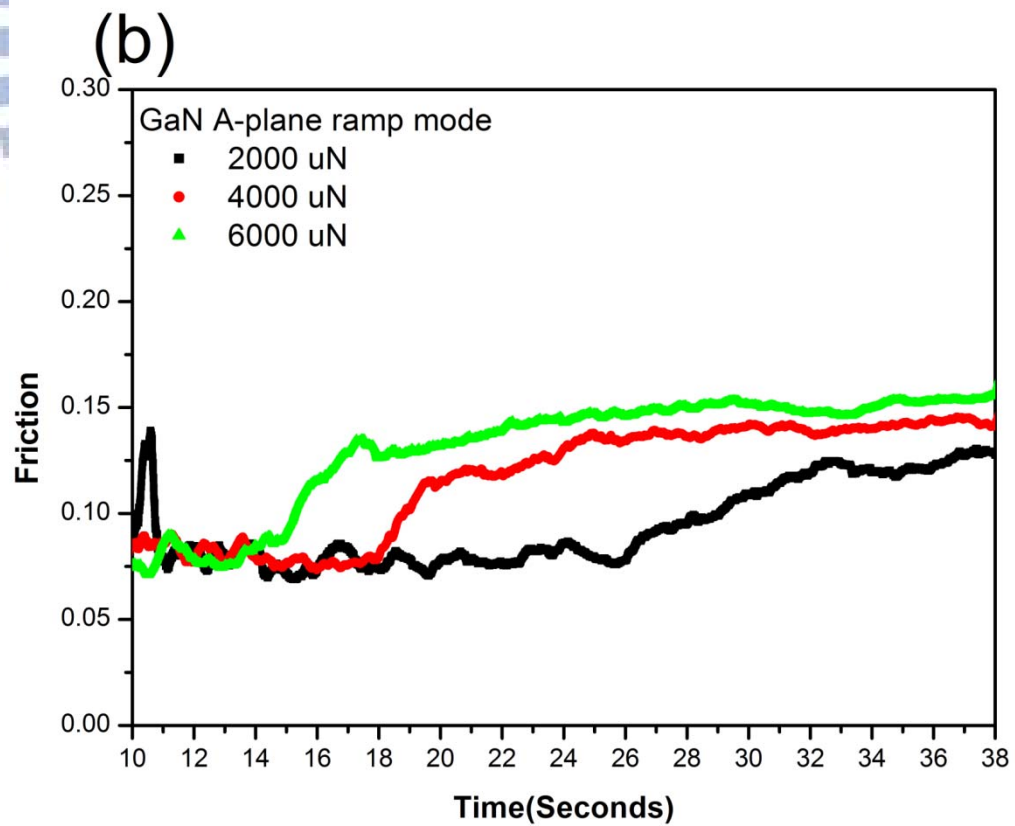
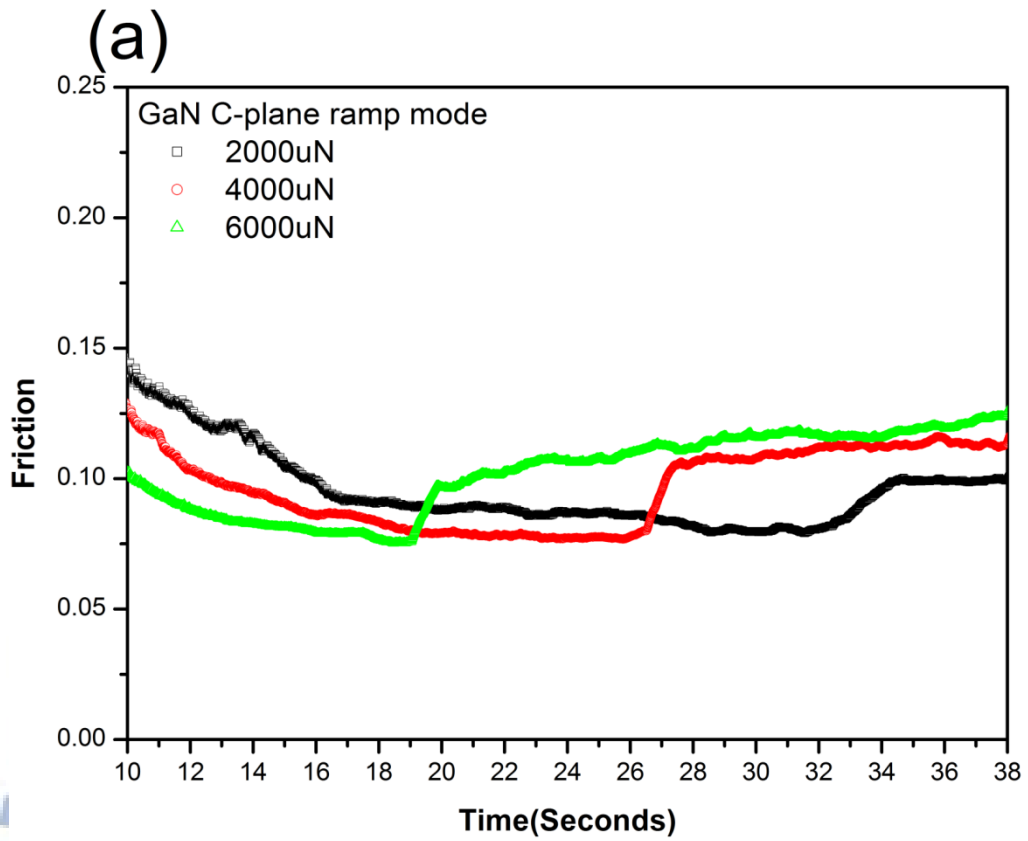


Fig. 4.9 Typical profiles of the coefficient of friction (μ) plotted with respect to the scratch duration at ramped loads of 2000, 4000, 6000 μN for GaN films on (a) c-axis and (b) a-axis sapphire substrates.

Tab. 4.1 Hardness and elastic modulus of GaN films obtained from various measurement methods.

	Average Hardness (GPa)	Average Modulus (GPa)	Indenter Tip
A-plane GaN*	15.9 ± 0.8	394.6 ± 12	Berkvich
C-plane GaN [124]	22.5		Berkvich
C-plane GaN [129]	19 ± 1	286 ± 25	Berkvich
C-plane GaN [119]	13.4	233	Spherical

*This study.

Tab. 4.2 Critical lateral forces and values of μ determined from nanoscratch trace depths within GaN films on c- and a-axis sapphire substrates.

Sample	Normal Load (uN)	Coefficient of Friction	Lateral Force (uN)
GaN C-plane	2000	0.10511	-91.323
GaN C-plane	4000	0.10516	-200.21
GaN C-plane	6000	0.10615	-328.63
GaN A-plane	2000	0.09614	-100.56
GaN A-plane	4000	0.11785	-256.17
GaN A-plane	6000	0.12966	-425.92

Chapter 5 Conclusions and Future Work

5-1 Conclusions

In short, a systematic study of the contact-induced deformation behaviors/mechanisms on GaN films with the aid of nanoindentation technique have demonstrated. The main conclusions are summarized and discussed.

The deformation mechanisms of the GaN films/a-axis sapphire substrate result in a "pop-in" event during loading-unloading cycle, especially lead to deviations in the penetration depth versus indentation load curves. The punching out of the threading dislocations beneath the deformed region may contribute to the 'pop-in' event, which has been shown as one of the mechanisms responsible for the plastic deformation of the GaN films. Furthermore, the repetition pressure-induced impairment of the GaN films/a-axis sapphire substrate was investigated by using nanoindentation and atomic force microscopy techniques. From atomic force microscopy scans, the pop-ins resulted in impressions with depths that corresponded to the extent of residual penetration, or plastic deformation, registered in the first cycle. A material pile-up was also seen around the impressions. The deformation mechanisms of the GaN films were observed in the form of a pop-in event during loading-unloading cycle, especially leading to deviations in the penetration depth vs cyclic nanoindentation loading/unloading. A cathodoluminescence images study of the indentation impressions show the clear evidence on the observation of the defects transform. In addition, the transformation of strain hardening of GaN is occurred under the cyclic nanoindenter test. The strain energy is transformed to mobile dislocation and resulted in a pop-in event initially. It is speculated that the repetition pressure-induced impairment was contributed by the multiple pop-in events, and are revealed over the indentation load and penetration depth.

Finally, the contact-induced deformation behaviors of GaN films on c- and a-axis sapphire substrates have been systematically investigated with the aid of the nanoscratch and atomic force microscopy techniques. Three separate scratch processes in the ductile, brittle transition (elastic–plastic deformation), and brittle regions were observed. AFM morphological studies of the bulge edge scenarios provided evidence for significant reductions in the average scratch depth for the GaN/c-axis sapphire. It suggested that the substrate orientation dominated the extent of ploughing in the GaN films during the scratching process. In addition, this discrepancy suggested that c-axis sapphire–grown GaN films have higher shear resistance than those grown on a-axis sapphire. Pile-up events indicated the generation and motion of individual dislocations measured under the critical brittle transition part of the scratch track, result in ductile and/or brittle properties.

5-2 Future Work

(1) The deformation features underneath the indented spot of GaN films.

The deformation features underneath the indented spot are primarily manifested by dislocation activities. The dislocation activities with repetition pressure-induced impairment has been analyzed qualitatively by the focused ion beam (FIB) and the cross-sectional transmission electron microscopy (XTEM).

(2) The deformation Behaviors with time-dependent nanoindentation experiments and unloading-reloading cycles on GaN films.

Nanoindentation is a useful tool to investigate the mechanical properties and fracture mechanism of thin films. Therefore, we can use this technique with different loading parameters in force mode such as number of times to load, maximum load, and peak hold time to observe loading and unloading curves. Besides, the morphology of indentation mark also includes some helpful information and can be observed by AFM analysis.

References

- [1] J. Black, et. al., "Recombination Radiation in GaAs", J. Appl. Phys. 34(1963)178.
- [2] F. A. Ponce and D. P. Bour, "Nitride-based semiconductors for blue and green light-emitting devices", Nature 386(1997)351.
- [3] S. Agarwal, et. al., "Design Guidelines for True Green LEDs and High Efficiency Photovoltaics Using ZnSe/GaAs Digital Alloys", Electrochemical and Solid-State Lett. 13(1)(2010)H5.
- [4] S. Leone, et. al., "High Growth Rate of 4H-SiC Epilayers on On-Axis Substrates with Different Chlorinated Precursors", Crystal Growth & Design 10(12)(2010)5335.
- [5] S. J. Pearton, et. al., "GaN and Related Materials", Gordon and Breach Science Publishers (1997) 471.
- [6] M. Fukuda, Optical Semiconductor Devices, John Wiley & Sons, New York (1999).
- [7] H. J. Round, "A note on carborundum", Electrical World 49 (1907) 309.
- [8] O. V. Lossev, "Luminous carborundum detector and detection effect and oscillations with crystals", Philosophical Magazine Series 7 6(1928)1024.
- [9] R. Braunstein, "Radiative Transitions in Semiconductors", Physical Review 99(1955)1892.
- [10] J. I. Pankove, et. al., "Luminescence properties of defects in GaN", J. Luminescence 5(1992)84.
- [11] H. Amano, et. al., "P-Type Conduction in Mg-Doped GaN Treated with Low-Energy Electron Beam Irradiation (LEEBI)", Appl. Phys. Lett. 48(1986)353.
- [12] A. Zukauskas, et. al., "Introduction to Solid State Lighting", John Wiley & Sons (2002) 15.
- [13] N. M. P. Low, et. al., "Effects of preparation on the anti-stokes luminescence of Er-activated rare-earth phosphors", Journal of Luminescence 4(4) (1971)357.
- [14] M. Berggren, et. al., "Multicolour electroluminescent diode made from poly(3-(4-octylphenyl)-2,2'-bithiophene) and an oxadiazole derivative", J. Appl. Phys. 76(1994)7530.
- [15] S. Nakamura, et. al., "The Blue Laser Diode: GaN Based Light Emitters and Lasers", Springer (1997)343.
- [16] S. Strite, and H. Morkoc, "GaN, AlN, and InN: A review", J. Vac. Sci. Technol. 10(1992)1237.
- [17] H. Morkoc, et. al., "A Review of Large Bandgap SiC, III-V Nitrides, and ZnSe Based II-VI Semiconductor Structures and Devices", J. Appl. Phys. 76(1994)1363.
- [18] S. Yoshida, et. al., "Improvements on the electrical and luminescent properties of reactive molecular beam epitaxially grown GaN films by using AlN-coated sapphire substrates", Appl. Phys. Lett. 42(1983)427.

- [19] S. C. Jain, et. al., “III–nitrides: Growth, characterization, and properties”, *J. Appl. Phys.* 87(2000)965.
- [20] J. A. Vechten, et. al., “Defeating Compensation in Wide Gap Semiconductors by Growing in H that is Removed by Low Temperature De-Ionizing Radiation”, *Jpn. J. Appl. Phys.* 31(1992)3662.
- [21] S. Nakamura, et. al., “Hole Compensation Mechanism of P-Type GaN Films”, *Jpn. J. Appl. Phys.* 31(1992)1258.
- [22] S. Nakamura, “Nichia’s 1cd blue LED paves way for full-color display. *Nikkei Electronics Asia*”, 6(1994)65.
- [23] S. Nakamura, et. al., “Candela-class high-brightness InGaN/AlGaN double-heterostructure blue-light-emitting diodes *Appl. Phys. Lett.* ”, 64(1994) 1687.
- [24] Cheng Liao, “Effects of Surface Microstructures on the Optoelectronic Properties of GaN-based Light-Emitting Diodes”, NCTU, Department of Material Science and Engineering, 2010.
- [25] S. D. Lester, et. al., “High dislocation densities in high efficiency GaN-based light-emitting diodes”, *Appl. Phys. Lett.* 66(1995)1249.
- [26] K. Dennis, et. al., “Development of Gallium Nitride Photoconductive Detectors”, *Johns Hopkins APL Tech. Dig.* 18(2)(1997)217.
- [27] S. Nakamura, et. al., “Room-temperature continuous-wave operation of InGaN multi-quantum-well structure laser diodes”, *Appl. Phys. Lett.* 69(1996) 4056.
- [28] S. Nakamura, et. al., “High-brightness InGaN/AlGaN double-heterostructure blue-green-light-emitting diodes”, *J. Appl. Phys.* 76(1994)8189.
- [29] T. Nagatomo, et. al., “Properties of Ga_{1-x}In_xN Films Prepared by MOVPE”, *Jpn. J. Appl. Phys.* 28(1989)L1334.
- [30] N. Yoshimoto, et. al., “Photoluminescence of InGaN films grown at high temperature by metalorganic vapor phase epitaxy”, *Appl. Phys. Lett.* 59(1991)2251.
- [31] L. Liu, J.H. Edgar, “Substrates for gallium nitride epitaxy”, *Mater. Sci. Eng. R* 37(2002)61.
- [32] S.J. Pearton, et. al., “Fabrication and performance of GaN electronic devices”, *Mater. Sci. Eng. R* 30(2000)55.
- [33] T. Miyajima, et. al., “GaN-based blue laser diodes ”, *J. Phys. Cond. Matter* 13 (2001) 7099.
- [34] E.T. Yu, et. al., “Spontaneous and piezoelectric polarization effects in III-V nitride heterostructures”, *J. Vac. Sci. Technol. B* 17 (1999) 1742.
- [35] O. Ambacher, et. al., “Role of Spontaneous and Piezoelectric Polarization Induced Effects in Group-III Nitride Based Heterostructures and Devices”, *Phys. Stat. Sol. (b)* 216(1999)381.

- [36] R. Dimitrov, et. al., "Two-dimensional electron gases in Ga-face and N-face AlGa_N/Ga_N heterostructures grown by plasma-induced molecular beam epitaxy and metalorganic chemical vapor deposition on sapphire", *J. Appl. Phys.* 87(2000) 3375.
- [37] J. H. Edgar, et. al., "Gallium Nitride and Related Semiconductors", Exeter, UK, 45(1999).
- [38] D. C. Look, J.R. Sizelove, "Predicted maximum mobility in bulk Ga_N" *Appl. Phys. Lett.* 79(2001)1133.
- [39] U. Kaufmann, et. al., "Hole Conductivity and Compensation in Epitaxial Ga_N:Mg Layers", *Phys. Rev. B.*, 62(2000)10867.
- [40] D. Doppalapudi, T.D. Moustakas, "Epitaxial growth and structure of III-V nitride thin films", *Handbook of Thin Film Mater.* 4(2002)57.
- [41] S. Porowski, Grzegory, in: J.H. Edgar (Ed.), *Properties of Group III Nitrides*, INSPEC, The Institution of Electrical Engineers, Stevenage, UK, (1994)76.
- [42] R. R. Reeber, K. Wang, *Mater. Res. Soc. Symp.* 622 (2000) T6.35.1.
- [43] D. I. Florescu, et. al., "Thermal conductivity of fully and partially coalesced lateral epitaxial overgrown Ga_N/sapphire (0001) by scanning thermal microscopy", *Appl. Phys. Lett.* 77(2000) 1464.
- [44] S. Krukowski, et. al., "The Institution of Electrical Engineers, Stevenage", UK, INSPEC(1999) 21.
- [45] S. O. Kucheyev, et. al., "Nanoindentation of epitaxial Ga_N films", *Appl. Phys. Lett.* 77(2000) 3373.
- [46] I. Yonenaga, et. al., "Hardness of Bulk Single-Crystal Gallium Nitride at High Temperatures", *Jpn. J. Appl. Phys.* 39(2000) L200.
- [47] I. Yonenaga and K. Motoki, "Yield strength and dislocation mobility in plastically deformed bulk single-crystal Ga_N", *J. Appl. Phys.* 90 (2001) 6539.
- [48] E.S. Hellman, *MRS Internet J. Nitride Semicond. Res.* 3 (1998) 11.
- [49] S. Nakamura, "Candela-class high-brightness InGa_N/AlGa_N double-heterostructure blue-light-emitting diodes", *Appl. Phys. Lett.* 64 (1994) 28.
- [50] S.D. Lester, et. al., "High dislocation densities in high efficiency Ga_N-based light-emitting diodes", *Appl. Phys. Lett.* 66 (1995) 1249.
- [51] S. Mutsumi, et. al., "Reduced Defect Densities in Cubic Ga_N Epilayers with AlGa_N/Ga_N Superlattice Underlayers Grown on (001) GaAs Substrates by Metalorganic Vapor Phase Epitaxy", *Jpn. J. Appl. Phys.* 43(3)(2004) 958.
- [52] D. K. Wickenden, et. al., "Development of Al_xGa_{1-x}N Alloy Semiconductors for Solar-Blind Ultraviolet Seeker Applications", *Johns Hopkins APL Tech. Dig.* 6(3)(1995) 246.
- [53] S. Strite, and H. Morkoc, "Ga_N, AlN, and InN: A Review", *J. Vac. Sci. Technol. B* 10(4) (1992) 1237.

- [54] I. Akasaki, et. al., “High Efficiency Blue LED Utilizing GaN Film with AlN Buffer Layer Grown by MOVPE”, *Inst. Phys. Conf. Ser.* 91(1988)633.
- [55] H. Amano, et. al., “P-Type Conduction in Mg-Doped GaN Treated with Low-Energy Electron Beam Irradiation (LEEBI)”, *Jpn. J. Appl. Phys.* 28(1989) L2112.
- [56] M. A. Khan, et. al., “Metal Semiconductor Field Effect Transistor Based on Single Crystal GaN”, *Appl. Phys. Lett.* 62(1993) 1786.
- [57] K. Itoh, et. al., “Metalorganic Vapor Phase Epitaxial Growth and Properties of GaN/Al_{0.1}Ga_{0.9}N Layered Structures”, *Jpn. J. Appl. Phys.* 30(1991)1924.
- [58] H. Amano, et. al., “Stimulated Emission in MOVPE-Grown GaN Film”, *J. Luminescence* 48/49(1991) 889.
- [59] M. A. Khan, et. al., “High Electron Mobility GaN/Al_xGa_{1-x}N Heterostructures Grown by Low-Pressure Metalorganic Chemical Vapor Deposition”, *Appl. Phys. Lett.* 58(1991) 2408.
- [60] S. Nakamura, et. al., “High-Power InGaN/GaN Double Heterostructure Violet Light Emitting Diodes”, *Appl. Phys. Lett.* 62(1993) 2390.
- [61] S. Nakamura, et. al., “High-brightness InGaN/AlGaIn double-heterostructure Blue-Green-light-emitting diodes”, *J. Appl. Phys.* 76(1994) 8189.
- [62] S. Nakamura, et. al., “High-Brightness InGaN Blue, Green and Yellow Light-Emitting Diodes with Quantum Well Structures”, *Jpn. J. Appl. Phys.* 34(1995) L797.
- [63] I. Akasaki, et. al., “Stimulated Emission by Current Injection from an AlGaIn/GaN/GaInN Quantum Well”, *Jpn. J. Appl. Phys.* 34 (1995) L1517.
- [64] S. Nakamura, et. al., “InGaN-based Multi-Quantum-Well- Structure Laser Diodes”, *Jpn. J. Appl. Phys.* 35(1996) L74.
- [65] M. A. Khan, et. al., “High-Responsivity Photoconductive Ultraviolet Sensors Based on Insulating Single-Crystal GaN Epilayers”, *Appl. Phys. Lett.* 60(1992) 2917.
- [66] M. A. Khan, et. al., “Gated Photodetector Based on GaN/AlGaIn Heterostructure Field Effect Transistor”, *Electron. Lett.* 31(1995) 398.
- [67] Razeghi, M., and Rogalski, A., “Semiconductor Ultraviolet Detectors”, *J. Appl. Phys.* 79(1996) 7433.
- [68] P. Waltereit, et. al., “Growth of M-Plane GaN(11-00): A Way to Evade Electrical Polarization in Nitrides”, *Phys. Stat. Sol. (a)* 180(2000) 133.
- [69] E.S. Hellman, et. al., “Growth of Ga-face and N-face GaN films using ZnO substrates”, *MRS Internet J. Nitride Semicond. Res.* 1(1996)16.
- [70] F. Hamdani, et. al., “Microstructure and optical properties of epitaxial GaN on ZnO (0001) grown by reactive molecular beam epitaxy”, *J. Appl. Phys.* 83 (1998) 983.
- [71] Y. Xin, et. al., “Microstructural characterisation of GaN(As) films grown on (001) GaP by molecular beam epitaxy”, *J. Cryst. Growth* 171 (1997) 321.
- [72] V. Y. Davydov, et. al., “Raman characterization of cubic GaN epitaxial layers grown on (001)GaAs and GaP substrates”, *J. Cryst. Growth* 189/190 (1998) 430.

- [73] H. P. Maruskas, and J.J. Tietjen, "The preparation and properties of Vapor-deposited single-crystalline GaN", *Appl. Phys. Lett.* 15 (1969) 327.
- [74] E. V. Etzkorn, and D.R. Clarke, "Cracking of GaN films", *J. Appl. Phys.* 89 (2) (2001) 1025.
- [75] J. E. Van Nostrand, et. al., "Dissociation of Al₂O₃(0001) substrates and the roles of silicon and oxygen in n-type GaN thin solid films grown by gas-source molecular beam epitaxy", *J. Appl. Phys.* 87 (2000) 8766.
- [76] W. E. Lee, K.P.D. Lagerlof, *J. Electron. Microsc. Technol.* 2 (1985) 247.
- [77] O. Ambacher, "Growth and applications of Group III-nitrides", *J. Phys. D: Appl. Phys.* 31 (1998) 2653.
- [78] D. A. Stocker, et. al., "Facet roughness analysis for InGaN/GaN lasers with cleaved facets", *Appl. Phys. Lett.* 73(1998) 1925.
- [79] S. Nakamura, et. al., "InGaN Multi-Quantum-Well-Structure Laser Diodes with Cleaved Mirror Cavity Facets", *Jpn. J. Appl. Phys.* 35 (1996) L217.
- [80] T. Shibata, Y. Hori, et. al., "2.4GHz SAW filters using AlN deposited on off-angle r-plane sapphire substrates by MOCVD", *IEEE Ultrasonics Symposium*, (2000)287.
- [81] S. Tripathy, et. al., "Optical properties of GaN layers grown on C-, A-, R-, and M-plane sapphire substrates by gas source molecular beam epitaxy", *J. Appl. Phys.* 85 (1999) 8386.
- [82] T. Matsuoka, and E. Higiwara, "GaN Growth on Novel Lattice-Matching Substrate: Tilted M-Plane Sapphire", *Phys. Stat. Sol. (a)* 188 (2001) 485.
- [83] B. Bhushan, Micro/Nanotribology and Micro/Nanomechanics of MEMS, Handbook of micro/nanotribology. 2nd ed. Boca Raton (FL): CRC Press, 1999.
- [84] J. B. Pethica, et. al., "Hardness measurement at penetration depths as small as 20 nm", *Philos Mag A* 48 (1983)593.
- [85] W. C. Oliver, and G. M. Pharr, et. al., "An improved technique for determining hardness and elastic-modulus using load and displacement sensing indentation experiments", *J Mater Res* 7(1992)1564.
- [86] G. M. Pharr, "Measurement of mechanical properties by ultra-low load indentation", *Mater Sci Eng, A* 253(1998)151.
- [87] X. Li, et. al., "Fracture mechanisms of thin amorphous carbon films in nanoindentation", *Acta Mater.* 45(1997)4453.
- [88] X. Li X, and B. Bhushan, "Measurement of fracture toughness of ultra-thin amorphous carbon films", *Thin Solid Films* 315(1998) 214.
- [89] T. Y. Tsui and G. M. Pharr, "Substrate effects on nanoindentation mechanical property measurement of soft films on hard substrates", *J. Mater. Res.* 14(1999) 292.
- [90] R. Saha, and W. D. Nix, "Effects of the substrate on the determination of thin film mechanical properties by nanoindentation", *Acta Mater.* 50(2002)23.

- [91] X. Li, and B. Bhushan, "A review of nanoindentation continuous stiffness measurement technique and its applications", *Materials Characterization* 48(2002)11.
- [92] J. L. Hay, G. M. Pharr, "ASM Handbook: Material Testing and Evaluation (10th edition)", International Materials Park, Ohio, USA, 8(2002) 232-242.
- [93] H. Hertz, *Journal Reine and Angewandte Mathematik* 92(1882)156.
- [94] J. Boussinesq, "Applications despotentials a l'etude de equilibre et du mouvement de solides elastiques", Gauthier-Villars, Paris(1885).
- [95] I. N. Sneddon, "The relation between load and penetration in the axisymmetric Boussinesq problem for a punch of arbitrary profile", *Int. J. Eng. Sci.* 3(1965)47-56.
- [96] W. C. Olivera, and C. J. McHargue, "Characterizing the hardness and modulus of thin films using a mechanical properties microprobe", *Thin Solid Films*161(1988)117.
- [97] D. Tabor, The hardness of metal, Oxford Univ. Press(1951).
- [98] J. E. Bradby, et. al., "Mechanical deformation of InP and GaAs by spherical indentation", *Appl. Phys. Lett.* 78(2001) 3235.
- [99] D. Tabor, "Indentation hardness: fifty years on a personal view", *Philos. Mag. A*, 74(1996) 1207.
- [100] G. M. Pharr, and A. Bolshakov, "Understanding nanoindentation unloading curves", *J. Mater. Res.* 17(2002)2660.
- [101] B. Bhushan, "Nanoindentation and picondentation measurements using a capacitive transducer system in atomic force microscopy", *Philos. Mag. A* 74(1996) 1117.
- [102] B. Bhushan, "Mechanical and tribological characterization of ultra-thin and hard amorphous carbon coatings as thin as 3.5 nm: recent developments", *Diamond Relat. Mater.* 8(1999)19895.
- [103] Z. C. Li, et. al., "Shear-activated indentation crack in GaAs single crystal", *J. Mater. Res.* 16(2001)2845.
- [104] C. R. Taylor, et. al., "Nanoscale dislocation patterning by ultralow load indentation", *Appl. Phys. Lett.* 87(2005) 073108.
- [105] X. Li X., and B. Bhushan, "Evaluation of fracture toughness of ultra-thin amorphous carbon coatings deposited by different deposition techniques", *Thin Solid Films* 355(1999) 330.
- [106] Y. Ando, R. Kaneko, *Microwear process*, in: *Proceedings of the International Conference in Tribology*, Yokohama, JAST Press, Tokyo, Japan(1995).
- [107] S. Miyake, and J. Kim, "Fabrication of Silicon Utilizing Mechanochemical Local Oxidation by Diamond Tip Sliding", *Jpn. J. Appl. Phys.* 40 (11B) (2001) L1247.
- [108] S.W. Youna, C.G. Kang, "A study of nanoscratch experiments of the silicon and borosilicate in air", *Mater. Sci. and Eng. A* 384 (2004) 275.
- [109] R. C. Chang, "Nanoindentation and nanoscratch behaviors of evaporation thin films", *The 29th National Conference on Theoretical and Applied Mechanics*, p16-17, Hsinchu, Taiwan, R.O.C., December, 2005.

- [110] J. Gong, et. al., “Analysis of the nanoindentation data measured with a Berkovich indenter for brittle materials: effect of the residual contact stress”, *Acta Mater.* 52(3)(2004)785-793.
- [111] P. F. Yang, et. al., “Characteristics of ZnO thin films prepared by radio frequency magnetron sputtering”, *Microelectronics Reliability* 48(2008)389.
- [112] W. C. Oliver, and G. M. Pharr, “Measurement of hardness and elastic modulus by instrumented indentation: Advances in understanding and refinements to methodology”, *J. Mater. Res.* 19(1994)3.
- [113] N. K. Mukhopadhyay, and P. Paufler, “Micro- and nanoindentation techniques for mechanical characterisation of materials”, *Inter. Mater. Rev.* 51(2006)209
- [114] K. Geng, et. al., “Nanoindentation-induced delamination of submicron polymeric coatings”, *Polymer* 48 (2007) 841.
- [115] M. H. Lin, et. al., “Effect of repetition nanoindentation of GaN epilayers on a-axis sapphire substrates”, *Surf. Interface Anal.* 43(2011) 918.
- [116] T. Gühne, et. al., “Cathodoluminescence spectroscopy of epitaxial-lateral-overgrown nonpolar (11-20) and semipolar (11-22) GaN in relation to microstructural characterization”, *Appl. Phys. Lett.* 101(2005) 113101.
- [117] R. Nowak, et. al., “Elastic and plastic properties of GaN determined by nano-indentation of bulk crystal”, *Appl. Phys. Lett.* 75(1999) 2070.
- [118] S. Basu, et. al., “Spherical nanoindentation and deformation mechanisms in freestanding GaN films”, *J. Appl. Phys.* 101 (2007) 083522.
- [119] S. O. Kucheyev, et. al., “Deformation behavior of ion-beam-modified GaN”, *Appl. Phys. Lett.* 78 (2001) 156.
- [120] S. R. Jian, “Mechanical Deformation Induced in Si and GaN Under Berkovich Nanoindentation”, *Nanoscale Res Lett.* 3(2008) 6.
- [121] D. Caceres, et. al., “Nanoindentation on AlGaIn thin films”, *J. Appl. Phys.* 86 (1999) 6773.
- [122] T. Wei, et. al., “Mechanical Deformation Behavior of Nonpolar GaN Thick Films by Berkovich Nanoindentation”, *Nanoscale Res. Lett.* 4 (2009) 753.
- [123] D. Hanser, et. al., “Surface preparation of substrates from bulk GaN crystals”, *J. Cryst. Growth* 305 (2007) 372.
- [124] J. E. Bradby, et. al., “Indentation-induced damage in GaN epilayers”, *Appl. Phys. Lett.* 80 (2002) 383.
- [125] R. Navamathavan, et. al., “Pop-in’ phenomenon during nanoindentation in epitaxial GaN thin films on c-plane sapphire substrates”, *Mater. Chem. Phys.* 99 (2006) 410.
- [126] X. J. Ning, et. al., “Growth defects in GaN films on sapphire: The probable origin of threading dislocations”, *J. Mater. Res.* 11 (1996) 580.
- [127] B. N. Sverdlov, et. al., “Formation of threading defects in GaN wurtzite films grown on nonisomorphic substrates”, *Appl. Phys. Lett.* 67 (1995) 2063.

- [128] C. D. Lee, et. al., "Role of Ga flux in dislocation reduction in GaN films grown on SiC(0001)", *Appl. Phys. Lett.* 79 (2001) 3428.
- [129] C. H. Tsai, et. al., "Berkovich nanoindentation and deformation mechanisms in GaN thin films", *Appl. Surf. Sci.* 254 (2008) 1997.
- [130] M. A. Haase, et. al., "Blue-green laser diodes", *Appl. Phys. Lett.* 59(1991)1272.
- [131] H. Jeon, et. al., "Blue and green diode lasers in ZnSe-based quantum wells", *Appl. Phys. Lett.* 60(1992)2045.
- [132] T. Nagatomo, et. al., "Properties of Ga_{1-x}In_xN Films Prepared by MOVPE", *Jpn. J. Appl. Phys.* 28(1989)L1334.
- [133] O. Lopatiuk-Tirpak, et. al., "Cathodoluminescence studies of carrier concentration dependence for the electron-irradiation effects in p-GaN", *Appl. Phys. Lett.* 90(2007)172111.
- [134] H. Okumura, et. al., "Growth and characterization of cubic GaN", *J. Cryst. Growth* 178(1997)113.
- [135] H. M. Kim, et. al., "Preparation of large area free-standing GaN substrates by HVPE using mechanical polishing liftoff method", *Mater. Lett.* 47 (2001)276.
- [136] K. Motoki, et. al., "Preparation of large GaN substrates", *Mater. Sci. Eng. B* 93(2002)123.
- [137] R. P. Vaudo, et. al., IWN 2000, IPAP Conference Series C1, Nagoya, Japan, 2000, p. 15.
- [138] Y. Oshima, et. al., "Preparation of Freestanding GaN Wafers by Hydride Vapor Phase Epitaxy with Void-Assisted Separation", *Jpn. J. Appl. Phys.*, 42(2003) L1.
- [139] S. Dhara, et. al., "Recrystallization of epitaxial GaN under indentation", *Appl. Phys. Lett.* 92(2008) 143114.
- [140] S. J. Bull, "Nanoindentation of coatings", *J. Phys. D: Appl. Phys.* 38 (2005) R393.
- [141] C. Coupeau, et. al., "Nanoindentation-induced deformation in Al-Pd-Mn single quasicrystals", *J. Appl. Phys.* 88 (2006) 073106.
- [142] R. Navamathavan, et. al., "Nanoindentation 'pop-in' phenomenon in epitaxial ZnO thin films on sapphire substrates", *Mater. Characterization* 59(2008)359.
- [143] M. Albrecht, et. al., "Carrier recombination at single dislocations in GaN measured by cathodoluminescence in a transmission electron microscope", *J. Appl. Phys.* 92(2002) 2000.
- [144] A. C. Fischer-Cripps, "A simple phenomenological approach to nanoindentation creep", *Mater. Sci. Eng.* 385(2004)74.
- [145] N. Armani, et. al., "Raman and cathodoluminescence study of dislocations in GaN", *J. Appl. Phys.* 92(2002) 6666.
- [146] M. H. Lin, et. al., "Nanoindentation characterization of GaN epilayers on A-plane sapphire substrates", *Appl. Surf. Sci.* 256(2010)3299.
- [147] C. A. Schuh, "Nanoindentation studies of materials", *Materials Today* 9(2006)580.

- [148] G. Yu, et. al., “Mechanical properties of the GaN thin films deposited on sapphire substrate”, *J. Cryst. Growth* 189-190(1998)701.
- [149] R. Navamathavan, et. al., “Nanoindentation studies of (111) GaAs/InP epilayers”, *Appl. Sur. Sci.* 256(2010)3299.
- [150] M. W. Barsoum, et. al., “Kink bands, nonlinear elasticity and nanoindentations in graphite”, *Carbon* 42(2004)1435.
- [151] W. H. Yau, et. al., “Luminescence properties of mechanically nanoindented ZnSe”, *Microelectronics Reliability* 51(2011)931.
- [152] R. Navamathavan, et. al., “A nanoindentation analysis of the influence of lattice mismatch on some wide band gap semiconductor films”, *Physica B* 403 (2008) 675.
- [153] M. Fujikane, et. al., “Elastic–plastic transition during nanoindentation in bulk GaN crystal”, *J. Alloys and Compounds* 450 (2008) 405.
- [154] G. Zhang, et. al., “Elastic modulus and hardness of muscovite and rectorite determined by nanoindentation”, *Appl. Clay Sci.* 43 (2009) 271.
- [155] W. G. Mao, et. al., “Nanoscale elastic–plastic deformation and stress distributions of the C plane of sapphire single crystal during nanoindentation”, *J. European Ceramic Society* 31 (2011) 1865.
- [156] M.W. Barsoum, et. al., “Kinking Nonlinear Elastic Solids, Nanoindentations, and Geology”, *Phys. Rev. Lett.* 92(2004)255508.
- [157] S. Basu, et. al., “Sapphire: A kinking nonlinear elastic solid”, *J. Appl. Phys.* 99(2006)063501.
- [158] S. R. Jian, et. al., “Cathodoluminescence and Cross-sectional Transmission Electron Microscopy Studies for Deformation Behaviors of GaN Thin Films Under Berkovich Nanoindentation”, *Nanoscale Res. Lett.* 3(2008)158.
- [159] X. Huang, A. A. Pelegri, “Finite element analysis on nanoindentation with friction contact at the film/substrate interface”, *Composites Sci. Tech.* 67 (2007) 1311.
- [160] W. C. Oliver, R. Hutchings, J.B. Pethica, in *ASTM STP 889*, ed. by P.J. Blau, B.R. Lawn (American Society for Testing and Materials, Philadelphia, 1986)
- [141] M. F. Doerner, and W.D. Nix, “A method for interpreting the data from depth-sensing indentation instruments”, *J. Mater. Res.* 1 (1986)601.
- [162] J. B. Pethica, in *Ion Implantation into Metals*, ed. by V. Ashworth, W. Grant, R. Procter (Pergamon Press, Oxford, 1982)
- [163] J. L. Loubet, et. al., “Vickers Indentation Curves of Magnesium Oxide (MgO)”, *J. Tribol* 106(1984) 43.
- [164] D. Newey, et. al., “An ultra-low-load penetration hardness tester”, *J. Phys. E: Sci. Instrum.* 15(1982)119.

- [165] D. Stone, et. al., “An investigation of hardness and adhesion of sputter-deposited aluminum on silicon by utilizing a continuous indentation test”, *J. Mater. Res.* 3(1988)141.
- [166] S. R. Jian, et. al., “Analysis of Physical Properties of III-Nitride Thin Films by Nanoindentation”, *J. Electronic Mater.* 32(2003)496.
- [167] R. Navamathavan, et. al., “Deformation behavior during nanoindentation of epitaxial ZnO thin films on sapphire substrate”, *Mater. Lett.* 61 (2007) 2443.
- [168] T. Ebisu, and S. Horibe, “ Analysis of the indentation size effect in brittle materials from nanoindentation load–displacement curve”, *J. European Ceramic Society* 30(2010)2419.
- [169] M. H. Lin, et. al., “Nanoscratch Characterization of GaN Epilayers on c- and a-Axis Sapphire Substrates”, *Nanoscale Res. Lett.* 5(2010)1812.
- [170] L.L. Sohn, and R.L. Willet, “Fabrication of nanostructures using atomic-force-microscope-based lithography”, *Appl. Phys. Lett.* 67(1995)1552.
- [171] K. Ashida, et. al., “Study on Nano-machining Process Using Mechanism of a Friction Force Microscope”, *JSME – Int. J., Ser. C* 44(2001)244.
- [172] W. Meredith, et. al., “Microprobe Raman study of the variation of LO phonon frequency with the Cd concentration in the ternary compound $Zn_{1-x}Cd_xSe$ ”, *J. Cryst. Growth* 159 (1996)103.
- [173] C. Jin, et. al., “Growth and optical characterization of diluted magnetic semiconductor $Zn_{1-x}Mn_xSe/ZnSe$ strained-layer superlattices”, *J. Appl. Phys.* 81(1997)5148
- [174] J. M. Sanchez, et. al., “Cross-sectional nanoindentation: a new technique for thin film interfacial adhesion characterization”, *Acta Mater.* 47(1999)4405.
- [175] T. H. Fang, et. al., “Nanoindentation and nanoscratch characteristics of Si and GaAs”, *Microelectronic Engineering* 77 (2005) 389.

Curriculum vitae and list of publications

Personal data

Name: Meng-Hung Lin

Birthday: July 6, 1981 at Taichung, Taiwan.

Education

⇒ 9/2008-6/2012-6 Ph.D.

in Mechanical Engineering, National Chiao Tung University, Hsinchu, Taiwan.

⇒ 9/2006-7/2008-7 Master

in Mechanical Engineering, National Chin-Yi University of Technology, Taichung, Taiwan.

⇒ 9/2002-7/2005-2 Bachelor

in Mechanical Engineering, National Chin-Yi University of Technology, Taichung, Taiwan.

⇒ 9/1997-7/2002-6 Junior College

in Power Mechanical Engineering, National Formosa University, Yunlin, Taiwan.

SCI Journal papers

- [1] **Meng-Hung Lin**, Hua-Chiang Wen, Shyh-Chi Wu, Wen-Fa Wu, Chang-Pin Chou, “Effect of Repetition Nanoindentation of GaN Epilayers on a-axis Sapphire Substrates” , Surface and Interface Analysis, 43(2011)918-922.
- [2] **Meng-Hung Lin**, Hua-Chiang Wen, Yeau-Ren Jeng, Chang-Pin Chou, “Nanoscratch Characterization of GaN Epilayers on c- and a-Axis Sapphire Substrates”, Nanoscale Research Letters, 5(2010)1812-1816.
- [3] **Meng-Hung Lin**, Hua-Chiang Wen, Chih-Yung Huang, Yeau-Ren Jeng, Wei-Hung Yau, Wen-Fa Wud, Chang-Pin Chou, “Nanoindentation characterization of GaN epilayers on A-plane sapphire substrates”, Applied Surface Science 256 (2010) 3464-3467
- [4] Bo-Ching He, Chun-Hu Cheng, Hua-Chiang Wen, Yi-Shao Lai, Ping-Feng Yang, **Meng-Hung Lin**, Wu-Ching Chou, Wen-Fa Wu, Chang-Pin Chou, “Evaluation of the nanoindentation behaviors of SiGe epitaxial layer on Si substrate”, Microelectronic Reliability, 50 (2010) 63-69.
- [5] Bo-Ching He, Hua-Chiang Wen, **Meng-Hung Lin**, Yi-Shao Lai, Wen-Fa Wu, Chang-Pin Chou, “Effect of annealing treatment and nanomechanical properties for multilayer Si_{0.8}Ge_{0.2}-Si films”, Microelectronic Reliability, 50(2010)851-856.

Conference Papers

- [1] 李其澧, 何柏青, **林孟泓**, 吳明璋, 溫華強, 吳文發, 周長彬, ”碲化鋅機械與光學特性研究”, 中國材料科學學會97年會論文集, P07-032, 11月21日, 台北市, 2008.
- [2] 王凱億, 何柏青, **林孟泓**, 吳明璋, 李其澧, 溫華強, 吳文發, 周長彬, ”栓塞結構結合奈米碳管定機械性質之探討”, 中國材料科學學會97年會論文集, P07-034, 11月21日, 台北市, 2008.
- [3] 林金雄, 吳明璋, 彭麟皓, **林孟泓**, 周長彬, “不同鉛鈹合金元素奈米線複合陽極處理氧化鋁模板之機械特性探討”, 台灣中國材料科學學會97年會論文集, 十一月P21-22, 台北, 台灣, 2008.
- [4] **M.H. Lin**, B.C. He, H.C. Wen, C.H. Chiang, W.F. Wu, and C.P. Chou, “Nanomechanical and Cathodoluminescence Characteristics of GaN Epitaxial Layers”, Symposium on Nano Device Technology, Hsinchu, Taiwan, 2009.
- [5] Ming-Jhang Wu, Neng-Tung Liao, Jin-Shyong Lin, **Meng-Hung Lin**, Chang-Pin Chou, Wen-Fa Wu, “The microstructure and mechanical properties of Pb-Bi alloy nanowires/anodic aluminum oxide template”, Symposium on Nano Device Technology, Hsinchu, Taiwan, 2009.
- [6] **林孟泓**, 蕭元駿, 溫華強, 何柏青, 朱貞慈, 吳文發, 周長彬, ”氮化鎵結構施力參數研究”, 中國材料科學學會98年會論文集, 花蓮市, 2009。
- [7] C.T. Chu, B.C. He, **M.H. Lin**, Y.C. Hiao, C.P. Chou, W.F. Wu, “The characteristic of epitaxial SiGe thin films during high-temperature treatment”, 中國材料科學學會98年會論文集, 花蓮市, 2009。
- [8] **Meng-Hung Lin**, Hua-Chiang Wen, Yi-Shao Lai, Ping-Feng Yang, “Evaluation of nanomechanical properties on multi-layer SiGe-Si films”, ASE Technology Journal, Kaohsiung, Taiwan, 2009.
- [9] Chen-Tzu Chu, Bo-Ching He, **Meng-Hung Lin**, Yuan-Chin Hiao, Chang-Pin Chou, Wen-Fa Wu, “The Characteristic of Epitaxial SiGe Thin Films During High-Temperature Oxidation Treatment”, Symposium on Nano Device Technology, Hsinchu, Taiwan, 2010.
- [10] Yuan- Chun Hsiao, Chi-Hsiu Yeh, **Meng-Hung Lin**, Bo-Ching He, Wen-Fa Wu, Chang-Pin Chou, “Deformation Behaviors of A-plane GaN Epilayers Under Berkovich Nanoindentation”, Symposium on Nano Device Technology, Hsinchu, Taiwan, 2010.
- [11] **Meng-Hung Lin**, Hua-Chiang Wen, Ping-Feng Yang, Yi-Shao Lai, “Nanoindentation ‘Pop-in’ Phenomenon of GaN Epilayers on a-plane Sapphire Substrates”, ASE Technology Journal, Kaohsiung, Taiwan, Vol.3, No1, 2010.
- [12] 何柏青, 彭麟皓, 林金雄, **林孟泓**, 吳世基, 周長彬, ”Si/SiGe多層薄膜經熱處理之表面形貌分析”, 第四屆積體光機電科技與智慧財產權實務會議論文集, 2010.
- [13] 何柏青, 彭麟皓, 林金雄, **林孟泓**, 吳文發, 周長彬, ”探討矽/矽鍺多層薄膜結構經熱處理後之機械特性”, 第四屆積體光機電科技與智慧財產權實務會議論文集, 2010.

- [14] 葉吉修, 彭麟皓, 林孟泓, 林金雄, 吳文發, 周長彬, "C軸氮化鎵磊晶薄膜之機械特性與潛變特性探討", 第四屆積體光機電科技與智慧財產權實務會議論文集, 2010.
- [15] 何柏青, 彭麟皓*, 林金雄, 林孟泓, 吳世基, 周長彬, "熱處理溫度對矽鍺薄膜結構及機械特性之分析", 第四屆積體光機電科技與智慧財產權實務會議論文集, 2010.
- [16] 何柏青, 彭麟皓*, 林金雄, 林孟泓, 吳文發, 周長彬, "Si/SiGe多層結構之機械特性", 第16屆化學感測技術研討會, 2010.
- [17] 何柏青, 彭麟皓*, 林金雄, 林孟泓, 吳文發, 周長彬, "探討矽/矽鍺多層薄膜結構經高溫氧化後鍺擴散情形", 第16屆化學感測技術研討會, 2010.
- [18] 林孟泓, 彭麟皓, 林金雄, 吳世基, 吳文發, 周長彬, "多層矽鍺磊晶層之奈米壓痕性質探討", 台灣中國材料科學學會, 2010.
- [19] 林孟泓, 彭麟皓, 林金雄, 何柏青, 吳文發, 周長彬, "探討多層矽鍺薄膜經熱處理後之奈米微硬度變化", 台灣中國材料科學學會, 2010.
- [20] Meng-Hung Lin, Lin-Hao Peng, Ming-Jhang Wu, Wen-Fa Wu, Chang-Pin Chou, "Nanoscratch Characterization of GaN Epilayers on c-axis Sapphire Substrates", 台灣中國材料科學學會, 2010.
- [21] 林金雄, 彭麟皓, 林孟泓, 吳文發, 周長彬, "多層矽鍺薄膜結構之反覆負載機械特性", 台灣中國機械年會, 2010
- [22] 林孟泓, 彭麟皓, 林金雄, 吳世基, 周長彬, "矽緩衝層對機械特性影響", 2010國防科技學術研討會, 十二月十九, 桃園, 台灣, 2010
- [23] 曾瑞軒, 彭麟皓, 林孟泓, 吳世基, 周長彬, "A與C軸向氮化鎵之反覆負載機械性質", 2010國防科技學術研討會, 十二月十九, 桃園, 台灣, 2010.
- [24] 吳明璋, 吳世基, 林孟泓, 劉治平, 謝統生, 彭麟皓, 周長彬, "D6AC高強度合金鋼經由旋形加工後之機械特性與顯微組織探討", 2010國防科技學術研討會, 十二月十九, 桃園, 台灣, 2010.
- [25] 林孟泓, 彭麟皓, 吳雪, 林金雄, 周長彬, "氮化鎵磊晶層之彈塑性變形機制探討", 2010第四屆海峽兩岸科技與人文教育暨產學合作研討會, 十二月二日, 台中, 台灣, 2010
- [26] 林金雄, 彭麟皓, 林孟泓, 周長彬, "多層矽鍺薄膜缺陷機制探討", 2010第四屆海峽兩岸科技與人文教育暨產學合作研討會, 十二月二日, 台中, 台灣, 2010
- [27] Meng-Hung Lin, Lin-Hao Peng, Ming-Jhang Wu, Wen-Fa Wu and Chang-Pin Chou, "Repetition Nanoindentation-induced Deformation in GaN Epilayers on A-axis Sapphire Substrates", Symposium on Nano Device Technology, Hsinchu, Taiwan, 2011.
- [28] Ming-Jhang Wu, Meng-Hung Lin, Wen-Fa Wu, Chang-Pin Chou, "Nanoscratch Characteristics of Annealed Si/SiGe Superlattices", Symposium on Nano Device Technology, Hsinchu, Taiwan, 2011.